The Ecca Type Section (Permian, South Africa): An Outcrop Analogue Study of Conventional and Unconventional Hydrocarbon Reservoirs

By Stuart Alexander Campbell

Supervisor: Professor Annette E. Götz (Rhodes University)

Co-supervisor: Dr. Emese Bordy (University of Cape Town)

This thesis is submitted in fulfilment of the requirements of a Master of Science degree in the Department of Geology, Rhodes University.

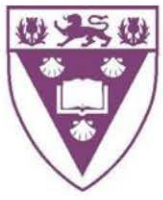

RHODES UNIVERSITY

Grahamstown • 6140 • South Africa

Acknowledgements

I would like to thank Rhodes University and the National Research Foundation for providing me with the opportunity to undertake this M.Sc study by sponsoring me during the year of study.

I would also like to express my utmost gratitude to all those who assisted me during the course of this study. Firstly, I would like to thank my supervisor Professor Annette E. Götz and my co-supervisor Dr. Emese M. Bordy for their invaluable time, patience and assistance with the completion of this project. I would like to thank and acknowledge Dr. Sebastian Homuth of Geotechnical Laboratory at TU Darmstadt for valuable assistance with the poroperm analysis of samples. I would also like to thank Dr. Herman Läuferts of Shell International Exploration and Production B.V. for arranging the TOC analysis.

I would like to thank Mr. Jan Pavluš for his invaluable support during the field work portion of this project which was often in the company of unsavoury and often disagreeable members of the local fauna. I would also like to thank my fellow M.Sc colleagues for their constant advice and support during our numerous coffee breaks.

Lastly I would like to thank the staff of the Rhodes University Geology Department: Mr. John Hepple and his staff for preparation of thin sections and for allowing me to prepare samples with their equipment.

Amat Victoria Curam.

Declaration

I declare that this thesis is my own work, and information from other publications is adequately referenced.

_____	_____
Name of candidate	signature

Signed on _____ day of _____ 2014

Abstract

The Karoo Basin of South Africa holds an estimated 906 billion to 11 trillion cubic meters of unconventional shale gas within the shales of the Whitehill and Collingham formations of the Ecca Group. Evaluation of this potential resource has been limited due to the lack of exploration and a scarcity of existing drill core data. In order to circumnavigate this problem this study was undertaken to evaluate the potential target horizons exposed in outcrops along the southern portion of the Karoo Basin, north of Grahamstown in the Eastern Cape Province.

Detailed field logging was done on the exposed Whitehill and Collingham formations as well as a possible conventional sandstone (turbidite) reservoir, the Ripon Formation, along road cuttings of the Ecca Pass. Palaeocurrent data, jointing directions and fossil material were also documented. Samples were analysed for mineralogy, porosity, permeability, and total organic carbon content (TOC).

The extensively weathered black shales of the Whitehill Formation contain a maximum TOC value of 0.9% and the Collingham Formation shales contain a maximum TOC value of 0.6%. The organic lithic arkose sandstones of the Ripon Formation are classified as ‘tight rock’ with an average porosity of 1% and an average permeability of 0.05 mD. The Whitehill Formation in the southern portion of the Karoo Basin has experienced organic matter loss due to low grade metamorphism as well as burial to extreme depths, thus reducing shale gas potential. The Ripon Formation is an unsuitable conventional reservoir along the southern basin boundary due to extensive cementation and filling of pore spaces.

Table of Contents

List of Figures

List of Tables

List of Photo Plates

Chapter 1 - Introduction

Turbidites, second only to carbonates, host the majority of the world's crude oil reserves, with deep water turbidites playing an increasingly important role as shallow water reservoirs are depleted (Bouma and Stone, 2000; Poupon, pers. comm., 2014). South Africa has a vested interest in unconventional natural gas resources contained in shales of the Karoo Basin with recent estimates of shale gas reserves between 32 Tcf and 485 Tcf (Decker and Marot, 2012). The Karoo Basin of South Africa contains both turbidites and shales within close stratigraphic proximity, excellently exposed in road cuttings along the Ecca Pass northeast of Grahamstown in the Eastern Cape. The Ecca Pass descending to the Brack River, the original of which was the Ecca River, is the type location for the Ecca Group (Mountain, 1946; Johnson, 1976).

The aim of this study is to compare and contrast conventional and unconventional reservoirs exposed in outcrops found in the lower stratigraphy of the Ecca Group of the Karoo Supergroup, with a focus on palaeo-environmental and depositional environmental determination as well as comparing reservoir characteristics to modern day productive and well-studied reservoirs.

1.1 Turbidites

Deep-water sands (submarine fans or turbidite systems) form a great portion of the total sediment body in the present day oceans and in many ancient sedimentary basins (*Figure 1.1*). These deposits are significant in deep basins adjacent to continents (*Figure 1.2*) and form via mass flows and turbulent suspension currents triggered by progressive accumulation of material on a submarine slope. When the angle of repose is exceeded material accumulated on the slope slides down, giving rise to a high-density current. It is well known that these potentially major oil and gas reservoirs lack the level of knowledge that is available from other depositional environments. Deposits of turbidity currents (turbidites) form fan complexes up to kilometres in thickness with individual beds ranging in thickness from a few millimetres to several metres in thickness with grain sizes ranging from mud to gravel (Einsele, 1992; Bouma, 2000; Casnedi, 2005).

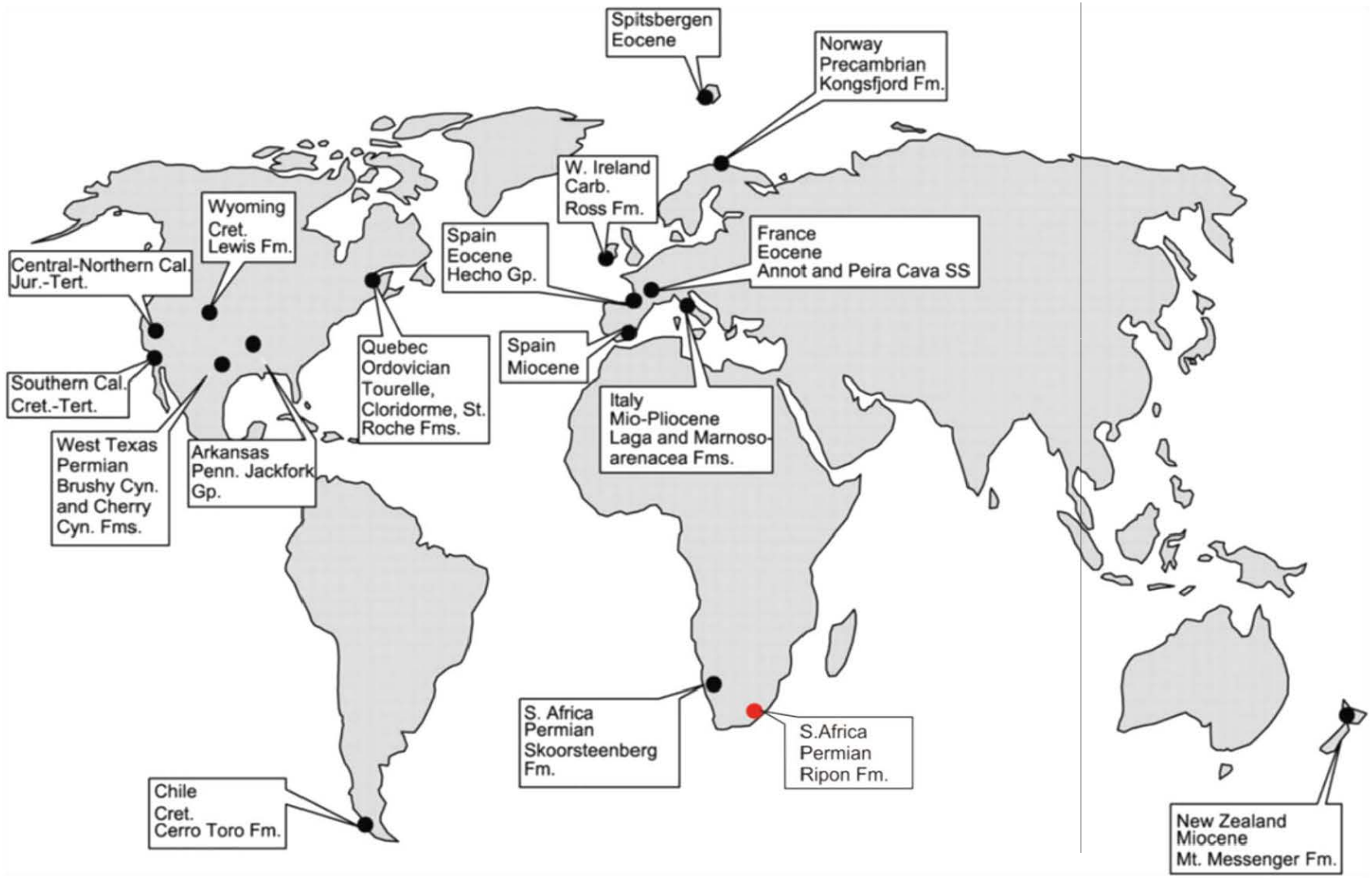

Figure 1.1: World map illustrating distribution of studied turbidite complexes . Diagram modified from Weimer et al. (2000).

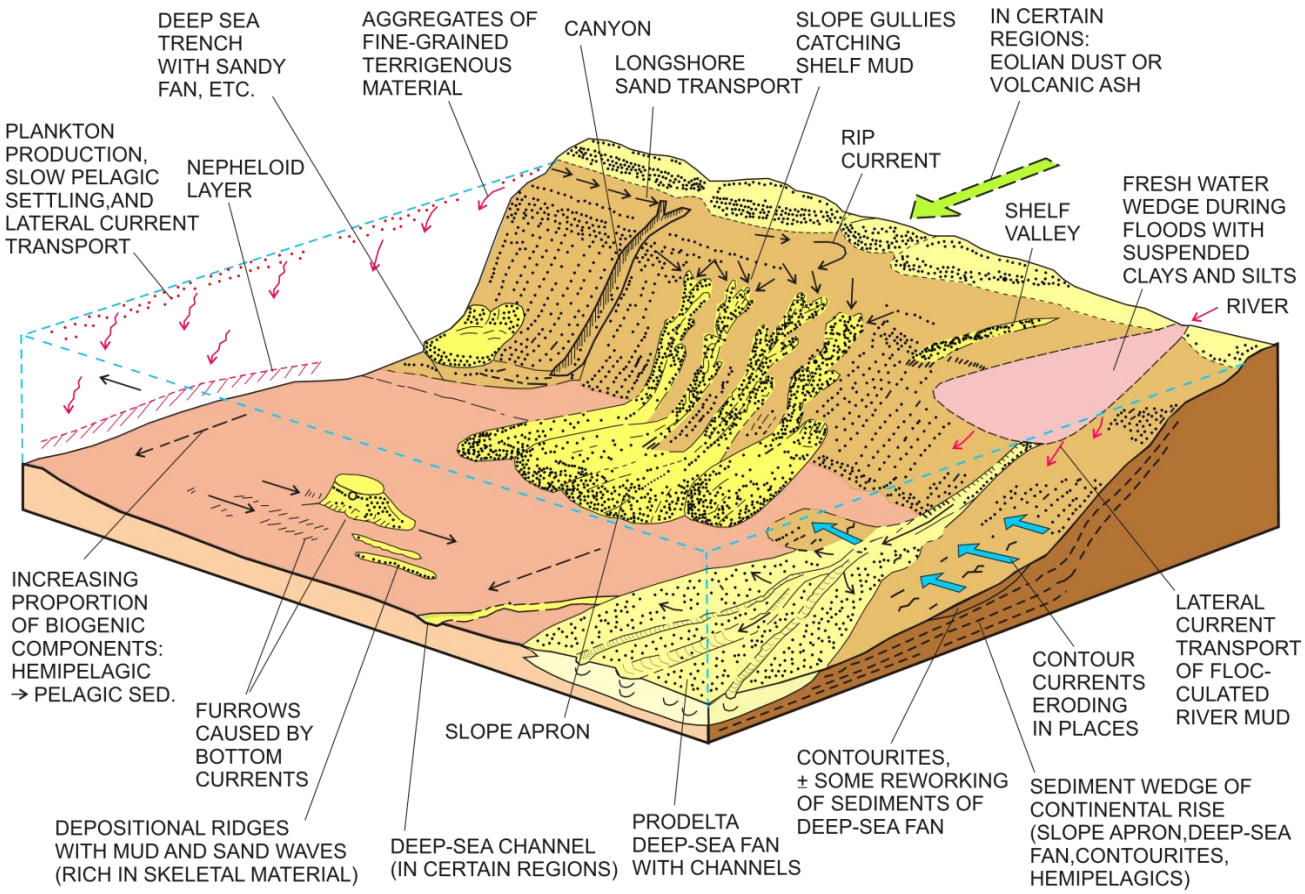

Figure 1.2: Sediment distribution systems in the deep sea. **Note**: Variety of settings in which fans are produced and thus where turbidites can be deposited. Diagram modified from Einsele (1992).

1.1.1 Classification Schemes

Over time many aspects of early fan models have fallen out of favour with geoscientists but physiographic regions are however still used in defining turbidite systems. Differences in methodology exist in the study of modern day fan complexes compared to ancient turbidite systems. Modern day fans are characterised based on sea-floor bathymetry and geomorphologic features at progressively greater distances from the shelf edge. Ancient turbidite systems are defined according to facies associations observed in outcrop exposures that reflects progressive changes in a vertical or stratigraphic sense of these facies associations. Differences in geomorphic facies associations exist between fine-grained, mud-rich systems and coarse-grained, sand-rich systems (Bouma *et al.*, 2000).

Bouma Sequence

The classic model for medium-grained sand-mud turbidites was presented by Bouma (1962) and recognises five divisions 'a' to 'e' (*Figure 1.3*) also annotated as 'Ta' to 'Te'. *Ta* is the lowest part of the succession and is composed of poorly sorted structureless sand deposited on the scoured base with rapid deposition prohibiting the formation of bedforms. *Tb* is composed of laminated sand that is finer grained than in 'a' and the material is better sorted. Parallel laminae are generated by the suspension of grains in the upper flow regime transport.

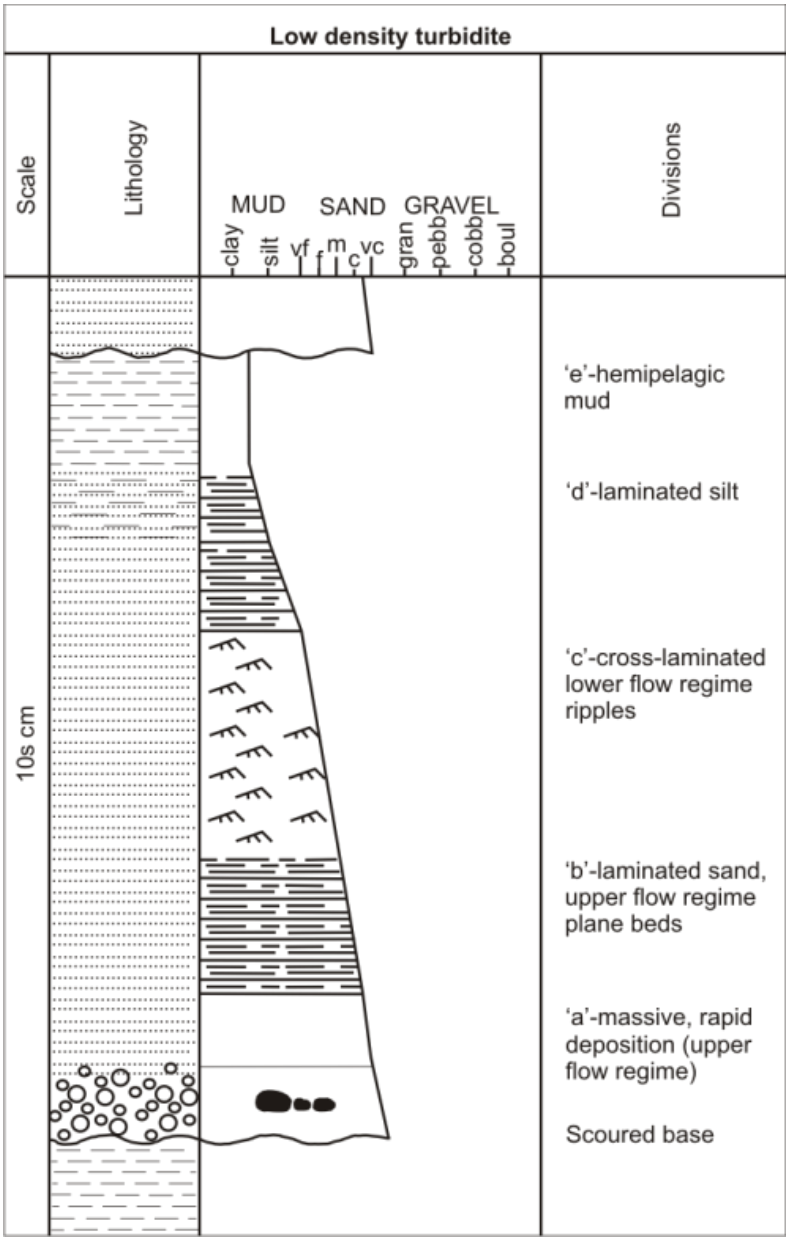

Figure 1.3: Idealised log of a complete Bouma sequence from 'a' through to 'e' with commonly associated bedforms. Log modified from Nicols (2009).

Tc contains cross-laminated medium to fine sand within the ripple bedform stability field and indicate moderate flow velocities and high sedimentation rates. Convoluted laminations can also occur in this division. *Td* is composed of fine sand and silt and is the result of waning flow in the turbidity current. Horizontal laminae may occur but the lamination is less well defined than in the 'b' layer. *Te* is the top part of the turbidite and consists of fine-grained sediment of silt and clay grade. It is deposited from suspension after the turbididty current has come to rest and is therefore a hemipelagic deposit (Nicols, 2009). Turbidity currents are declining flows and decrease velocity through time as they deposit material and decrease velocity with distance from the source. There is therefore a decrease in the grain size deposited with distance (Stow, 1994). The lower parts of the Bouma sequence are only present in more proximal parts of the flow and with distance the lower divisions are progressively lost as the flow carries only finer sediment. At the distal end only the Tc to Te or perhaps just Td and Te divisions are deposited. In more proximal regions the flow turbulence may be strong enough to cause scouring and completely remove the upper parts of a previously deposited bed. The Td and Te divisions may therefore be absent due to erosion and the eroded sediment incorporated into the overlying deposit as mudclasts (Nicols, 2009).

Sediment Supply Based Models

Four models have been proposed in Nicols (2009) to accommodate the range in grain sizes other than the Bouma model which focuses on medium-grained sand-mud turbidites. The four models include gravel-dominated, sandy, mixed sand and mud and muddy turbidites with a variety of combinations possible, each having a distinct sequence of internal structures within beds. The model also divides submarine fan systems according to physiographic regions such as inner, middle and outer for ancient turbidite systems and- upper fan, mid fan and lower fan for modern day systems (Bouma *et al.*, 2000).

Gravel-rich systems are deposited at basin margins in delta's consisting of coarse grained sediment supplied by braided rivers and alluvial fans. Sand is deposited by high-density turbidites and gravel is deposited by debris flows, usually abruptly grading into thin bedded distal turbidites and hemipelagic mudstones. Fan systems are considered 'sand-rich' if 70% of the deposits are composed of sandy material. Sand is supplied by waves, storms and tidal currents from sand-rich shelves where mud has been removed by the high energy processes. Sandy deposits do not travel

very far, thus creating small sediment bodies. Mixed sand-mud systems are deposited by large rivers or deltas and are defined as having between 30-70% sand. Deposits of this type are tens to hundreds of kilometres in diameter and usually contain well developed channel levee systems and depositional lobes. Mud-rich systems are the largest sub-marine fan systems in modern oceans (over 1000km in radius) and are fed by very large rivers. They are defined as having less than 30% sand and predominantly consist of channels (Nicols, 2009).

Complete sequences are rarely observed and partial sequences are more common with top-absent or bottom-absent being the norm. Grading is a common feature of all four facies models although reverse grading and multiple grading also occur (Reading, 1996; Nicols, 2009). Basal surfaces of many turbidite beds contain erosional sole marks generated during the passage of the head of the flow. Tool marks due to the impact and scraping of objects carried in the flow are more common on thinner beds while flute marks and products of turbulent scour are often associated with thicker beds. Load casts formed by gravitational settling of the coarser layer into the muddier layer beneath are also common features (Reading, 1996).

Exploration for and the discovery of hydrocarbons in fine-grained, mud-rich turbidite systems in passive margin settings (Gulf of Mexico, North Sea, West Africa) led to a vast increase in research efforts in the 1990's. However, studies have verified that essential differences exist in how deep water sediments are deposited in fine-grained, mud-rich, turbidite systems compared to more comprehensively studied coarse-grained, sand-rich turbidite systems (Bouma *et al*, 2000).

1.2 Black Shales

Black shale is the general term for any fined-grained, dark-coloured, organic-rich sediment. Black shales are usually compacted sediments that display distinct lamination. Their dark colour is caused by dispersed iron sulphides and organic compounds. Many black shales are hemipelagites, pelagites or fine grained turbidites. Organic material from dead plants, animals and microbial organisms is abundant in the oceans and accumulates on the sea floor. Where the sea floor is oxygenated the organic matter is oxidised or consumed by scavengers. Where circulation is poor, oxygen is reduced in the water at the sea floor and conditions become anoxic and breakdown of organic matter becomes slower or non-existent. Organic matter accumulates and contributes to pelagic sedimentation and combined with burial and diagenesis may form black shales (Einsele, 1992;

Reading, 1996; Nicols, 2009). Factors leading to the formation of black shales are therefore determined by organic input, consumption by microbial activity and dilution by terrigenous clastic, biogenic carbonate or silica. The most favourable sites for the deposition of organic rich sediments are therefore deep seas where there is poor circulation between oxygenated surface waters and the sea floor (*Figure 1.4*).

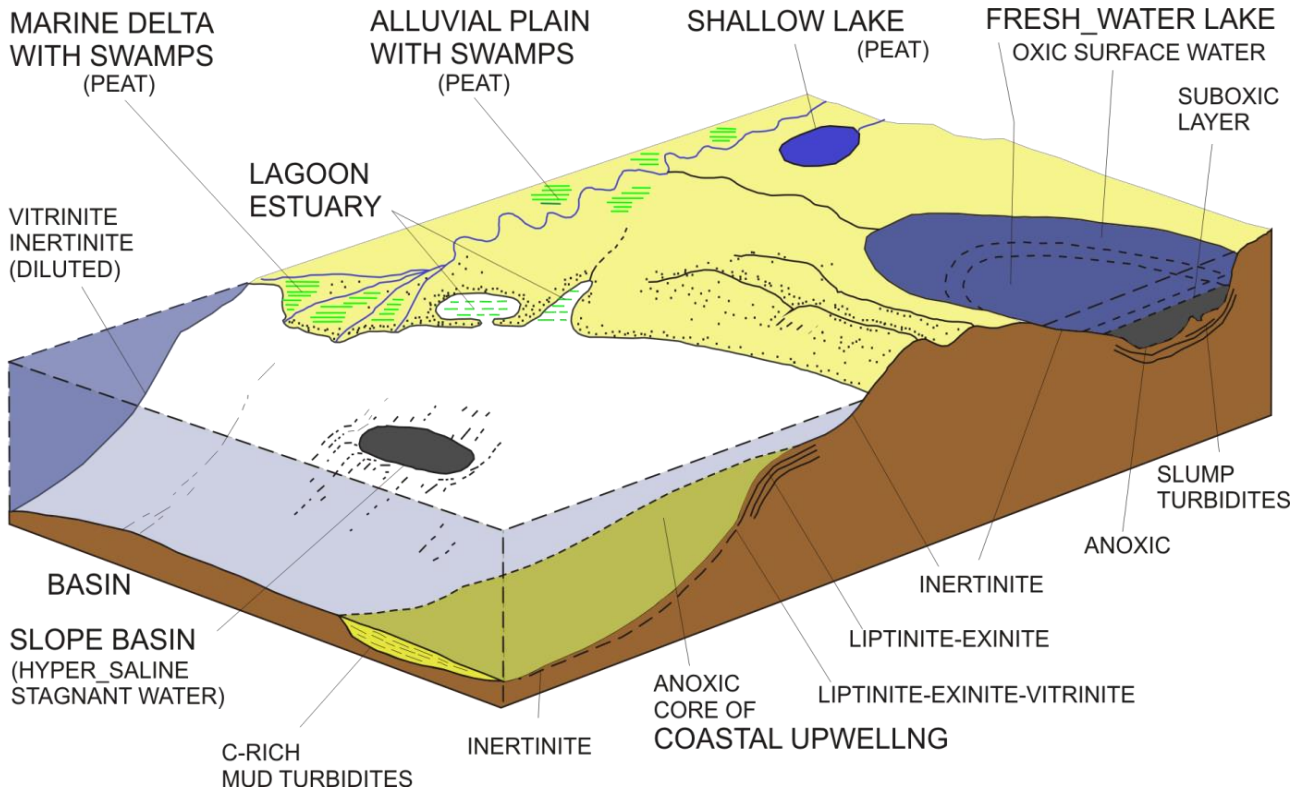

Figure 1.4: Schematic diagram showing major depositional environments for the accumulation of organic-rich sediments, with their dominant types of kerogen. Diagram modified from Einsele (1992).

Other favourable areas include reduced or anoxic swamps and tidal flat zones, estuaries, lakes and lagoons with high nutrient supply, shelves and upper continental slopes under zones of coastal upwelling and widely extended deep-sea regions during periods of sluggish ocean circulation (Einsele, 1992; Reading, 1996; Nichols, 2009). Total organic carbon (TOC) contents in black shales range from 1-15%. In the evaluation of petroleum source rocks the TOC concentration is a critical factor. Typically carbonate source rocks should contain 0.3% organic carbon and clastic source rocks at least 0.5% (Einsele, 1992).

1.2.1 Shale Gas

Organic matter preserved in shales may alter to oil and gas with increases in temperature and pressure. Intensity and duration of post- depositional burial are the main parameters controlling the transition of organic matter to natural gas. Gas is extracted from tight shales (less than 10% porosity and less than 0.1% millidarcy of permeability) by a process known as hydraulic fracturing (Geel, 2013).

Chapter 2 - Geological Setting

2.1 Palaeogeography

The Main Karoo Basin is part of a series of Gondwanan foreland basins including the Paraná Basin in South America, the Beacon Basin in Antartica and the Bowen Basin in Australia (De Wit and Ransome 1992; Veevers *et al*., 1994; Catuneanu *et al*., 1998; Catuneanu and Elango, 2001; Catuneanu and Bowker, 2002). The Karoo Basin of South Africa covers around 700,000 km² and represents approximately 100 million years of sedimentation from ca. 280 Ma to ca. 180 Ma (Johnson *et al*., 2006; Geel *et al*., 2013). The longstanding interpretation is that the Main Karoo Basin constitutes a retro-arc foreland basin developed by northward oblique subduction of oceanic lithosphere (palaeo-Pacific plate) under western Gondwana, from the late Carboniferous onwards and subsequent development of a wide fold thrust belt, the Cape Fold Belt (CFB) (Johnson *et al*., 2006). More recent interpretations of the Karoo Basin formation suggest strike-slip tectonics led to the development of the CFB and the adjacent Karoo Basin comparable to a flexural foreland basin (Tankard *et al*., 2012). By contrast the CFB has been compared to a Jura-type fold belt that formed due to arc-continent collision with subduction to the south (Lindeque *et al*., 2011; Pangaro and Ramos, 2012). However, Flint *et al*. (2011) contests that regionally pronounced large-scale subsidence occurred due to dynamic topography (mantle flow) related to the subducting slab. This resulted in a series of interconnected marine basins that are older than the generally accepted foreland basin stage of the Karoo Basin.

The Main Karoo Basin is underlain by a stable foundation comprising the Kaapvaal Craton in the north, the Namaqua-Natal Metamorphic Belt in the south and Cape Fold Belt along its southern margin (Johnson *et al*., 2006).

The Cape Fold Belt formed while sedimentation of at least the upper Karoo Formations was still in progress. Orogeny resulted in intense deformation of the Cape Supergroup, the underlying basement as well as lower units of the Karoo Supergroup. The major lithostratigraphic units of the Karoo Supergroup crop out concentrically around the basin (*Figure 2.1*) (Johnson *et al*., 2006).

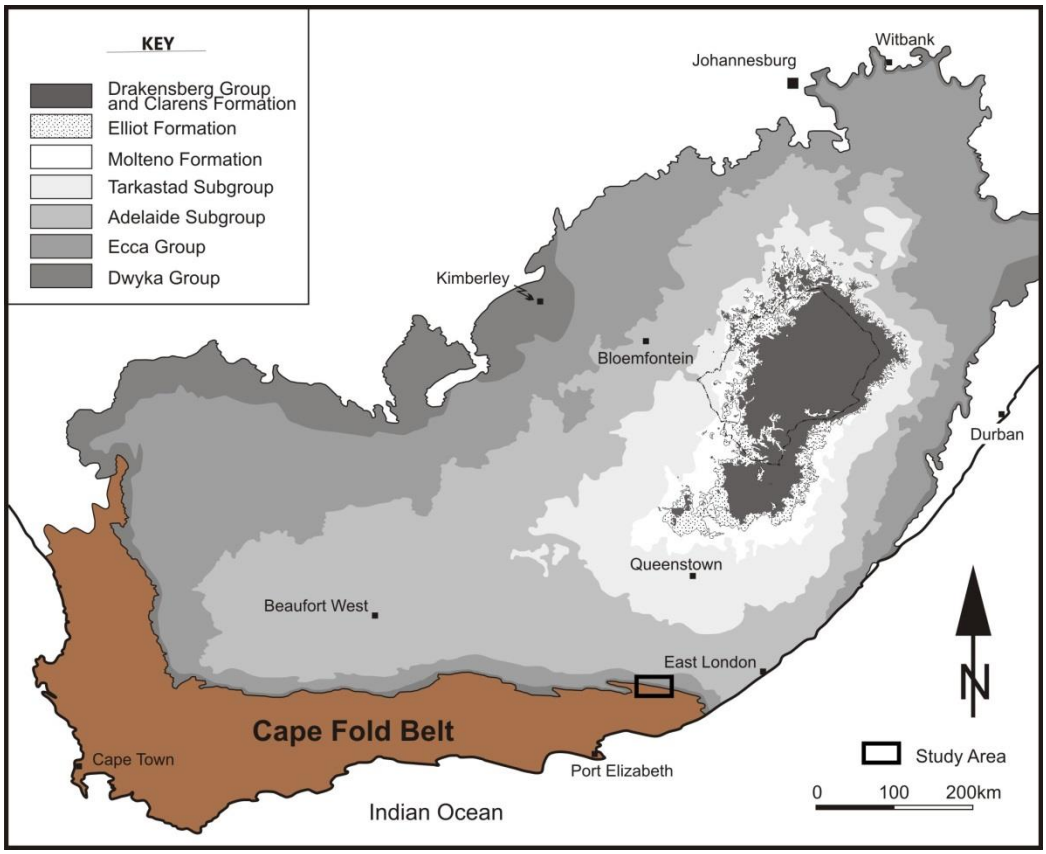

Figure 2.1. Stratigraphy and distribution of the Karoo Supergroup and location of the study area. Based on Catuneanu *et al*. (1998), modified from Bordy *et al.* (2004).

2.2 Stratigraphy

The onset of deposition of Karoo sedimentary rocks occurred during the late Carboniferous and continued until the break-up of Gondwana during the Middle Jurassic at ca. 183 Ma (Johnson *et al*., 2006; Geel *et al*., 2013). A total sediment infill thickness of 12 km is attained within the south-eastern part of the Main Karoo Basin with sediment sourced from the north (Cargonian Highlands) as well as from the south (Cape Fold Belt mountain range) (McCarthy and Rubidge, 2005). Flint *et al*. (2011) contests that during the Ecca Group time there was no source area nearby. The Karoo Supergroup is divided into the Dwyka Group (Late Carboniferous to Early Permian), the Ecca Group (Mid Permian), followed by the Beaufort Group (Permian-Triassic) and the Stormberg Group (Late Triassic to Early Jurassic) (Visser, 1996; Catuneanu, 1998; Johnson *et al*., 2006). The entire succession is capped by up to 1.4 km of basaltic lavas of the Drakensberg Group. The numerous formations of the Karoo Supergroup document changing environmental conditions from the

glacio-marine deposits of the Dwyka Group to the marine-deltaic deposits of the Ecca Group through to the fluvial-deltaic sediments of the Beaufort Group and the fluvial-lacustrine and aeolian sandstones of the Stormberg Group (Johnson *et al*., 2006) (*Figure 2.2*).

2.2.1 Dwyka Group

Deposition of the Late Carboniferous to Early Permian Dwyka Group, a succession of diamictites, varved glacial deposits and fluvial deposits up to 800 m thick, rests on glaciated Precambrian bedrock surfaces along the northern margin of the basin and in the south it overlies the Cape Supergroup unconformably or paraconformably (Johnson *et al*., 2006; Flint *et al*., 2011). The formation of the Dwyka Group coincided with the migration of Gondwana over the South Pole and marked the onset of Karoo Basin sedimentation at approximately 300-310 Ma (Flint *et al*., 2011). Rhyolitic/dacitic and basaltic/andesitic tuff beds within the glaciomarine sediments of the Dwyka Group in Namibia reveal new evidence for an early onset of proximal bimodal volcanic activity in southern Africa (Stollhofen, 2000).

2.2.2 Ecca Group

The Permian Ecca Group is composed of 16 formations reflecting the lateral facies changes that are characteristic of this group. The Ecca Group comprises predominantly siliciclastic sediments capped by the fluvial Beaufort Group (Johnson *et al*., 2006). The basal Prince Albert and Whitehill Formations are fairly extensive throughout the Karoo Basin but overlying formations are geographically dependant and for the sake of brevity only the formations pertinent to this study area are included.

The basal Prince Albert Formation has a maximum thickness of 100 m of predominantly dark grey mudrock. The overlying Whitehill Formation constitutes up to 80 m of black, carbonaceous pyrite-bearing shale. These units are highly condensed (low sedimentation rates) and contain almost no clastic input. The Collingham Formation is made up of 70 m of a rhythmic alteration of dark grey siliceous mudrock and very thin beds of yellow tuff (K-bentonite). The rhyodacitic volcanic ash may have been derived from volcanoes located in what is now northern Patagonia where Permian aged silicic-andesitic volcanic and plutonic rocks are exposed. A regional marker, the Matjiesfontein chert bed (uniformly thick over 5000 km^2) is found within the Collingham Formation.

The overlying Ripon Formation is up to 1000 m thick of fine-grained lithofeldspathic sandstone alternating with clastic rythmite and mudrock. The Fort Brown Formation consists of up to 1000 m of rhythmite and mudrock with intercalated sandstone (Johnson *et al*., 2006; Flint *et al.,* 2011). Palaeoclimatic modelling indicates a shift from tundra-like vegetation to more warm and humid conditions, with swamp-like vegetation and hence a change in depositional systems in the Permian (Götz and Ruckwied, 2013). The Prince Albert Formation contains shallow-water carbonates and clastics whilst the Whitehill Formation is indicative of marine anoxic conditions with pelagic Mesosaurid reptiles and palaeoniscid fishes preserved (Scheffer *et al*., 2006).

2.2.3 Beaufort Group

The Beaufort Group is subdivided into the Adelaide Subgroup (5000 m-800 m) and the Tarkastad Subgroup (2000 m-150 m). The dominant lithologies include fluvial-deltaic mudstones and sandstones with occasional granulestones and pebbles (Johnson *et al*., 2006).

2.2.4 Stormberg Group

The Stormberg Group is subdivided into the Molteno, Elliot and Clarens formations (*Figure 2.2*). The basal Molteno Formation (Late Triassic) is made up of alternating medium to coarse grained sandstones and grey mudrocks with secondary quartz overgrowths and has a maximum thickness of 600 m in the south. It formed as a result of bedload-dominated rivers flowing across extensive braid-plains. The Elliot Formation (Late Triassic) comprises an alternating sequence of mudrock and fine to medium grained sandstone, attaining a maximum thickness of 500 m in the south. The Elliot Formation is a typical “red bed” fluvial deposit (Johnson *et al*., 2006). The upper Clarens Formation (Late Triassic/Early Jurassic) is comprised of up to 300 m of primarily sandstone representing desert conditions and associated dune, playa lake, sheet flood and stream deposits (Johnson *et al*., 2006).

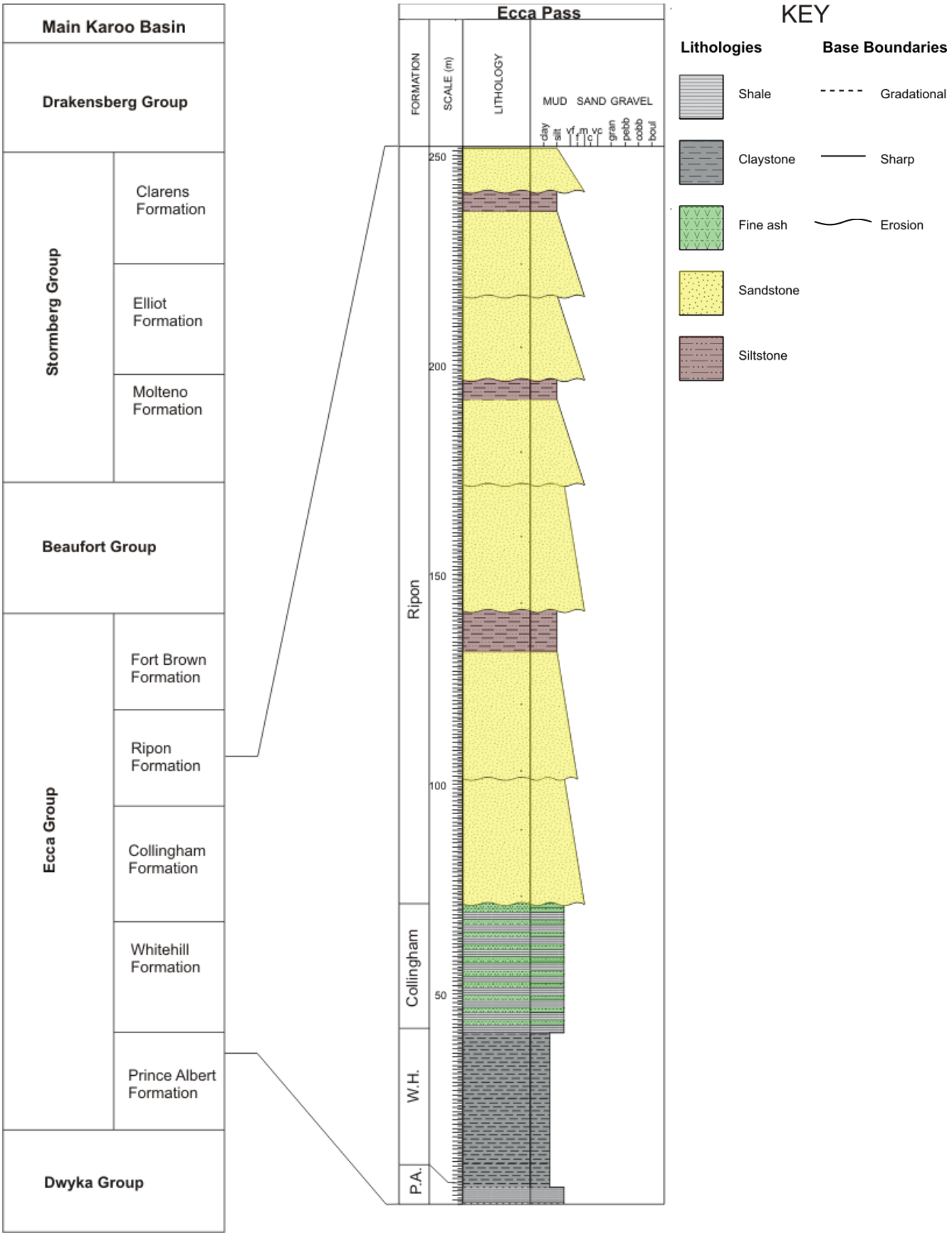

Figure 2.2: Stratigraphy of the Karoo Supergroup and overview log of the location of the study area (Ecca Pass). Used abbreviations: P.A. - Prince Albert, W.H. - Whitehill. Log created using Sedlog software.

2.3 Regional Geology

The city of Grahamstown, Eastern Cape, is located at the interface between the southern portion of the Karoo Basin and the eastern limb of the Cape Fold Belt (*Figure 2.3*). The sedimentary rocks of the Cape Fold Belt in this area belong to the Weltevrede, Witpoort and Kirkskraal formations of the Witteberg Group (Late Devonian to Early Carboniferous) with deformed shale and quartzite constituting the dominant lithologies (Council for Geoscience, 1995). The Waterloo Farm black shale N2 roadcut, famous for the preservation of Gondwana's oldest known tetrapod *Gondwanascorpio emzantsiensis*, is located on the south-eastern outskirts of Grahamstown (Gess, 2013). Immediately surrounding the city to the north, east and west are outcrops of silcrete and kaolinite (Tertiary and Quaternary) and Dwyka tillite, underlain by Witteberg Group quartzites and shales. To the north, the interface between the Cape Supergroup and Karoo Supergroup is delineated with a transition from quartzites and shales to deformed and weathered tillite. The lower most units of the Karoo Supergroup are excellently exposed in road cutting along the Ecca Pass (R67 to Fort Beaufort north of Grahamstown) with the Ecca Pass being the type locality for the Ecca Group (Johnson, 1976).

2.4 Previous Work

Numerous studies have been conducted on the Whitehill Formation and its stratigraphic equivalents of Middle Artinskian Age namely, the Whitehill Formation in S Namibia, the Huab Formation in NW Namibia, Irati Formation in the Paraná Basin Brazil and the Black Rock Member of the Port Sussex Formation of the Falkland/Malvinas Islands as well as the Collingham and Ripon formations (Thomas, 2001; Trewin *et al.,* 2002).

In the early 20th century Haughton (1925, 1928) was the first person to study trace fossils from the Ecca Shales of the Cape Province. He also described the geology between Grahamstown and Port Elizabeth. Next, Johnson (1966, 1976) logged and described the formations of the Ecca Group at the type locality. Then, Kingsley (1979, 1981) proposed a composite turbidite-delta-fluvial model for the sedimentation for the Permian Ecca and Lower Beaufort groups in the Eastern Cape of South Africa. Oelofsen (1987) compared the biostratigraphy of the Whitehill and Irati Shale formations of

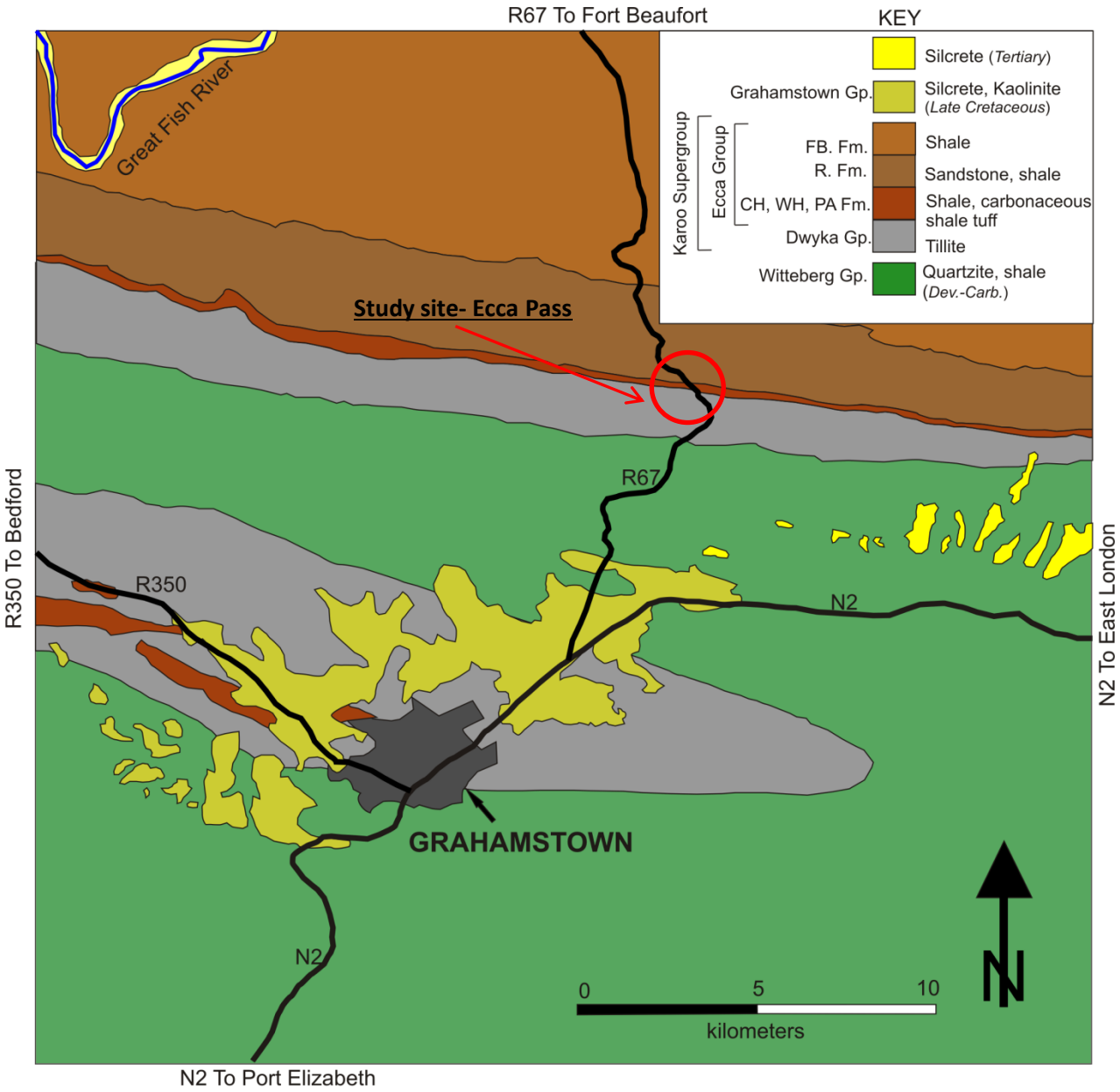

Figure 2.3: Geological map illustrating the regional geology of Grahamstown and surrounds. Map modified from the Counsel for Geoscience (1995). Used abbreviations: CH - Collingham, PA - Prince Albert, WH - Whitehill, R - Ripon, FB - Fort Brown, Dev - Devonian, Carb - Carboniferous, Fm - Formation, Gp - Group.

the Karoo and Paraná basins. He concludes that the two formations may represent a transcontinental isochronous unit based on the striking similarity in the biota of the two formations, and the presence of specimens of the same species of vertebrates in both basins. Visser (1992) suggested that the Whitehill Formation was deposited during a highstand sea-level in a juvenile foreland basin. He proposed a terrestrial source of the organic material stating that fresh-water plumes carried organic-rich mud from the basin margin into an anoxic deep marine setting. Faure and Cole (1999) presented geochemical evidence (C, O, S isotopes and hydrogen and oxygen indices) from the Whitehill, Irati and Huab formations and Black Rock Member, in the south-western Gondwana basins. The data suggest the manifestation of a microbial bloom event covering approximately 5 million km² that peaked in the upper half of the black shale units. Recently, Santos *et al*. (2006) presented the first SHRIMP zircon age data from bentonitic ash fall layers intercalated with the Irati sedimentary rocks of the Paraná Basin. SHRIMP analysis performed on the euhedral and prismatic grains revealed an age of ca. 278.4 ± 2.2 Ma interpreted as the crystallization age of the volcanic eruption. Based on this new dating, the Irati Formation should be placed on the Lower Permian (Cisuralian), Artinskian in age, modifying substantially the traditional ages previously attributed to this unit. Branch *et al*. (2007) acquired magnetotelluric (MT) data along three profiles across the Karoo Basin in South Africa and reported on electrical conductivity, vitrinite reflectance, and impedance spectroscopy studies that were undertaken. Flint *et al*. (2011) reported on the depositional architecture and sequence stratigraphy of the lower Karoo Supergroup and finally Geel (2013) undertook a comprehensive and detailed lithological, sedimentological, structural and geochemical description on a core (SFT2) of the lower Ecca Group with emphasis on the shale gas characteristics of the Whitehill Formation.

Chapter 3 - Materials and Methods

3.1 Materials

An outcrop analogue study with respect to reservoir characterisation of the Permian clastic deposits of the Eastern Cape was performed on the Ecca Pass road cuttings north of Grahamstown. A total of 50 samples were collected representing the dominant lithologies (sandstones and shales) of the area. The following is a breakdown of the number of samples used in this study: 30 for thin sections, ten samples for porosity and permeability analysis, four samples for total organic carbon analysis, four samples for X-ray diffraction.

3.2 Methods

3.2.1 Field Methods

Outcrop Logging

The variable nature of turbidite deposits warrants great attention to detail therefore the entire outcrop was logged on a centimetre scale. Particular attention was paid to observing lithological contacts and associated erosional features such as scouring and tool marks. Fossil rich horizons were well documented and relevant samples collected. Bouma Sequences and repetitive or cyclical sequences also warranted focused attention.

Sedimentary Structures

The sedimentary processes operating within a depositional sedimentary environment generate particular structures, textures and bedforms within the sediments. Observable characteristics preserved in the rock record define different sedimentary lithofacies. Therefore, a reasonable knowledge of the sedimentary processes and careful analysis of the preserved sedimentary features may provide a satisfactory explanation of the genesis of the sediments or sedimentary rocks (Reading, 1996; Einsele, 2000; Bordy, 2000). Special attention was paid to observing and documenting sedimentary structures in relation to stratigraphic position and lithology.

Sample Collection

Hand specimen sized samples were collected across all four (Prince Albert, Whitehill, Collingham, and Ripon) Formations exposed in the Ecca Pass (*Figure 2*). Hand specimens were collected if the specimen contained any of the following features:

- Dominant and minor lithologies
- Small scale structures
- Fossils (trace or body)
- Tool and scour marks
- Bouma Sequence or cyclicity
- Organic rich (black shales)
- Porosity, permeability
- Textures (rip-up clast conglomerate, spotted sandstone)

Hand specimens were photographed, recorded, and documented based on checklists for sedimentary rocks in hand specimens (Appendix A) and blocks were cut, where needed, for creation of thin sections and powders.

3.2.2 Facies Analysis

A sedimentary sequence exhibits the vertical progression and environmental evolution over time, and can be studied using sequential stratigraphy methods. Lateral facies variations highlight the environment's distribution in space according to the principle, expressed by Johannes Walther in 1894 that: "only facies that deposit in contiguous environments can overlie in sedimentary continuum" (Casnedi, 2005).

Slope to deep marine turbidite deposits can range in thickness from a few millimetres to tens of meters and range from high-energy coarse-grained sediments and related structures to pelagic 'rain' of mud sized particles (Nichols, 2009). In order to scientifically study, as accurately as possible, the entire plethora of available information in the form of an outcrop, an approach was undertaken that started with the macro-scale (outcrop sized) features and progressed to meso-scale (hand specimen sized) and finally to the micro-scale.

According to Casnedi (2005), facies analysis takes into consideration a range of sedimentary aspects including: a) inorganic sedimentary structures such as cross- bedding, graded beds, sole marks, palaeocurrents, etc.; b) the presence of flora and fauna and their habitat, along with the organic sedimentary structures (fossil moulds); c) granulometric distribution and sedimentary textures; d)

mineralogical composition; e) geochemical composition (trace elements and stable isotopes); f) stratigraphic relations (morphology of the environment, unconformities, magnetic polarity).

Facies analysis of sedimentary outcrops entails a step-wise approach, starting off with documentation of lithologies followed by detailed observation and description of all physical and biological structures recorded in the sedimentary strata. In the case of siliciclastic sedimentary rocks it is imperative to record the type, size, sorting, roundness, sphericity, orientation and, grading of the grains; the quality, type and size of the matrix; the grain/matrix ratio; the fossil content of the beds (trace and body fossils); the thickness and lateral extent of the strata; the bedform types; the shape and the length of the erosional surfaces and the syn-sedimentary deformation structures and so forth (Reading, 1996; Bordy, 2000; Einsele, 2000).

3.2.3 Analytical Methods

Microscopy

Normal thin sections (30 µm, uncovered) were prepared by The Rhodes University thin-section preparation laboratory using standard preparation techniques (Reed and Mergner, 1952). Thin sections were documented based on checklists for sedimentary rocks under the microscope (Appendix B) using a *LEICA DM EP* microscope.

X-ray Diffraction

Samples that were observed to be too fine grained under the microscope for mineral identification (50X maximum magnification) were powdered for XRD analysis. X-ray powder diffraction (XRD) is a rapid analytical technique primarily used for phase identification of a crystalline material. Samples were finely ground using a chromium-steel swing-mill and then an automated agate pestle and mortar. The samples were homogenised and the average bulk composition was determined (Moore and Reynolds, 1989).

Total Organic Carbon

Organic rich samples (black shales) were sent the Shell Geochemical Laboratory in The Hague for Total Organic Carbon (TOC) analysis. Samples were selected based on perceived freshness and quality of organic matter. Two samples were selected from the Whitehill Formation that appeared to be the least weathered specimens available from the outcrop. Two samples were selected from

the Collingham Formation that represented the average lithological composition of the formation based on colour and texture. TOC is the amount of carbon bound in an organic compound. Samples undergo acidification, oxidation, and then detection. TOC analysers measure the CO_2 formed when organic carbon is oxidized and/or when inorganic carbon is acidified.

TOC analysis was done using a CS-200 analyser (LECO Corporation, St. Joseph, Michigan, USA). The instrument is calibrated at least once a day against various carbon standards (LECO). Samples are ground, homogenised, and acidified with a 10% HCl solution and dried before analysis. Results are reported in % Carbon.

Porosity and Permeability Analysis

Ten sandstone samples (cylindrical plugs with dimension 3 mm x 4 mm) from the Ripon Formation that were considered suitable were sent to Geotechnical Laboratory at TU Darmstadt for Poro-Perm analysis (porosity and permeability). Total porosity is defined as the fraction of the bulk rock volume that is not occupied by solid matter but porosity does not give any information concerning pore sizes, their distribution, and their degree of connectivity.

Porosity is measured using Gas Expansion based on Boyle's Law. The rock is sealed in a container of known volume at atmospheric pressure. The container is attached by a valve to another container of known volume, containing gas at a known pressure. The value of the equilibrium pressure is used to calculate the volume of grains in the rock.

The permeability of a rock is a measure of the ease with which the rock will permit the passage of fluids. Permeability depends on porosity; the higher the porosity the higher the permeability. However, permeability also depends upon the connectivity of the pore spaces, in order that a pathway for fluid flow is possible.

Permeability is measured on cores in the laboratory by passing a fluid of known viscosity through a core sample of known dimensions at a set rate, and measuring the pressure drop across the core, or by setting the fluid to flow at a set pressure difference, and measuring the flow rate produced. The determination of the grain and bulk density as well as the porosity was done by measuring the grain and bulk volume of the samples, using a helium pycnometer and a powder pycnometer. For the determination of the rock permeability a combined column and mini-permeameter was used.

The method offers either the measurement of the apparent gas permeability, which afterwards is converted into permeability, or the direct measurement of the intrinsic permeability. The basis for the gas driven permeameter is the Darcy law, which is enhanced by the terms of compressibility and viscosity of gases. The maximal measurement error depending on the measurement setting is 10% whilst the minimal error is about 1% (Goggin *et.al*., 1988; Götz and Lenhardt, 2011; Sass and Götz, 2012; Götz *et al*., 2014).

Chapter 4 - Observations

4.1 Macroscopic and Mesoscopic Field Observations

4.1.1 Prince Albert Formation

The Prince Albert Formation of the Ecca Group is poorly exposed in the study area. The outcrop is less than 1 m high and 3 m wide and is partially covered by scree and soil. Only weathered and fractured shale is visible. The upper contact with the underlying Dwyka Group is not visible and the upper contact with the Whitehill Formation is not readily discernable and has been inferred.

Rock Descriptions

The shale is a greenish-grey colour and weathers a reddish-brown colour. The grain size of the shale is in the mud range, either fine silt or clay. The shale is very hard when struck with a hammer. The lower contact appears to be gradational over 1 meter with the shale changing from a reddish-brown colour to a light grey colour. Fresh rock from this transition zone is darker in colour than the Prince Albert Formation samples, but it is not as dark as the above Whitehill Formation samples.

Sedimentary Structures

The shale appears to be thinly bedded and not deformed.

Palaeontological Findings

No fossil material has been observed.

4.1.2 Whitehill Formation

The Whitehill Formation of the Ecca Group is 35.67 meters thick and well exposed in the study area. Exposures of this formation consist of a quarry with an exposed face approximately 50 m in length and 10 m in height. The formation is also exposed in road cuttings approximately 25 m in length and 5 m in height. All the exposures are highly weathered. The Whitehill Formation consists of white-weathering, laminated black shale. The contact between the Whitehill and overlying Collingham Formations is sharp.

Rock Descriptions

Fresh samples of shale are a uniform dark black colour and are micro-laminated with a grain size in the mud range between fine silt and clay (*Plate 1, Figure* 1). The fissile shale occurs in layers that are weathered on the surface and display a range of weathering colours (white, pink, red, rusty-brown) with white being the most dominant weathering colour (*Plate 1, Figure 2*). Layers of white gypsum nodules are visible. These layers cross-cut the stratigraphy and contain aggregates of gypsum nodules with individual nodules up to 5 cm in diameter (*Plate 1, Figure 3*). Some nodules have a noticeably higher density than others.

The outcrop contains shale layers ranging in thickness from 1 mm to 2 cm. Layers alternate from 'thickly bedded' (centimetre scale) to 'thinly bedded' (millimetre scale). Thickly bedded layers are more resistant to weathering and erosion compared to the thinly bedded layers (*Plate 1, Figure 4*). This alternating bedding pattern is visible throughout the majority of the outcrop with some exceptions, most notably the portion immediately above the lower contact with the Prince Albert Formation, which does not contain thicker layers.

Higher up the stratigraphic column the shale layers are bedded parallel to one another with minor deformation in places. This is followed by 9.9 m of outcrop that is deformed and possibly faulted. This section is also highly weathered. The remaining upper portion of the stratigraphy (7.8 m) is extensively eroded and weathered. Some beds are visible that display deformation.

Sedimentary Structures

Possible water escape or deformation structures are observed in the basal section of the outcrop (*Plate 1, Figure 5 & 6*).

Palaeontological Findings

No fossil material was observed in the Whitehill Formation.

PLATE 1

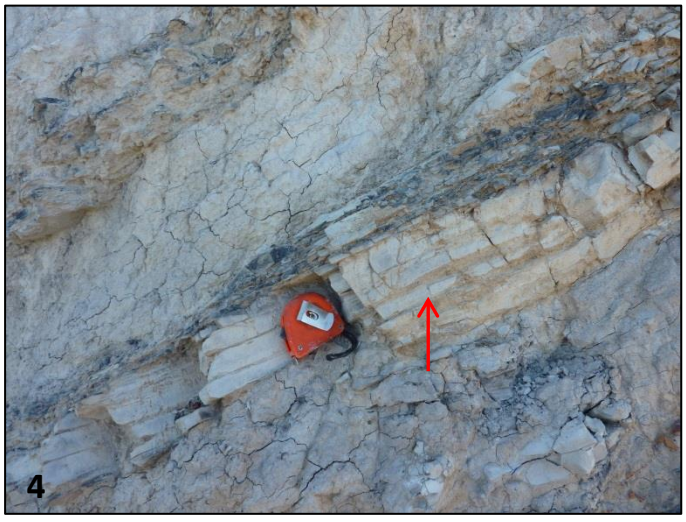

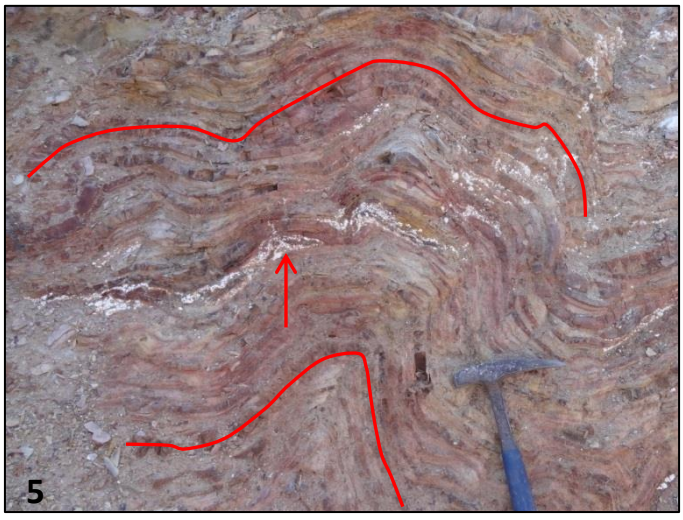

Plate 1: Outcropping Whitehill Formation rocks with lithologies, structures and weathering features. **Figure 1:** Laminated dark coloured fresh shale within white weathered shale, Whitehill Fm. **Figure 2:** Weathered shale with characteristic white and reddish weathering colours, Whitehill Fm. **Figure 3**: An aggregate of white gypsum nodules from the Whitehill Fm. **Figure 4:** Hard weathering resistant layer within weathered sediments, Whitehill Fm. **Figure 5** and **6**: Possible water escape or deformation structures with variation in height, width and orientation with white gypsum nodules in weathered shale, Whitehill Fm. **NOTE**: Gypsum nodules cross-cut bedding.

4.1.3 Collingham Formation

The Collingham Formation of the Ecca group is 28.3 m thick and is well exposed along road cuttings in the study area (*Plate 2, Figure 1*). The exposure is approximately 60 m in length and up to 10 m in height. The outcrop contains fresh and well preserved material. The formation consists of inter-bedded organic-rich fissile shales and tuffaceous material. The Collingham Formation has a sharp contact with the overlying Ripon Formation (*Plate 2, Figure 2*).

Rock Descriptions

This formation contains competent shale layers ranging in thickness from 1 to 110 cm. The shale has a grain size in the mud range between fine silt and clay. Fresh shale is a light grey to black colour and weathers a white to rusty-red colour. Some layers are similar to the Whitehill Formation in colour and weathering (*Plate 2, Figure 3*). All the shales are internally finely laminated with laminae of less than 1 mm. The shales are inter-bedded with yellow tuff (*Plate 2, Figures 4 & 5*). The tuff layers range in thickness from 0.2 to 5.5 cm. The tuffaceous material is less competent than the shale and is extensively weathered and crumbles under the slightest strain (*Plate 2, Figure 5*). No competent tuffaceous material was observed. A section of the outcrop 10.8 m in stratigraphic height from the lower contact (Collingham and Whitehill) contains a layer of very hard possibly siliceous material approximately 15 cm thick, unlike the surrounding shales.

The outcrop consists of alternating layers of grey shale and yellow tuffaceous material with variations in layer thicknesses. All strata are tabular in geometry with uniform sharp contacts between layers. The strata in the outcrop have an average dip angle of 40° to the north. The shales at the contact with the Ripon Formation are slightly deformed.

Sedimentary Structures

Lens shaped layers of low competency clay-like material (*Plate 2, Figure 6*) are present in the 15 cm thick non-shale basal layer. The lens shaped structures have an average thickness of 9 cm and an average length of 110 cm.

PLATE 2

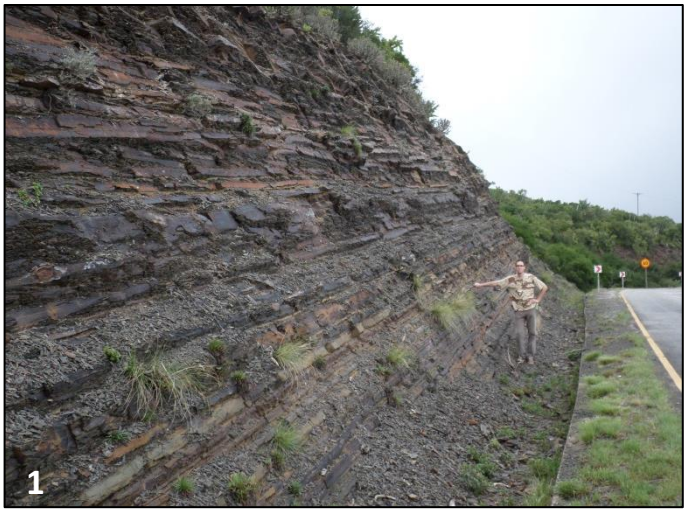

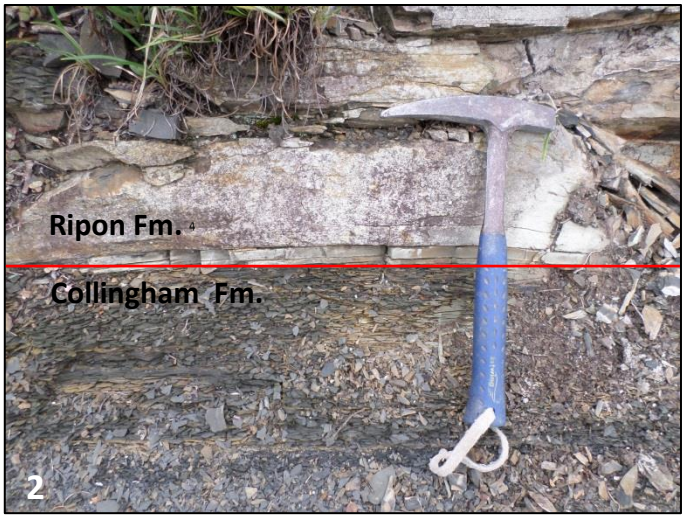

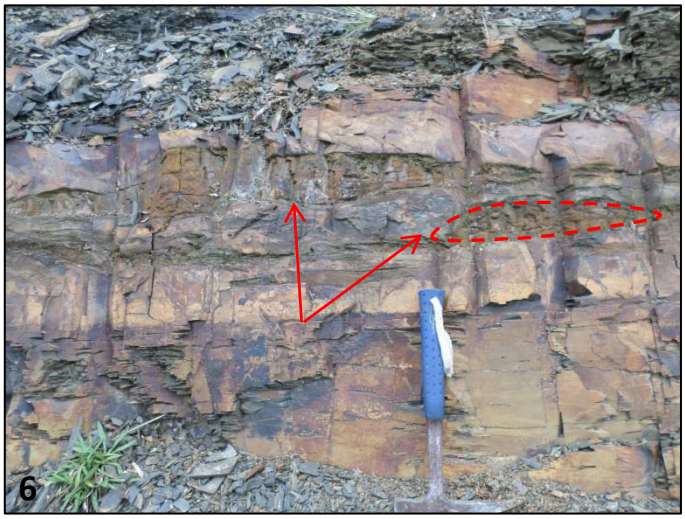

Plate 2: Outcropping Collingham Formation rocks with contacts, lithologies and, structures. **Figure 1:** Well exposed interbedded shales and tuffaceous material of the Collingham Fm. **Figure 2:** Sharp planar contact between the Collingham and Ripon formations. **Figure 3:** White weathering dark coloured shale of the Collingham Fm. **Figure 4**: Collingham Fm. shales exposed along road cutting displaying alternating shale and tuff layers. **Figure 5:** Fragmented tuff and competent shale of the Collingham Fm. **Figure 6:** Lenses of less competent clay-like material with average dimensions 110cm x 9cm within Collingham Fm. shale.

Palaeontological Findings

Fragmented plant detritus (*Plate 7, Figure 1*) was observed in distinct horizons within the outcrop. The fossils consist of fragmented stems and shoots. The majority of palaeontological findings were of poor quality. A small number of samples were recovered that preserved detailed structure of the plant stem with a possible girdle scar being visible (*Plate 7, Figures 2 & 3*).

4.1.4 Ripon Formation

The Ripon Formation of the Ecca Group is 217.84 m thick in the study area (*Figure 4.1*). The formation is exposed along road cuttings and contains fresh as well as weathered material. The formation consists of repetitive sequences of medium-grained sandstone, fine- grained sandstone and shale (*Plate 3*, *Figures 2-6*).

Rock Descriptions

The formation contains abundant sandstones with several variations being observed:

I. Very fine to fine grained laminated sandstone that ranges in colour from light to dark grey (*Plate 4, Figure 1*). Weathering colours range from light brown to rusty-red. This sandstone type is rich in organic matter and plant fossils. Individual sandstone layers range in thickness from 7 cm to 30 cm. Contacts between these sandstone layers appear erosive.

II. Medium grained sandstone that is usually upwards fining from medium grained to fine grained. It ranges in colour from grey to greenish-grey to brown. This sandstone weathers light grey to dark brown and displays 'onion skin' type as well as blocky weathering patterns. Internal banding is observed with bands from 2 -5 cm in thickness. Bands alternate from darker more silty bands to lighter coarser grained bands with the contact between bands occasionally displaying a reddish colouration. Where this lithology appears above a shale layer then the basal section usually contains a rip-up clast conglomerate of shale (*Plate 4, Figure 2*). Units of this lithology can attain a thickness of several meters. Some layers contain bands of dark organic matter that

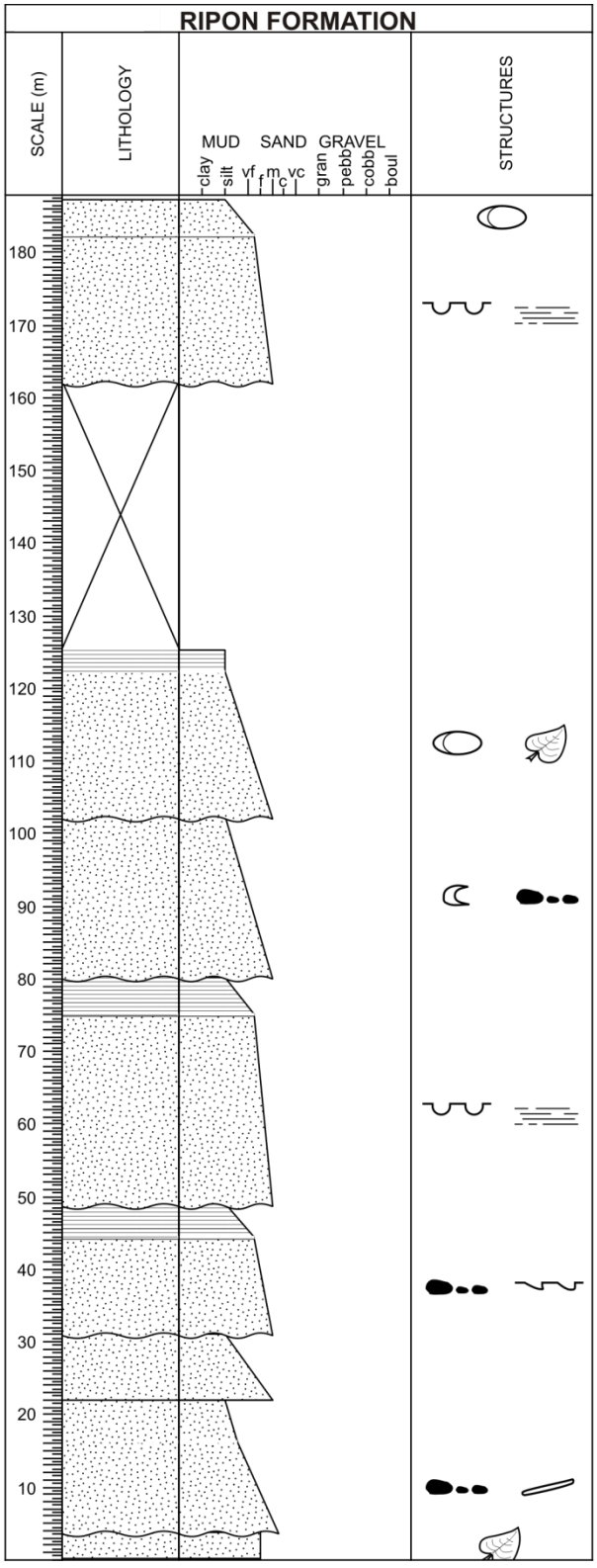

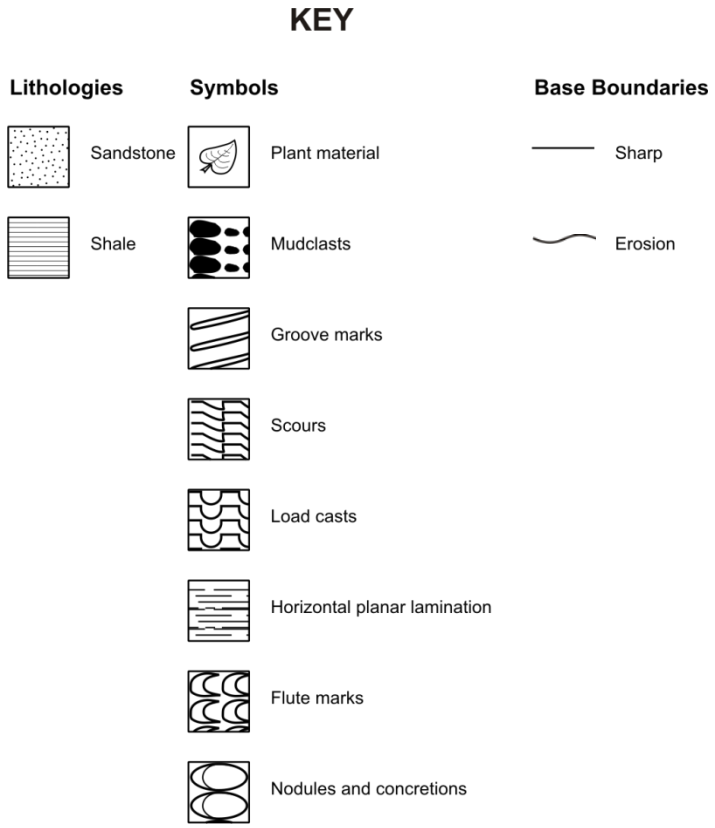

Figure 4.1: Simplified log of the Ripon Formation with major lithologies, structures and, palaeontological findings. Note: 37 meters in stratigraphic height was covered by regolith and vegetation and was therefore not logged. Log was created using Sedlog software.

reach a thickness of up to 0.5 cm. Large clasts of shale up to 10+ cm are occasionally visible in this lithology.

III. A medium grained white sandstone. This lithology is rare and all occurrences appear weathered and non-competent. Layer thicknesses are less than 1.5 m.

IV. A medium grained spotted sandstone (*Plate 4, Figures 3, 4 & 5*). This lithology appears to be a combination of lithology II and III although is much more abundant than lithology III. White spots are match-head sized and are usually evenly distributed through the sandstone that is otherwise the same as lithology II. Sandstone layers attain a maximum thickness of several meters. The white spotted sandstone (lithology IV) is inter-bedded with the grey medium grained sandstone (lithology II) in certain localities.

Various shale and clay lithologies have been observed and include the following:

V. Dark grey thinly bedded to laminated siltstone. This siltstone appears similar in nature to the Whitehill Formation but fresh samples are not as dark. The siltstone is however also white weathering. It ranges in thickness from 5 mm to 4.5 cm. It contains abundant organic matter and bioturbated samples have been documented from this lithology.

VI. Black shale. This black shale is highly weathered and fragmented. The shale occurs as pencil fragments- thin elongated shards of shale. The shale appears internally laminated.

VII. Light brown clay-like material. This material is very soft, being easily damaged by a geology hammer. This material occurs as basketball sized spheres occasionally linked to the next sphere by a thin layer less than 10cm thick. These spheres exhibit 'onion skin' type weathering patterns (*Plate 4, Figure 6*). It also occurs as lens shaped layers within sandstones with dimensions approximately 100 cm in length and 15 cm in height. Fresh material reacts with weak hydrochloric acid indicating the presence of carbonate.

All lithologies within the Ripon Formation, with the exception of clay lenses, are planar and tabular with an average dip of 40° to the north. The majority of shales and siltstones contain planar laminations and sandstones contain planar bedding. One sandstone layer was observed that appeared to be a channel fill approximately 5 meters in length.

The entire formation follows a regular and sequential pattern of deposition with upwards fining of grain size as well as upwards thinning of layer thickness within a sequence from medium grained, massive to laminated sandstone comprising the basal layer grading to fine/very fine grained, planar laminated sandstone with planar laminated shale or siltstone comprising the top of the sequence (*Plate 5, Figure 1*). This sequence is then repeated with changes only to the thickness of the representative lithologies and the type and content of the sandstone (spotted or non-spotted/ organic rich/ fossil rich etc.). Upwards fining was not always observed. A general trend of increasing grain size and increasing bed thickness is observed starting from the Collingham Formation and moving up stratigraphy through the Ripon Formation as illustrated in *Plate 3*. A section of the outcrop 37m in stratigraphic height was not exposed and is covered in regolith and vegetation. The section is most likely clay-rich shale that is easily eroded.

Erosive contacts are regularly observed between sequential sandstone layers (*Plate 5, Figure 2*). The basal layer/s have been eroded and the cavity subsequently filled by the depositing layer. In one instance an entire sequence of shale, medium grained sandstone and fine grained sandstone were eroded by a large sandstone layer being deposited. Remnants of the eroded stratigraphy are preserved in a lens.

Sedimentary Structures

One specific sandstone layer less than 50 cm thick (*Plate 5, Figure 3*) exhibits cross and convoluted bedding at the base followed by parallel laminae and then graded bedding from granule/pebble sized fragments up to fine sand. This is then followed by parallel laminations.

Load casts or 'ball and pillow' structures (*Plate 5, Figure 5*) occur at the contact between shale and sandstone layers with sandstone 'balls' up to 60 cm in length and 10 cm in height. Drag marks (*Plate 5, Figure 6*) as well as scour marks were used as palaeocurrent indicators with a north to north-north-east palaeocurrent direction recorded (*Figure 4.2*). Extensive sole marks and tool marks including grooves (*Plate 6, Figure 1*), bounce marks (*Plate 6, Figure 2*), scour marks, flute marks (*Plate 6, Figure 3*), ridges and furrows (*Plate 6, Figure 4*) and, gutter casts (*Plate 6, Figure 5*) were documented in the basal section of the sandstones. Sole marks are on the scale of centimetres. Pinching out of sandstone layers was also observed.

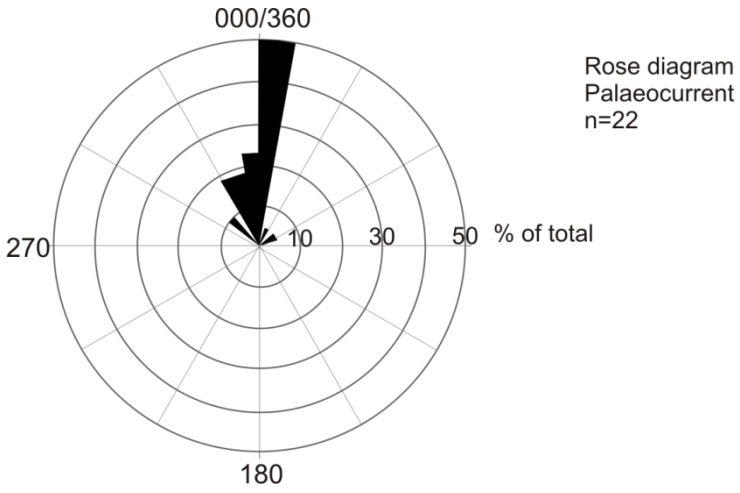

Figure 4.2: Rose diagram illustrating prominent northerly palaeocurrent direction from sandstones, Ripon Formation.

Palaeontological Findings

Fragmented plant detritus was again observed in distinct horizons within the outcrop (*Plate 7, Figure 4*). Fossil material recovered from the Ripon Formation consists of fragmented stems and shoots (*Plate 7, Figures 5 & 6*). The majority of palaeontological findings were of poor quality. One sample documented (*Plate 7, Figure 6*) contains a portion of a branch or stem 4 cm thick and 15 cm long with perfectly preserved internal cellular structures.

An exceptionally fossil rich horizon was identified at the contact between the Ripon and Collingham Formations. Numerous plant stems were documented (*Plate 8, Figures 1, 2 & 3*) from this horizon as well as a tentative leaf or insect wing with visible veins (*Plate 9*). Two samples of bioturbated siltstones were documented. Bioturbation consists of crisscrossing burrows or trails 2 mm thick and up to 5 cm in length (*Plate 8, Figure 4*). Detailed internal cellular structures are visible in some of the plant remains (*Plate 8, Figures 5 & 6*).

PLATE 3

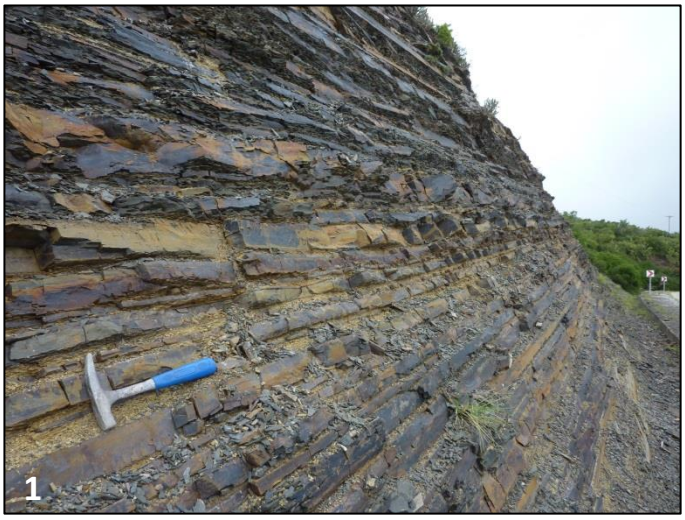

Plate 3: Outcrop overview of the Collingham and Ripon formations moving up stratigraphy. **Figure 1** through **6:** Increasing grain size and bed thickness on outcrop scale from predominantly thinly bedded laminated shale (Figure 1) to massive sandstone (Figure 6) and gradual variations in between (Figures 2-5).

PLATE 4

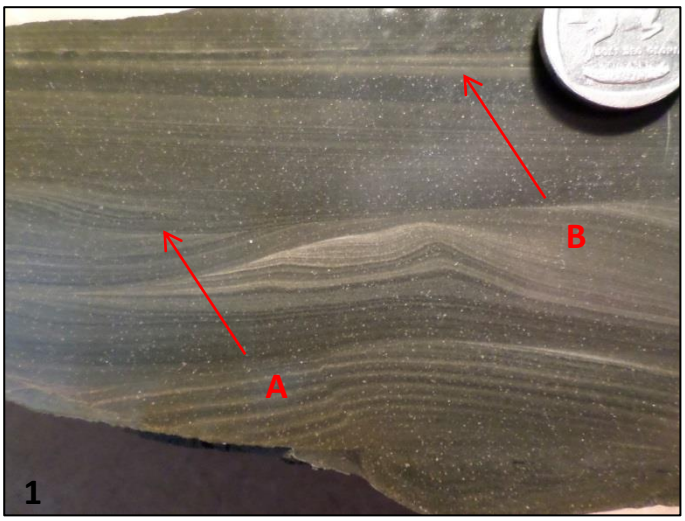

Plate 4: Ripon Formation lithologies, structures and, diagenetic features. **Figure 1**: Cut and polished sample displaying cross-bedded fine grained sandstone (A), and planar laminated silt (B), Ripon Fm. **Figure 2**: Rounded shale fragments in medium grained sandstone, Ripon Fm. **Figure 3**: Cut and polished sample displaying layers of spotted sandstone within normal medium grained grey sandstone, Ripon Fm. **Figure 4**: Disseminated white spots in normal grey sandstone. **Figure 5**: 20 cm thick spotted sandstone layer exposed in the outcrop, Ripon Fm. **Figure 6**: 'Onion skin' weathering of soft clay-like material within sandstone of the Ripon Fm.

PLATE 5

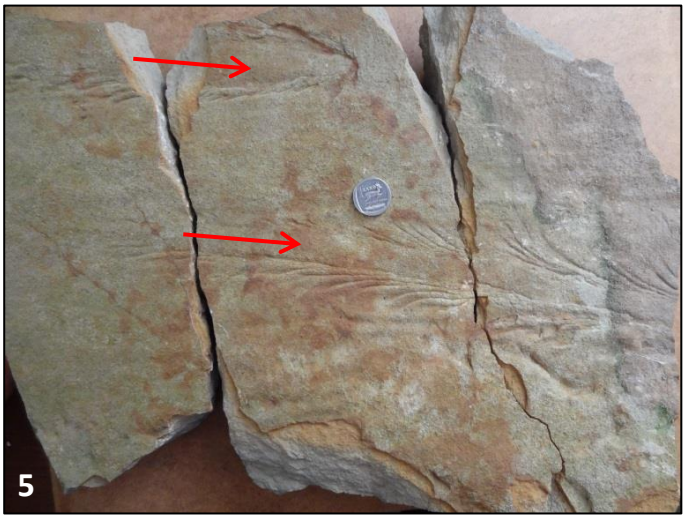

Plate 5: Ripon Formation upwards fining sequences and structures. **Figure 1:** Repetitive upwards fining sequences from medium grained sandstone to fine grained sandstone followed by siltstone and then shale, Ripon Fm. **Figure 2:** Erosive contact between shale and overlying sandstone with visible sole-marks, Ripon Fm. **Figure 3**: Sedimentary structures in medium to fine sandstone: From bottom- cross and convoluted laminae, parallel laminae, and graded bedding from pebble conglomerate to laminated fine grained sand, Ripon Fm. **Figure 4:** Sandstone 'Ball-and-Pillow' structures at shale-sandstone contact, Ripon Fm. **Figure 5:** A cast of a drag mark or chevron mark in medium grained sandstone, Ripon Fm **NOTE**: Arrows indicate palaeocurrent direction.

PLATE 6

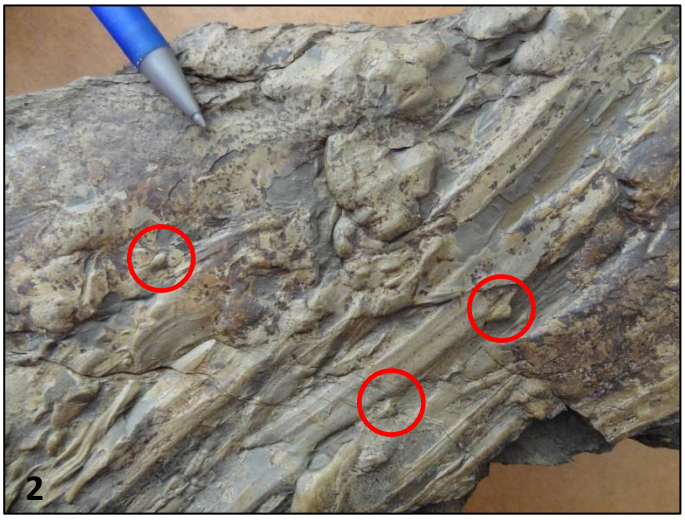

Plate 6: Ripon Formation sole marks. **Figure 1**: Grooves on the base of a medium grained sandstone layer, Ripon Fm. **Figure 2**: Fine grained sandstone with ridges and furrows, grooves and, skip and bounce marks in red circles, Ripon Fm. **Figure 3**: Flute cast with a bounce mark in red circle, Ripon Fm. **Figure 4**: Ridges and furrows in medium grained sandstone overlying shale, Ripon Fm. **Figure 5**: Gutter cast at the base of medium grained sandstone layer, Ripon Fm.

PLATE 7

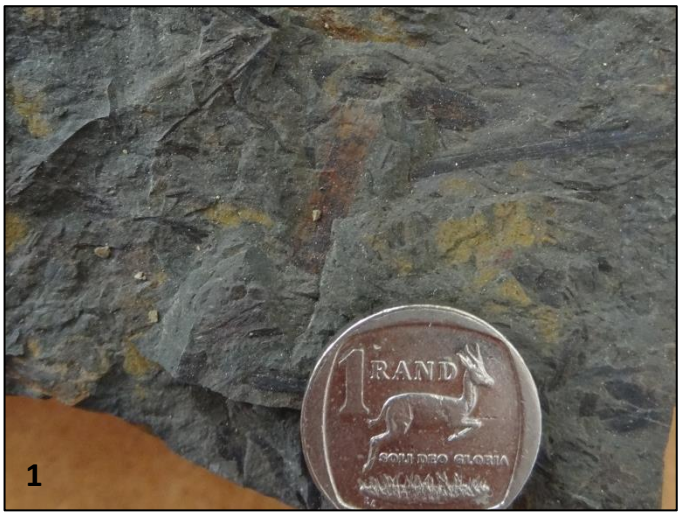

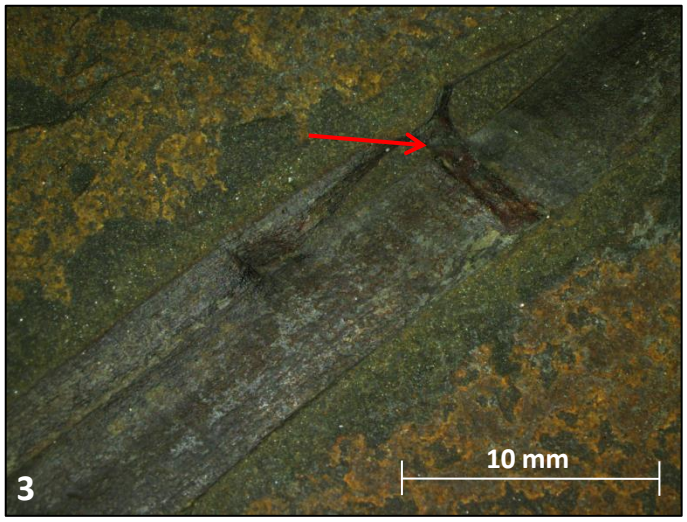

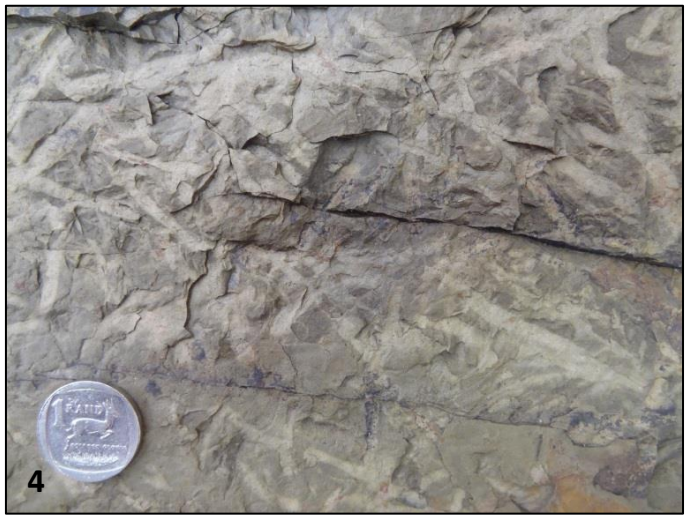

Plate 7: Fossil material from the Collingham and Ripon Formations**. Figure 1:** Abundant fragmented plant debris in organic rich shale, Collingham Fm. **Figure 2:** Plant stem in shale, Collingham Fm. **Note**: pencil tip for scale**. Figure 3:** The same plant stem with possible girdle scar, Collingham Fm. **Figure 4:** Abundant and fragmented plant debris in fine sandstone, Ripon Fm. **Figure 5:** Plant stem preserved in siltstone, Ripon Fm. **Figure 6:** Large terrestrial plant stem/branch with well-preserved internal cellular structure. **Note**: pencil tip for scale.

PLATE 8

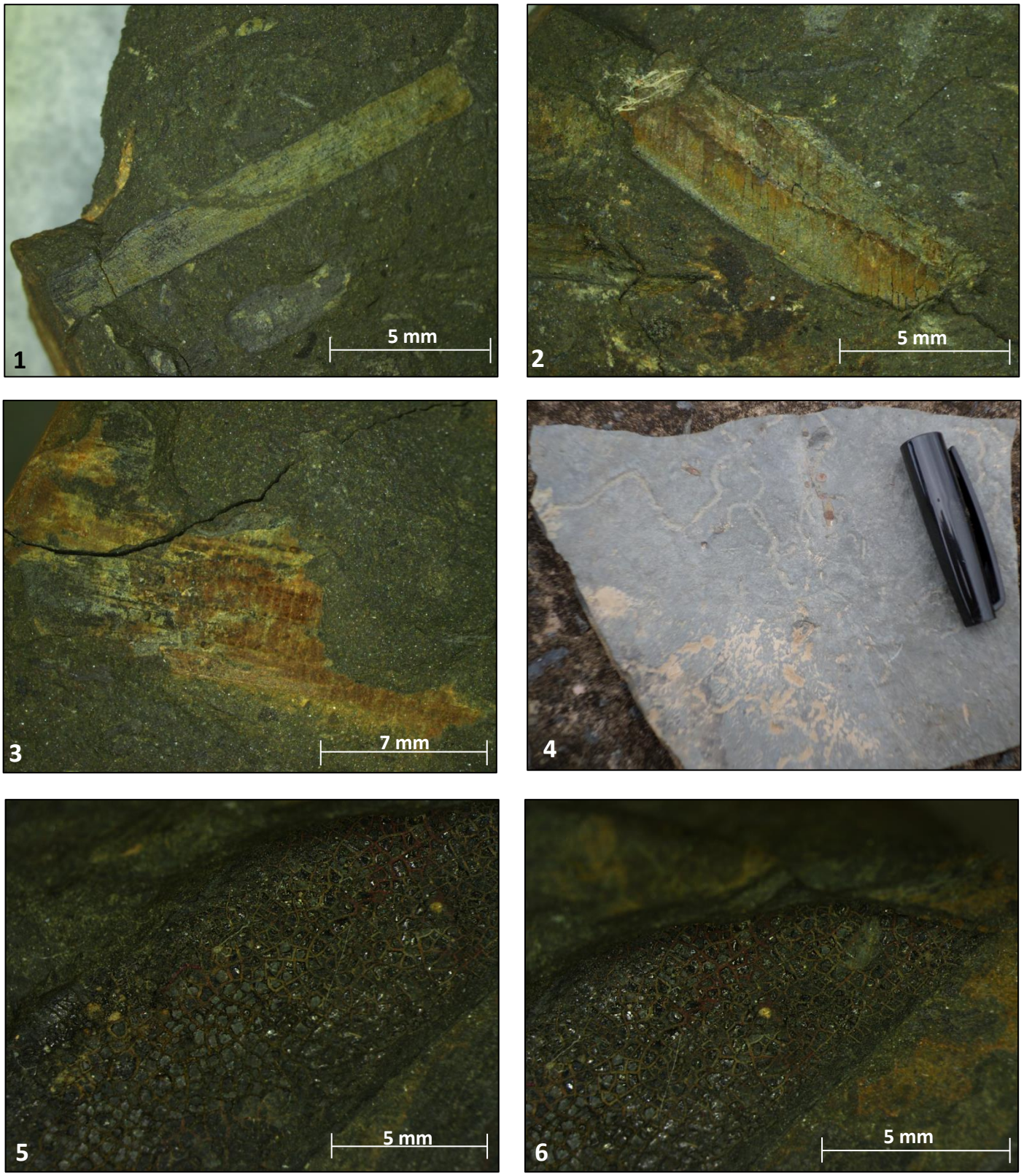

Plate 8: Ripon Formation fossil material and trace fossils. **Figure 1**: Plant stem in sandstone, Ripon Fm. **Figure 2**: Possible plant stem in sandstone, Ripon Fm. **Figure 3**: Fragmented possible woody remains (plant stem) in sandstone, Ripon Fm**. Figure 4**: Bioturbation in siltstones consisting of cross-crossing burrows and tunnels, Ripon Fm. **Figure 5 & Figure 6:** Plant stem in sandstone with preserved internal cellular structure, Ripon Fm.

PLATE 9

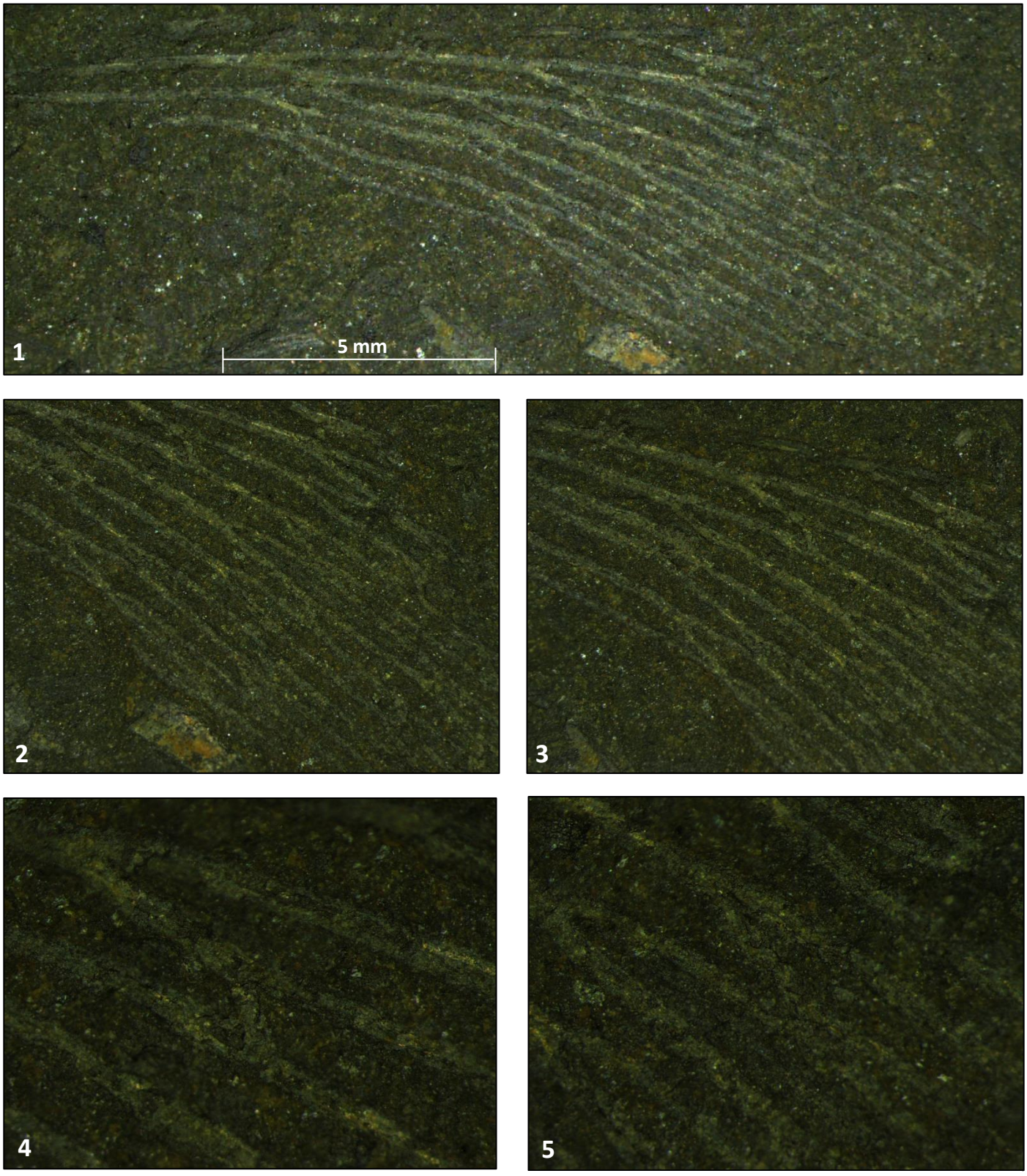

Plate 9: Leaf fragment in sandstone from the Ripon Formation. **Figure 1**: Overview of fossil in sandstone from Ripon Fm. 1.6X magnification. **Figure 2**: Linear arrangement of vein bifurcations. **Figure 3**: Parallel veins. **Figure 4 and 5**: Increased magnification of veins showing bifurcations and possible cross-vein, 8x magnification.

Joint Systems

Two predominant jointing directions were observed in the Ripon Formation sandstones and shales. The strike and dip of 40 joints were measured with an average of 242/53 and 143/73 with a nearly right angle intersection (99°).

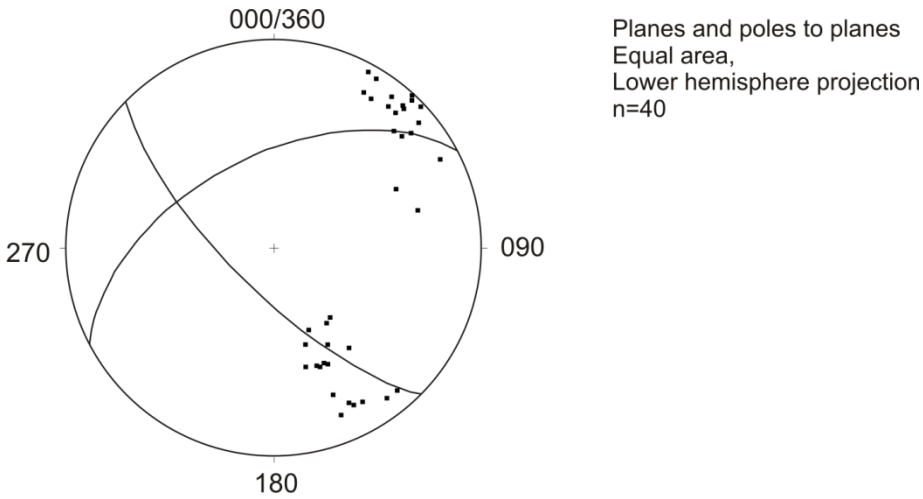

Figure 4.3: Stereonet projection of average values for planes and, poles to planes of two dominant joint systems in sandstone and shale, Ripon Formation.

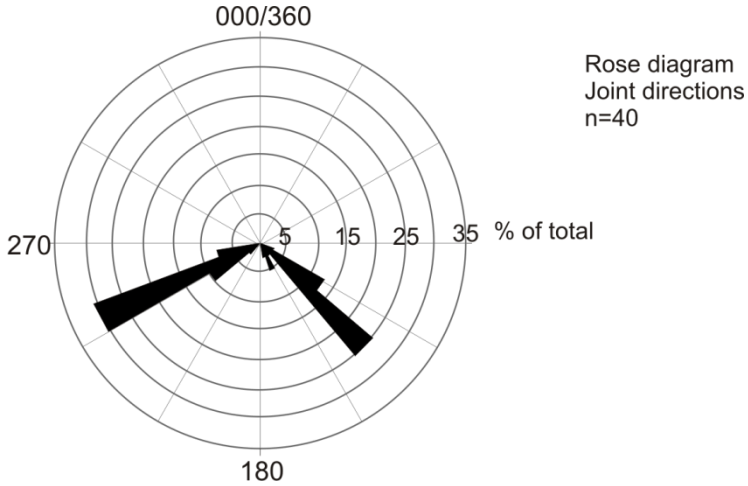

Figure 4.4: Rose diagram displaying two dominant joint systems in sandstone and shale, Ripon Formation.

4.2 Microscopic Observations

4.2.1 Thin Section Microscopy and X-ray Diffraction

30 samples were analysed to describe petrography. Selected thin section photographs are provided as *Plate 10* and *Plate 11*. For tabulated list of minerals from XRD see Appendix C.

Prince Albert Formation

Samples from the Prince Albert Formation (*Plate 10, Figure 1*) are too fine grained for normal thin section petrography (up to 50x magnification). X-ray diffraction (XRD) data from a powdered sample indicate that quartz, and iron and manganese oxides are among the most common constituents (*Figure 4.5*).

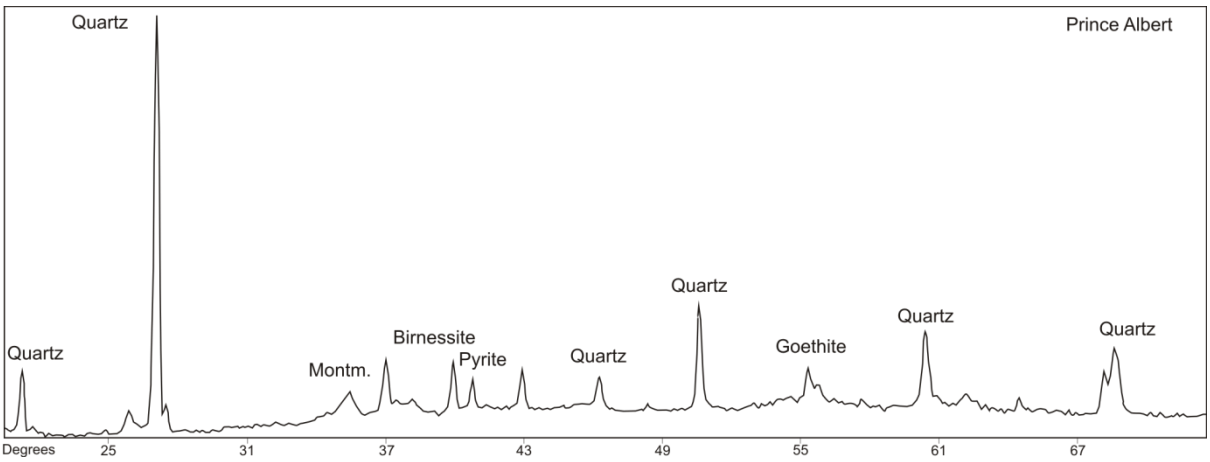

Figure 4.5: Mineral peaks from XRD analysis of the Prince Albert Formation. Quartz, montmorillonite, goethite, pyrite and birnessite are present in the sample.

Whitehill Formation

The samples from the Whitehill Formation range in the clay and silt fraction and were thus analysed by X-ray diffraction. XRD data indicates that quartz is the most common constituent (*Figure 4.6*).

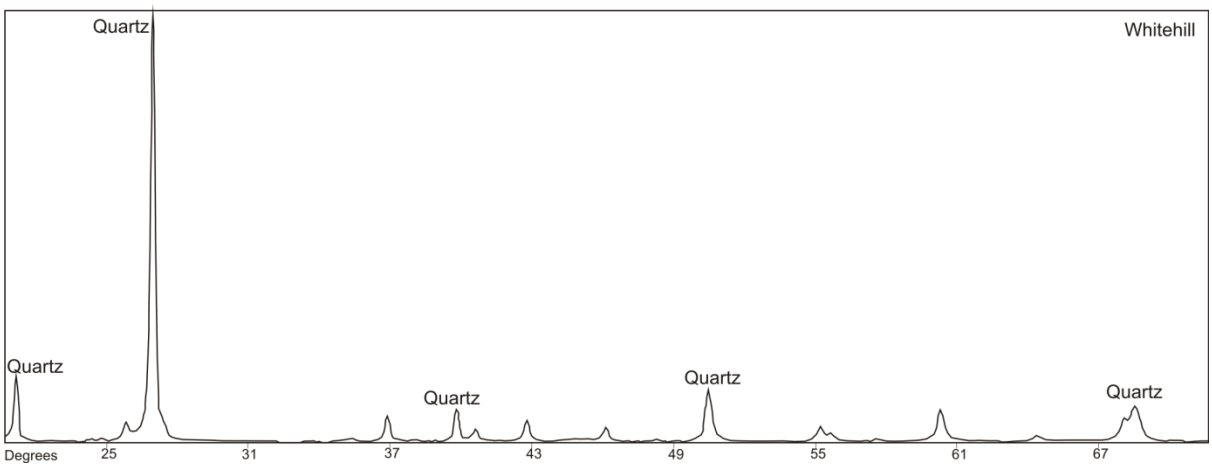

Figure 4.6: Mineral peaks from XRD analysis of the Whitehill Formation. Only quartz was detected in the sample.

Collingham Formation

The Collingham Formation (*Plate 10, Figure 2*) also comprises fine grained clastics and thus XRD analyses were conducted to identify mineral constituents. Some thin sections contain visible mica's and quartz grains with the rest comprising laminated dark organic matter and very fine grained material. XRD analysis from powdered samples indicates that quartz, illite (oneillite), and montmorillonite and, calcite are present in the sample (*Figure 4.7*).

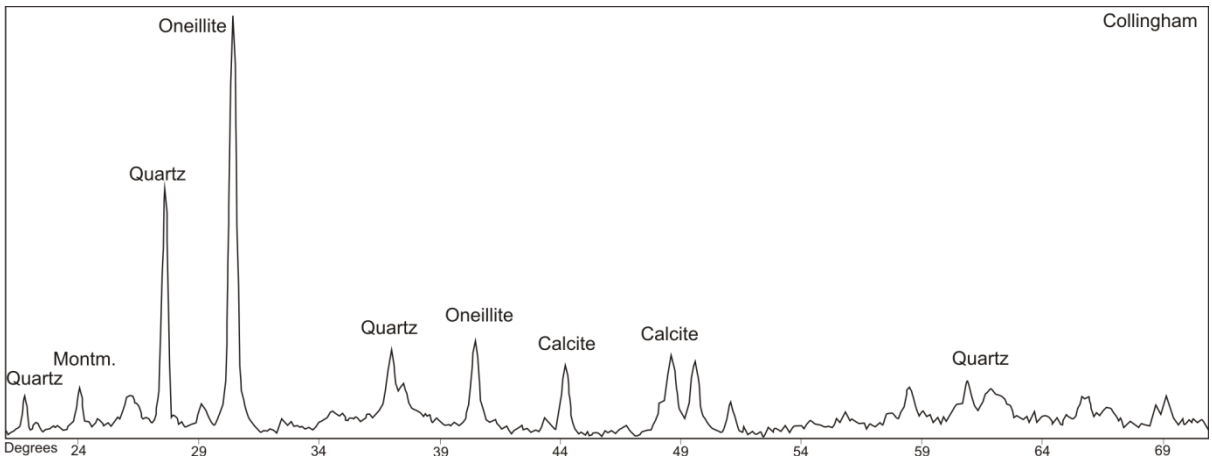

Figure 4.7: Mineral peaks from XRD analysis of the Collingham Formation. Quartz, calcite, montmorillonite, and oneillite were detected in the sample.

Ripon Formation

Non-Spotted Sandstone

Samples contain an amalgamation of poorly sorted, very well rounded to sub-rounded grains of varying size (*Plate 10, Figure 3*). Texture is massive to laminated with bands of organic matter (*Plate 10, Figure 3; Plate 11, Figure 1*) and closely packed (grain supported) with point contacts between grains. Grains consist of internally fractured monocrystalline undulatory quartz (*Plate 10, Figure 4*), twinned and zoned feldspar, chert, lithic fragments containing altered feldspar and others organic rich (*Plate 10, Figure 5*), glauconite (*Plate 10, Figure 6*), elongated biotite (being replaced by limonite in some samples), and organic fragments in a matrix of very fine yellow-brown to black clay-like material (*Plate 11, Figure 2*). Iron oxides (hematite) are present in organic rich sections. The majority of the samples are composed of quartz, feldspar, organic matter, lithic fragments, clay matrix, and other minerals (biotite, muscovite, glauconite, limonite).

Classification

Abundances of constituents (quartz, feldspar, lithic fragments, clay) were estimated visually using the 'Comparison Chart for Visual Percentage Estimation' after Terry and Chilingar (1955).

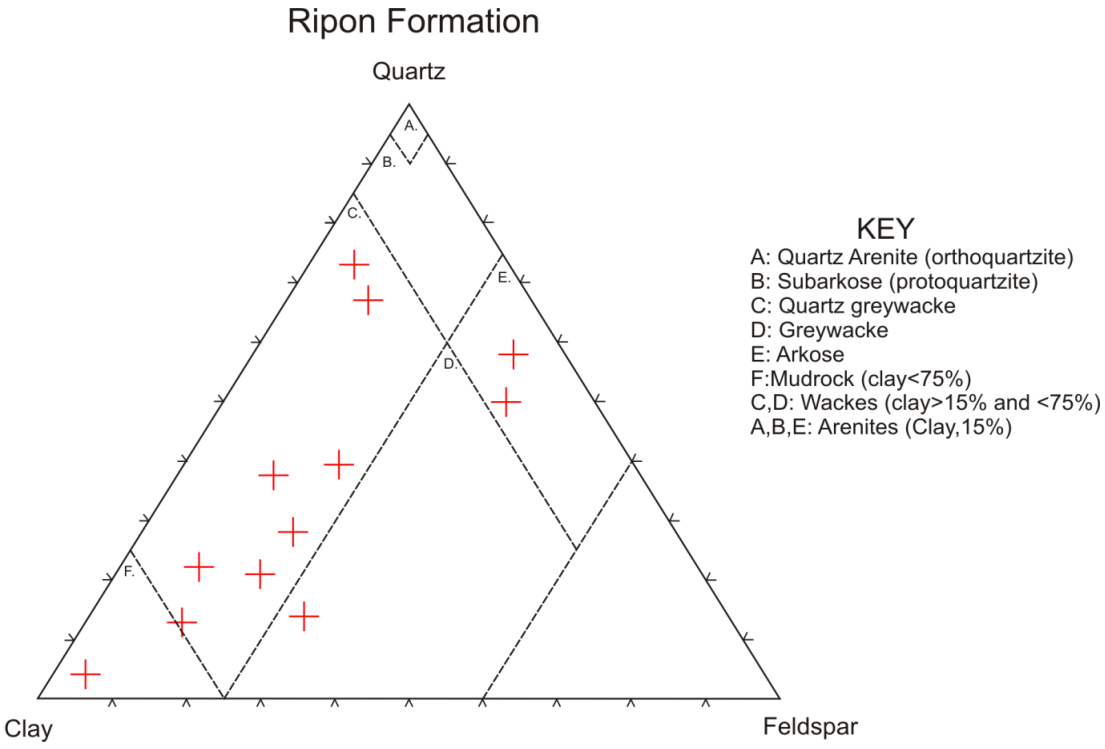

Figure 4.8: Classification of 12 sandstone samples from the Ripon Formation based on Selley (1984). Classification was done using WinRock software.

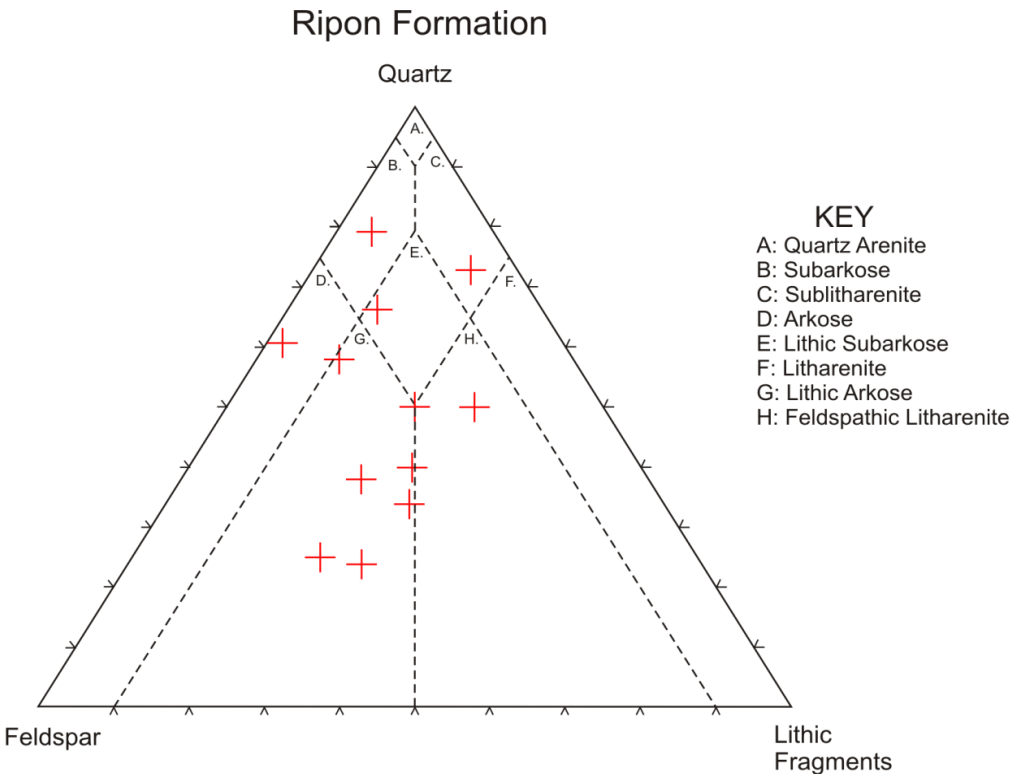

Figure 4.9: Classification of 12 sandstone samples from the Ripon Formation based on Pettijohn (1975). Classification was done using WinRock software.

Soft Sphere

XRD analysis was performed on a soft sphere of clay-like material from the Ripon Formation (*Plate 4, Figure 6*) and the material was found to contain quartz, calcite and illite (oneillite).

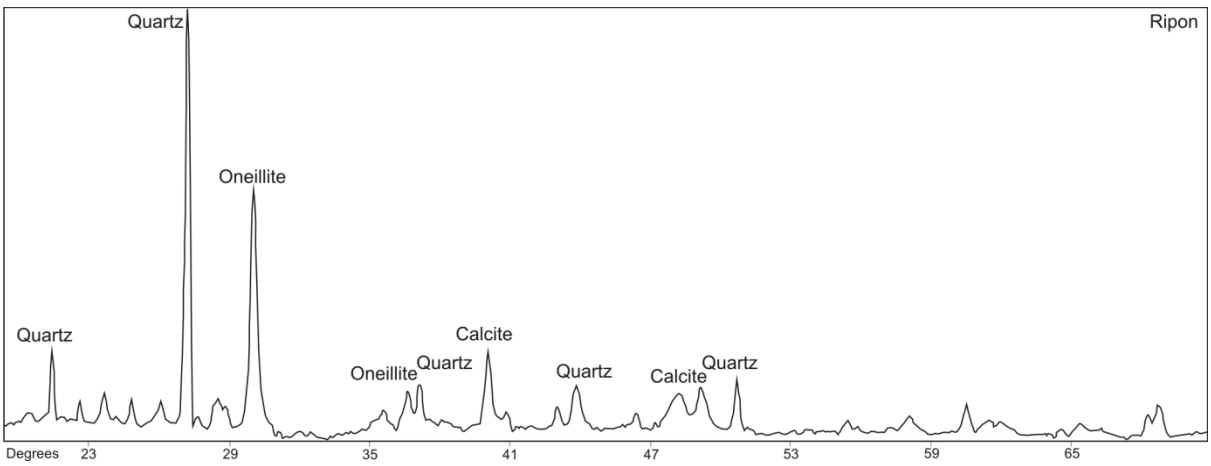

Figure 4.10: Mineral peaks from XRD analysis of a spherical lens from the Ripon Formation. Quartz, calcite, and oneillite were detected in the sample.

Spotted Sandstone

Spotted sandstone contains moderately to well-sorted monocrystalline quartz and feldspar grains that appear equigranular in size, up to 300 µm (*Plate 11, Figure 3*), and are grain supported with line contacts (*Plate 11, Figure 4*). Grains are angular to sub-rounded and quartz grains are not internally fractured as observed in non-spotted sandstone samples (*Plate 11, Figure 4*).

Samples of spotted sandstone contain little or no clay either as matrix or as alteration products and organic matter is virtually absent (less than 5%). The fine grained groundmass of quartz, feldspar, limonite, organic matter and other clays observed in non-spotted sandstone is absent from the spotted sandstone. Feldspar grains display a lesser degree of alteration in comparison to non-spotted sandstone. Spotted sandstone contains slightly altered biotite grains that bend around quartz and feldspar grains (*Plate 11, Figure 5*). Other observed minerals include chlorite and muscovite (*Plate 11, Figure 6*).

4.2.2 Total Organic Carbon

Shales presumed to be rich in organic matter, based on field observations, were tested for TOC as well sulphur and TMax. Only a very small sample size was collected (n=4) from the outcrop due to the weathered state of the study site. For the full range of tabulated data see (Appendix D).

Whitehill Formation

TOC of the Whitehill Formation ranges between 0.6-0.9 wt% with an average of 0.75 wt%. No sulphur (wt%) was detected and no TMax (C°) was detected.

Collingham Formation

TOC of the Collingham Formation ranges between 0.2-0.6 wt% with an average of 0.4 wt%. Again no sulphur (wt%) was detected and no TMax (C°) was detected.

Plate 10

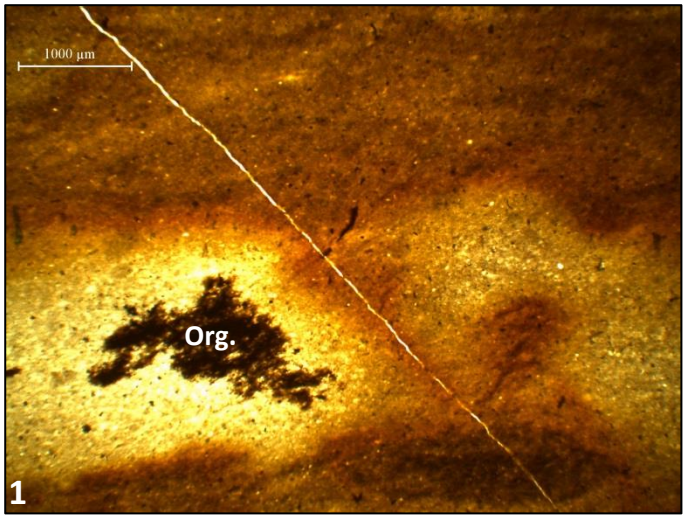

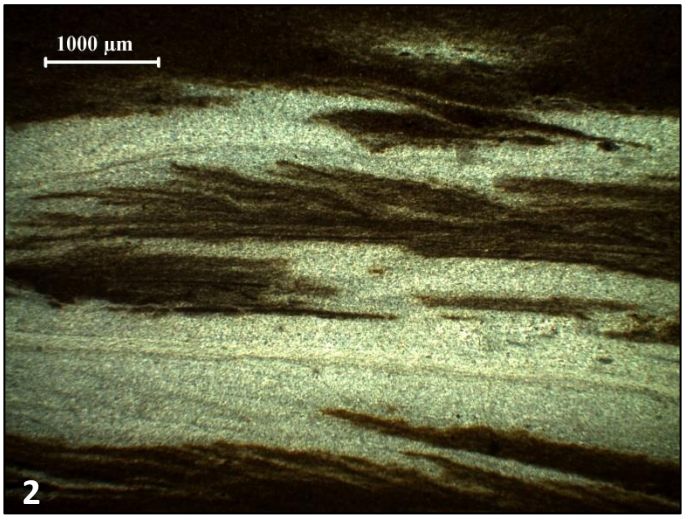

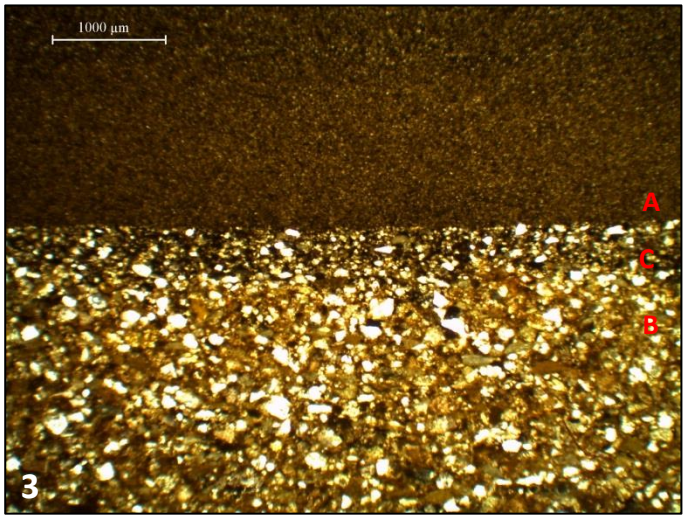

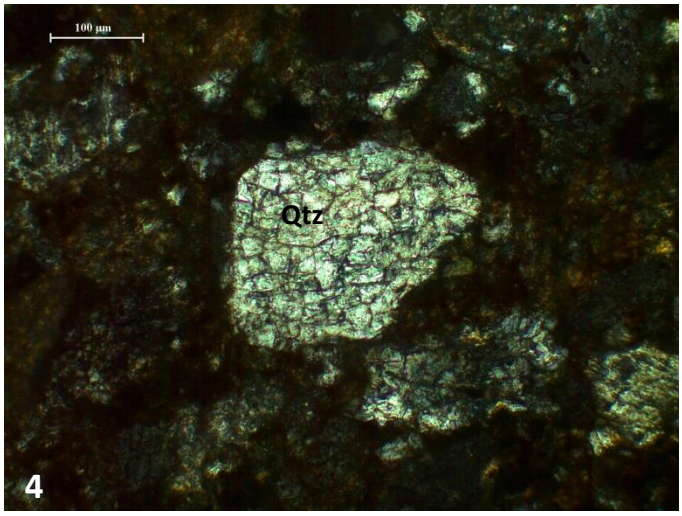

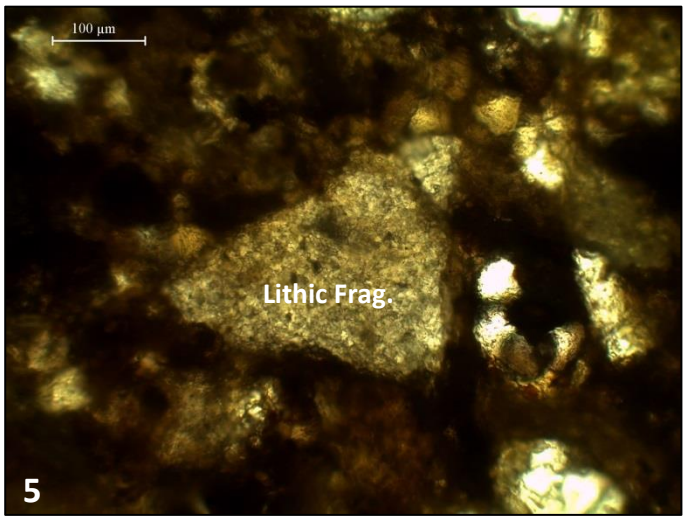

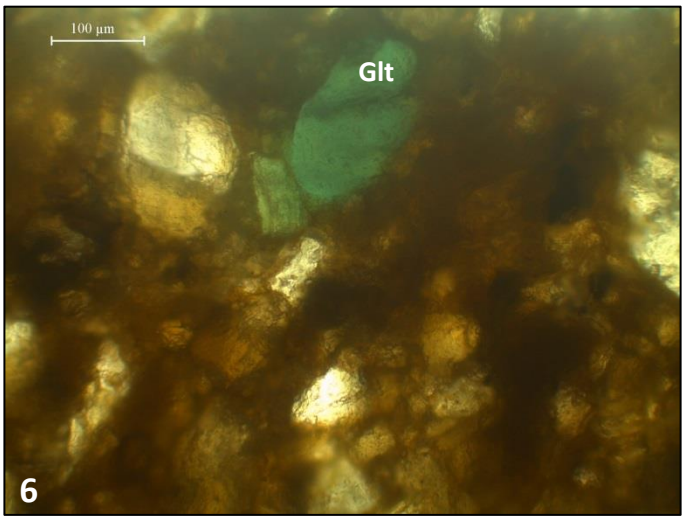

Plate 10: Photomicrographs from Prince Albert, Collingham and Ripon formations' thin sections. **Figure 1:** Shale with abundant organic matter and laminated clay, Prince Albert Fm. **Figure 2:** Shale with clay laminations and organic matter, Collingham Fm. **Figure 3:** Fine grained clast (A) in poorly sorted mixture of quartz, feldspar, clay and organic matter (B) with organic rich contact (C), Ripon Fm. **Figure 4**: Internally fractured quartz grain in mixture of clay and organic matter, Ripon Fm. **Figure 5:** Lithic fragment in clay and organic matter with quartz and feldspar, Ripon Fm. **Figure 6:** Glauconite grain in clay with quartz and feldspar, Ripon Fm.

Plate 11

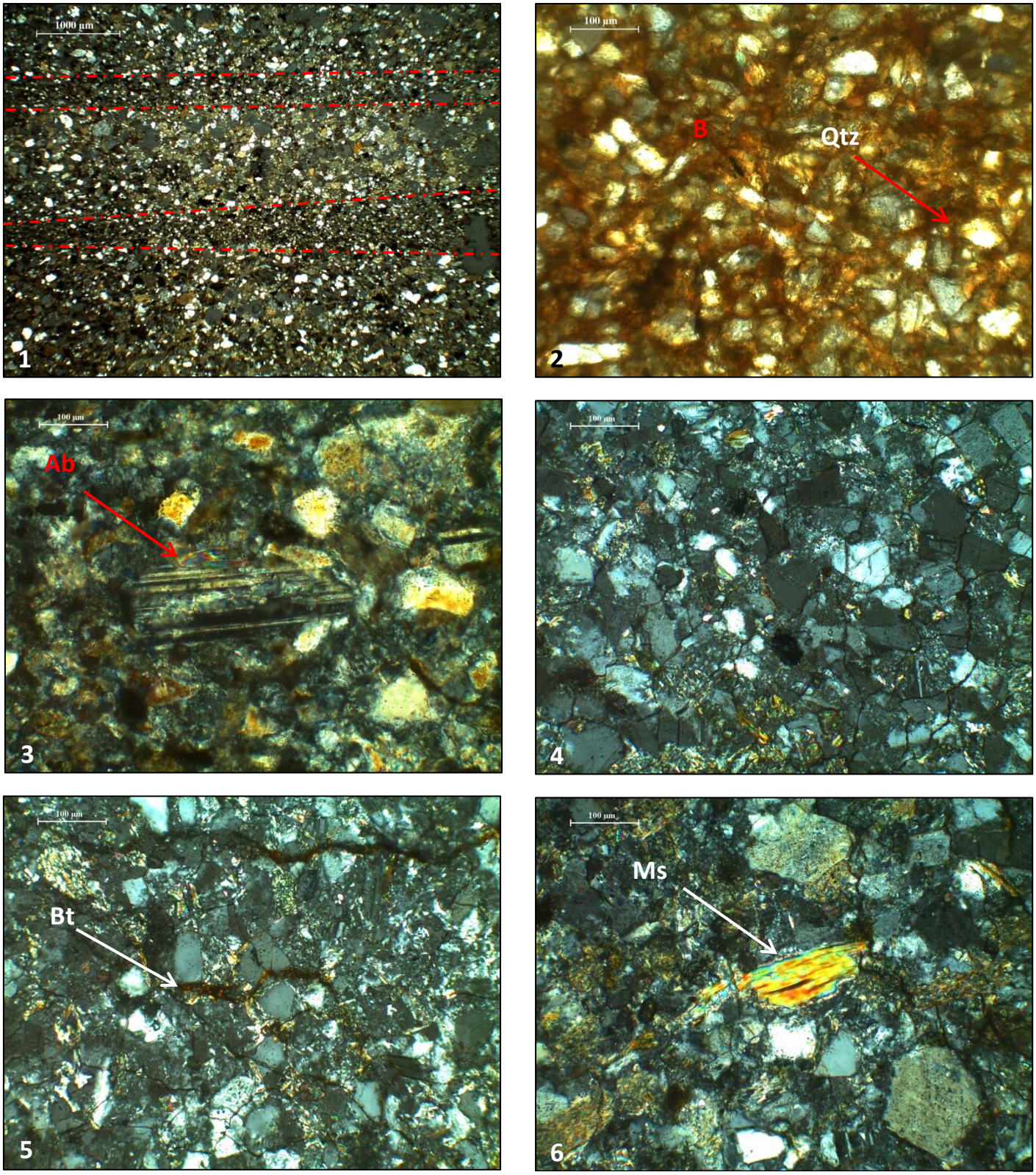

Plate 11: Photomicrographs from Ripon Formation thin sections**. Figure 1:** laminations in sandstone, Ripon Fm. **Figure 2:** Rounded quartz and feldspar grains in a clay matrix (B). **Figure 3:** Large feldspar displaying twinning (albite) and slight alteration in spotted sandstone, Ripon Fm. **Figure 4**: Equigranular, well sorted, angular to sub-rounded quartz and feldspar grains with 'granoblastic' texture in spotted sandstone, Ripon Fm. Note: absence of clay and organic matrix compared to non-spotted sandstone. **Figure 5:** Elongated curved biotite in spotted sandstone, Ripon Fm. **Figure 6:** Muscovite amongst quartz and feldspar grains in spotted sandstone, Ripon Fm.

4.2.3 Porosity and Permeability

Sandstone units of the Ripon Formation were tested for porosity and permeability (poroperm) in order to characterise and classify conventional reservoir potential. Ten sandstone samples were tested for poroperm and samples were selected from the base of largest sandstone units in order to sample the coarsest possible fraction and thus determine maximum poroperm values. Samples were also evenly selected from the base of the formation up to the highest exposed stratigraphic point of the formation in order to determine if reservoir characteristics change with stratigraphic height.

Porosity values range from 0 to 4% with a mean of 1%. Permeability values range from 0.01mD to 0.1mD with a mean of 0.05mD. Grain density values had a mean of 2.67g/cm³.

See Appendix E for tabulated values.

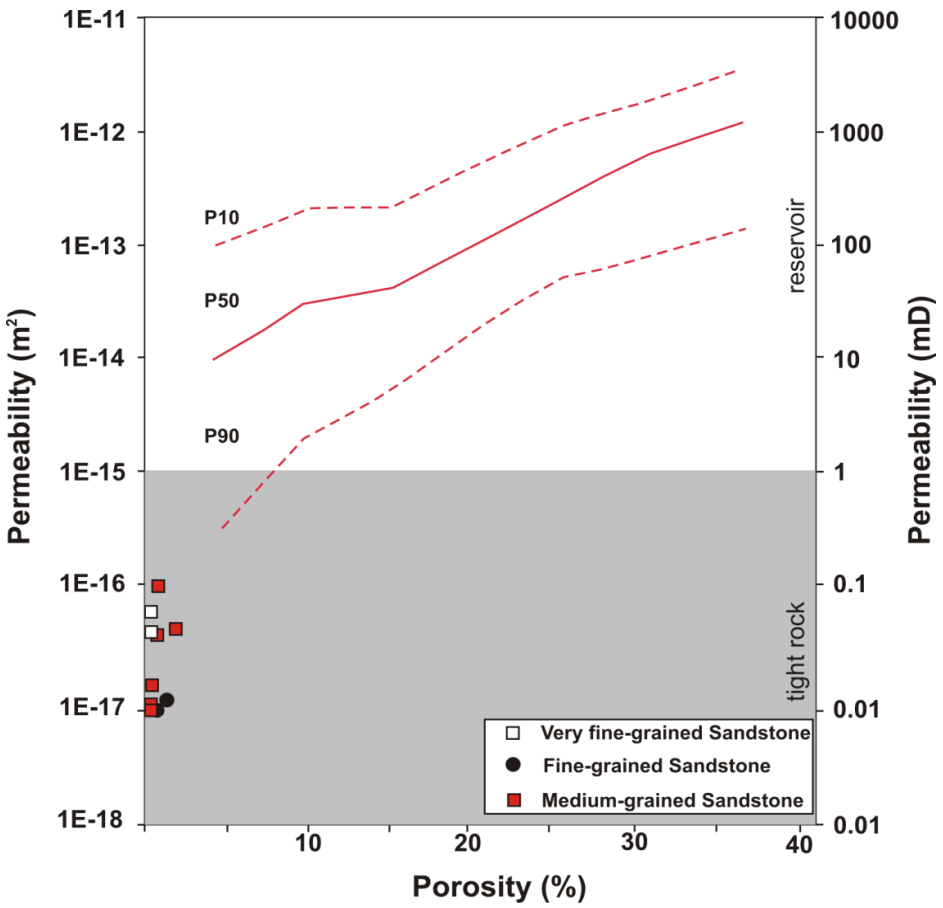

Figure 4.11: Porosity versus permeability plot for Ripon Formation sandstones (turbidites). Included are global statistical trends: P90 (90% of sandstone reservoirs have porosity greater than this value), P50 (median), P10 (10% of sandstone reservoirs have porosity greater than this value).

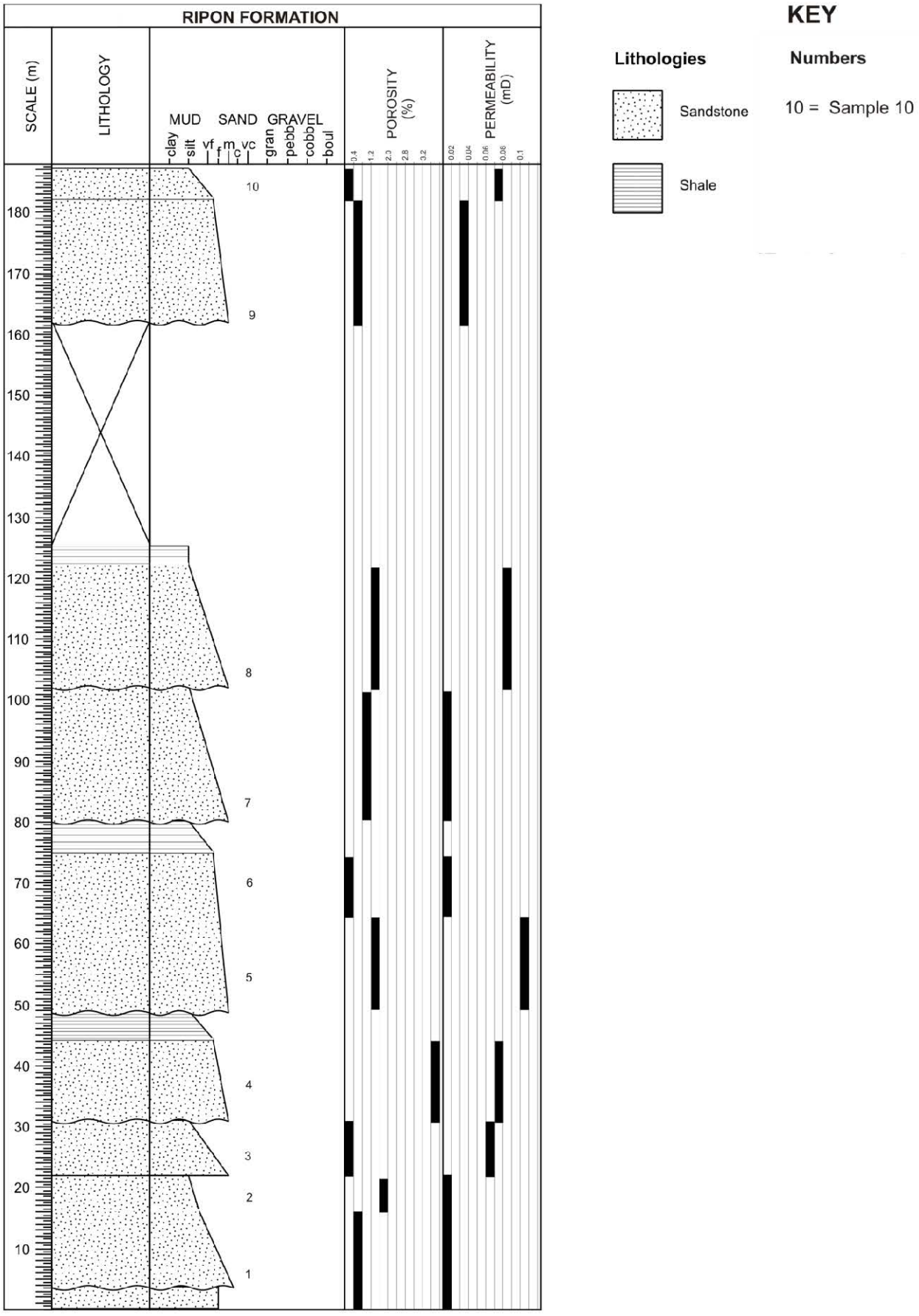

Figure 4.12: Simplified log of the Ripon Formation with major lithologies as well as porosity and permeability values (right) for selected samples (left). Log was created using Sedlog software.

Chapter 5 - Process Interpretations

5.1 Prince Albert Formation

5.1.1 Syndepositional Processes

The sediment grain size in the range of fine silt and mud and the laminated nature of the shale, denoted by lithofacies Fl, is indicative of deposition from suspension in a low energy setting (*Table 1*)

5.2 Whitehill Formation

5.2.1 Syndepositional Processes

The features observed in outcrop exposures of the Whitehill Formation namely, the finely planar laminated, fissile, dark-black coloured, organic-rich rock with a grain size between mud and silt, denoted by lithofacies Flo, identify this lithofacies as a black shale.

The laminated, laterally extensive planar bedding of this formation is indicative of a depositional environment that is very low energy with low rates of sediment accumulation. Deposits of this type are typical of deep water settling of suspended fine grained sediment.

5.2.2 Diagenetic and Weathering Features

The majority of the observed outcrop weathers white in colour and contains nodules of gypsum. Non-weathering hard dark-black layers most likely contain black-chert i.e. silicified black shale. The silicification and high degree of weathering are most likely due to leaching by percolating fluids, and exposure to oxygen of previously anoxic sediments. The organic matter is leached and decomposed and the disseminated pyrite is broken down (*Table 3*). The iron is oxidised resulting in red, pink and rusty colours observed in the shales.

The formation of gypsum possibly incorporates sulphate from the weathering of pyrite and calcium from calcite, which is abundant in marine sediments, with the formula $CaSO_4.2H_20$, (Nicols, 2009). The denser gypsum nodules could contain barium which would substitute for calcium. The abundance of gypsum and lack of organic matter in the weathered shale is evidence that the original sediment must have accumulated in an environment conducive to the preservation of reduced sulphur and organic matter, i.e. anoxic (Song *et al*., 2014).

TABLE 1: Syn-depositional lithofacies from Bordy (2000), modified from Miall (1996).

Formation	Facies Code	Facies	Sedimentary Structures	Interpretation
Prince Albert	Fl	Fine silt to clay	Horizontal planar laminations	Low energy settling from suspension
Whitehill	Flo	Organic rich silt to clay	Horizontal planar laminations	Low energy settling from suspension
Collingham	Flo	Organic rich silt to clay	Horizontal planar laminations, laterally extensive	Low energy settling from suspension
	Th	Tuff	Horizontal bedding, laterally extensive	Rapid deposition of wind-blown sediment, air-fall
	Cm	Chert	Thickly bedded, laterally extensive	Siliceous ooze
Ripon	Sm	Medium sand, may contain mud-clasts, to fine sand	Faintly laminated to massive	Rapid deposition, sediment gravity flow
	Sr	Fine sand	Convoluted bedding	Lower flower regime ripples
	Sl	Fine sand	Planar laminations	Upper flow regime plane beds
	Fl	Fine silt to clay	Planar laminations	Settling from suspension
	Sb	Fine sand to silt	Alternating bands within beds	Secondary sediment gravity flows causing sorting
	Ml	Mud	Laminated	Pelagic settling
	Ssm	Medium sand, may contain mud clasts	Sole marks	Scour fill

TABLE 2: Post-depositional lithofacies from Bordy (2000), modified from Miall (1996).

Formation	Facies Code	Facies	Sedimentary Structures	Interpretation
Ripon	Sb	Medium to fine sand	Ball-and-pillow structure	Soft sediment deformation

TABLE 3: Diagenetic and weathering structures and interpretations.

Formation	Feature	Interpretation
Whitehill	Gypsum nodule	Weathering of pyrite
Ripon	Soft clay sphere	Concretion

TABLE 4: Tectonic structures and interpretations.

Formation	Feature	Interpretation
Whitehill	Synformal and antiformal deformation of sediment	Tectonic folding

5.2.3 Tectonic Features

Structures observed in the field labelled as possible 'water escape structures' may in fact be tectonic in origin (*Table 4*). Water escape structures or dewatering structures, as they are often called, are caused by the expulsion of pore water from a bed. Dish structures are concave disruptions to the layering in sediments a few centimetres to tens of centimetres across formed by the upward movements of fluid through pillar structures or elutriation pipes (vertical water-escape channels). Dish and pillar structures often form together (Nichols, 2009).

The features observed in the Whitehill Formation are a series of synformal and antiformal structures that range in height, width and orientation. The structures incorporate bent shale layers, none of the shale layers having been broken, as would be expected to occur with the upward movement of escaping fluid and the formation of pillar structures. The structures are laterally continuous but are vertically limited in the outcrop. Water escape structures would be expected to

continue to occur up-stratigraphy where-ever fluid saturated sediment is to be found, but this was not observed.

A plausible explanation for the formation of these structures is the nearby Cape Fold Belt. Limited tectonic strain may have caused the laminated shale layers to be compressed horizontally leading to the formation of the synformal and antiformal structures. The up-stratigraphy laminae are horizontal and not deformed due to the lack of strain on the sediments. Unfortunately the Prince Albert Formation beneath the Whitehill Formation is not exposed, limiting observations to support this theory.

5.3 Collingham Formation

5.3.1 Syndepositional processes

The Collingham Formation shale is characterised by finely laminated, laterally extensive tabular beds, denoted by lithofacies Flo, and was most likely deposited by the settling of suspended very fine grained sediment in a low energy environment.

The laterally extensive, incompetent, thin, yellow layers, lithofacies Th, observed between shale layers, are believed to be weathered volcanic ash of rhyodacitic origin as mentioned by Johnson *et al*, (2006). This interpretation is based on the fact that the observed sediment is completely different in colour, texture, and structure from the surrounding sediment and no other sediment source can readily account for the rhythmically deposited, laterally extensive, layers of uniform thickness observed in the outcrop. A thin layer of volcanic ash is present in a hand specimen of chert. The volcanic ash must have been deposited during a hiatus in the formation of the chert or alternatively the ash must have been deposited in sufficient volume to temporarily overwhelm and disrupt chert formation as was most likely the case with the shale formation. The rate of sediment accumulation during the formation of shale is in orders of magnitude slower than the deposition of volcanic ash, therefore layers of nearly pure ash can be deposited during normal shale formation.

The chert layer observed, lithofacies Cm, can form directly from siliceous ooze deposited on the sea floor and these primary cherts occur in layers associated with other deep-water sediments (Nicols, 2009).

5.4 Ripon Formation

5.4.1 Syndepositional Processes

The sequences of upwards fining sandstones and shales exposed in the Ripon Formation along with the erosive contacts at the base of sequences and associated sole and tool marks are indicative of sediment gravity flows in a deep water setting.

The observed sequential pattern of deposition comprises a thick basal layer of medium grained sandstone, massive to laminated, with an erosive lower contact. This basal layer may also contain rounded mud clasts. This lithofacies, Sm, represents high energy sediment transport with erosion of the underlying lithology (usually mud) followed by rapid deposition. This unit is comparable to the Ta division of the Bouma sequence.

The sandstone then grades into a thinner unit of planar laminated fine sandstone, lithofacies Sl. This lithofacies was deposited by the next phase of deposition of the sequence, upper flow regime plane beds. This unit is comparable to the Tb division of the Bouma sequence.

Planar laminated very-fine sandstone to siltstone, lithofacies Fl, follows. This lithofacies was most likely deposited as a result of settling of the fine fraction of the sediment gravity flow that was left in suspension after the termination of the event. This lithofacies is comparable to the Td division of the Bouma sequence. The entire sequence is then capped by a mudstone layer, lithofacies Ml, which represents normal background sedimentation that continues until the initiation of the next high energy event. This lithofacies represents the Te division of the Bouma sequence.

The capping mudstone layer, lithofacies Ml, is occasionally absent having most likely been reworked by the subsequent event with remnants of the layer being preserved as large mud-clasts or lenses in the overlying sandstone. In one instance a lens comprising a sequence of shale, fine sandstone and then shale was observed in a large sandstone layer in the upper end of the studied Ripon Formation stratigraphy. The lens (representing only two lithofacies) had been completely removed by the overlying sandstone body. The lithofacies Sr is generally absent in the turbidites of the Ripon Formation, with only one example of convoluted bedding being recorded. This may be due to rapid deposition preventing the formation of cross or convoluted bedding (Nicols, 2009).

The banding observed in some sandstone layers, lithofacies Sb, could have been formed by secondary events after an initial turbidite had settled. Smaller secondary flows could result in alternating bands of basal coarser sediment followed by an overlying siltier band. More oxidising coarser bands reacting with more reducing organic-matter rich, siltier, bands would explain the red iron oxide staining observed at the interface between the bands.

The small scale erosional features observed on the bed surface of shale layers and beneath medium to coarse grained sandstone beds, lithofacies Ssm, were interpreted in the field as sole marks. Nicols (2009) states that sole marks are particularly common in successions of turbidites where the sole mark is preserved as a cast at the base of the overlying turbidite. Sole marks may be divided into those that form as a result of turbulence in the water causing erosion (scour marks) and impressions formed by objects carried in the water flow (tool marks). Both scour marks and tool marks were observed in the field.

Documented scour marks include flute casts, ridges and furrows, and gutter casts. Nicols (2009) states that turbulent eddies in a flow erode into the underlying bed and create a distinctive erosional scour called a flute cast. Flute casts are asymmetric in cross-section with one steep edge opposite a tapered edge. In plan view they are narrower at one end, widening out onto the tapered edge. The steep, narrow end of the flute marks the point where the eddy initially eroded into the bed and the tapered, wider edge marks the passage of the eddy as it was swept away by the current.

Ridges and furrows are linear features, on the scale of millimetres, on the bed surface caused by turbulence. Gutter casts are troughs on the scale of centimetres in width and depth and can extend for several metres along the bed surface (Nicols, 2009).

Documented tool marks include chevrons, grooves, and bounce marks. An object being carried in a flow over a bed can create marks on the bed surface. Grooves are sharply defined elongate marks created by an object (tool) being dragged along the bed. Chevrons are formed when the sediment is still soft and the object drags or rucks up the sediment. Bounce marks are caused by an object saltating in the flow and leaving impressions where it lands (Nicols, 2009).

The objects (tools) responsible for the creation of the observed marks are most likely plant material such as stems and branches and also semi-lithified mud clasts because no pebbles or shells were observed in the outcrop but fossilised plant material and mud clasts were observed in relative abundance. Mud clasts were observed in layers at the base of large turbidites and would have saltated during transport leaving bounce marks in soft sediment upon which the turbidite was scouring. Branches or stems travelling in a similar manner would have made contact with the underlying soft sediment leaving drag marks and rucking up the soft mud before bouncing up and disturbing the sediment again further down current.

5.4.2 Post-depositional Processes

Load cast structures observed were interpreted as being ball-and-pillow structures in the field (*Table 2*). Nicols (2009) states that an unstable situation is created if a body of material of relatively low density is overlain by a mass of higher density. In relatively wet conditions the lower density mass will be under pressure and will try to move upwards by exploiting weakness in the overlying unit, forcing it to deform. Load casts form where higher density sand has partially sunk into the underlying mud to form a downwards-facing bulbous structure. As sand is forced downwards and mud upwards, load balls of sand may become completely isolated within the muddy bed. These load-cast features are sometimes referred to as ball-and-pillow structures.

These bulbous load casts were observed in the Ripon formation where higher density medium grained sand overlies lower density mud. The sand has sunk into the mud but has not become completely isolated as sometimes occurs. Only two instances of these structures being formed were observed in the studied section of the Ripon Formation and in both instances a sandy turbidite base was overlying a muddy layer.

5.4.3 Diagenetic and Weathering Features

Spheres of clay-like material observed in the field, often containing a shale centre, are interpreted as being calcareous concretions. Johnson (1976) states that roughly spherical concretions 10-15 cm in diameter are fairly common in the sandstones of the Ripon Formation. He also noted the presence of a shale centre in some of the concretions.

Nicols (2009) states that most sedimentary deposits are heterogeneous with variations in grain sizes and compositions occurring at all scales. The passage of pore water through sediment will be affected by variations in the porosity and permeability due to this inherent heterogeneity. The same heterogeneity may lead to the processes that cause cementation to become unevenly dispersed, usually concentrated around a specific feature such as the body of an organism or plant debris in the sediment, although in some cases there is no obvious reason for the localised cementation.

Irregular cemented patches are usually referred to as nodules where as more symmetrical features are referred to as concretions. Nodules and concretions can form in any sediment that is porous and permeable and are commonly seen in sand beds, mudrock and limestone with a variety of different cementing mediums including calcite, siderite, pyrite and silica. Concretions are frequently concentrated in layers which deviated in their original composition and/or texture from the overlying and underlying sediments being higher in carbonate for example (Einsele, 1992; Nicols, 2009).

The observed concretions reacted strongly when applied with hydrochloric acid suggesting the presence of calcareous cement. XRD analysis indicates that quartz, oneillite and calcite are the primary constituents.

Certain sandstone layers must have contained percolating fluids enriched in calcium carbonate relative to silica. The calcium carbonate preferentially precipitated around a nucleus such as a shale fragment (shale fragment nuclei was observed in concretions studied by Horne and Taylor, 1969) or around a fragment of organic matter. The residual fluid, now relatively enriched in silica, cemented the rest of the sandstone body. At surface conditions the silica cement is more robust than calcareous cement which is prone to dissolution by acid fluid. The concretions are therefore more susceptible to weathering as observed in the outcrop.

Chapter 6 - Discussion

6.1 Sedimentology

6.1.1 Prince Albert Formation

XRD data (*Figure 4.5*) suggests that quartz, montmorillonite, and iron and manganese oxides are the dominant constituents. Quartz must have been derived from a clastic source with grains reaching a deep basinal setting probably via wind. The iron and manganese oxides are most likely secondary, formed by weathering. XRD analysis performed on fresh core material is known to contain quartz, illite, muscovite, chlorite and pyrite (Geel, 2013).

6.1.2 Whitehill Formation

Black Shale

The features observed in outcrop exposures of the Whitehill Formation- laminated, dark-black coloured organic-rich rock with a grain size between mud and silt, finely planar-laminated nature of the rock and the lateral extent and tabular nature of individual layers (*Plate 1, Figure 1*) are indicative of a depositional environment that is very low energy. The shales are interpreted as having been formed in an anoxic setting based on the high degree of organic matter preservation and reaction of the fresh rock to oxic atmospheric conditions with the formation of gypsum and high degree of weathering due to organic matter breakdown (*Plate 1, Figures 2 & 3*). The dark colour is due to the shale being rich in organic matter and also due to disseminated iron sulphides characteristic of anoxic sediments (Reading 1996; Nicols, 2009). Changes in thickness and competency of shale laminae can be attributed to rate and type of sedimentation. Increased rate of sedimentation or increased rate of preservation could lead to thicker laminae being developed. The dark coloured weathering resistant layers observed in the outcrop are interpreted as being black chert possibly formed by a siliceous ooze (*Plate 1, Figure 4*). XRD analysis only detected quartz in the Whitehill Formation (*Figure 4.6*). Interpretation of data from the Whitehill Formation should be done tentatively due to the extensively weathered nature of the outcrop. XRD analysis performed on fresh core material is known to contain quartz, calcite, albite, illite, muscovite, chlorite, pyrite and dolomite (Geel, 2013).

6.1.3 Collingham Formation

Shales of the Collingham Formation are composed of tabular, laterally extensive beds that are internally laminated with fine silt and mud representing the dominant lithology (*Plate 2, Figures 1 & 4*). Quartz, muscovite, oneillite (illite), montmorillonite, and calcite are the dominant mineral constituents contained in the Collingham Formation. The data attained from XRD analysis (*Figure 4.7*) of outcrop material compares well with data collected from core material with quartz, calcite, albite, muscovite, chlorite, biotite, illite and pyrite being recorded by Geel (2013). Weathering in outcrop conditions can account for the loss of phyllosilicates, albite and pyrite.

Tuff Layers

The large amount of illite observed, up to 13 %, (Geel, 2013), in the the Collingham Formation is mostly due to input of volcanic material. Tuff layers observed in the outcrop (*Plate 2, Figure 5*) represent periods of time when sedimentation of the Collingham Formation was completely overwhelmed by the settling of volcanic ash. Johnson *et al*, (2006) proposed a rhyodacitic source for the ash and the source of these tuffs has been suggested to be Patagonia and West Antarctica, forming part of an extensive volcanic arc which lay some 1500 to 2000 km to the south and west in their pre-break-up Gondwana positions (Stollhofen *et al.*, 2000). Volcanic ash commonly breaks down to K-Bentonite which is a form of illite. It is possible that during deposition of the Collingham Formation shales volcanic ash was present in quantities not sufficient to halt shale deposition, but sufficient enough to account for a large percentage of the rock forming material. This material was then converted to illite with time.

Fossil Material

Fragmented plant material (*Plate 7, Figures 1, 2 & 3*) is deemed to be terrestrial in origin by (Gess, pers. comm., 2014). Plant material was most likely carried out into a body of water where it sank and was preserved. Only the stems and shoots of the plants, some of which are quite delicate, are preserved indicating that the material must have been in a similar state before preservation. The plants may have travelled a long distance in conditions conducive to organic matter breakdown, thus loosing leaves and very fine stems and shoots before sinking to the bottom and into conditions of organic matter preservation.

Regional Chert Marker Layer

The 15 cm thick layer observed near the base of the Collingham Formation that is unlike the surrounding shales in thickness, hardness and competency is believed to be a the Matjiesfontein chert bed. Johnson (1976), states that a laterally extensive +- 30 cm thick chert layer located 10 m from the base of the Collingham Formation was used as a regional marker layer (uniformly thick over 5000 km²). It was used to delineate the boundary between the Whitehill and Collingham formations by Rossouw (1953). Similarities in observations (location and thickness) point to the layer observed by the current author being the same chert layer referred to by Johnson (1976).

6.1.4 Ripon Formation

Bouma Sequence

The Ripon Formation is characterised by fining upwards cycles of sandstone and shale (*Figure 6.1*). Cycles have erosive bases with occasional rip-up clast conglomerate and distinctive sole marks.

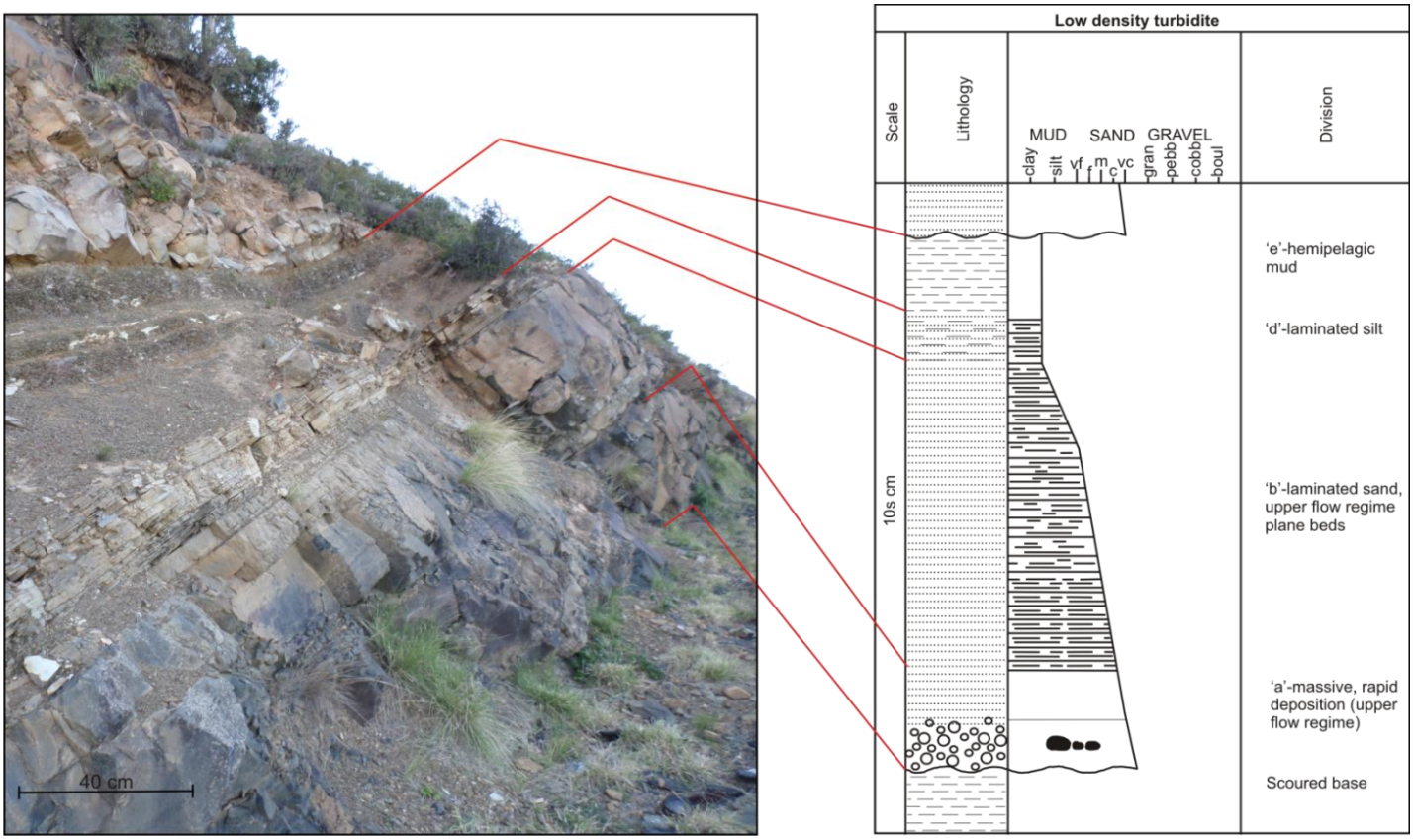

Figure 6.1: Turbidites of the Ripon Formation with a sequence of sandstones and shales corresponding to the idealised log of the Bouma sequence. Only division Tc of the Bouma sequence is missing. Log modified from Nicols (2009).

Internal structures closely follow the Bouma Sequence with the exception cross or convoluted bedding of division 'Tc'. The features observed in the Ripon Formation of the Ecca Pass study location are diagnostic of having been deposited by turbidity currents related to submarine fans. Hand specimens collected from the Ripon Formation appear to be products of the Bouma Sequence of turbidite deposition. One specimen, after being cut and polished, revealed very fine cross-bedded laminae of sand with a transition to planar laminated silt (*Plate 4, Figure 1*). This sample is an example of the transition from division 'Tc' to division 'Td' of the Bouma sequence with decreasing energy. As previously mentioned, examples of cross-laminated sand representing division 'Tc' of the Bouma sequence are rarely observed in the Ripon Formation indicating possible rapid deposition of sand inhibiting ripple formation.

Another specimen found contained well rounded shale fragments in medium sand (*Plate 4, Figure 2*). This sample was formed from the scouring of a semi-consolidated shale layer by a rapidly moving turbidity current as exemplified by division 'Ta' in the Bouma sequence. The fact that the shale fragments are rounded is an indication that the turbidity current transported the shale fragments over a distance long enough for the fragments to become rounded. Division 'Ta' of the Bouma sequence is usually structureless due to rapid deposition. Rapid deposition does not lend itself to the rounding of fragments during transport unless the fragments are easily and rapidly rounded due to the composition of the fragment, in this case mud, possibly semi-consolidated.

Palaeocurrent Indicators

Field measurements indicate a northward palaeocurrent direction (*Figure 4.2*). A northward transport of sediment into the basin fits with the model, as illustrated by (S.D. Johnson *et al*., 2001; M.R. Johnson *et al.,* 2006) that implicates northward subduction at the southern margin of Gondwana and subsequent volcanism and uplift with sediment being supplied northwards into the basin.

Fossil Material

As previously stated for the Collingham Formation, preserved plant material, (*Plate 7, Figures 4, 5 & 6*; *Plate 8, Figures 1-6*), observed in the Ripon Formation is interpreted as being terrestrial in origin. The tentative wing observed (*Plate 9*) is interpreted as being a leaf by Schneider, pers. comm. (2014).

The stems and shoots found in horizons in the Ripon Formation must have been transported out into a body of water, under-going partial breakdown in the process, and then sank to the sediment surface. The fact that plant matter was found within distinct horizons suggests that energy generated by turbidity currents served to mobilise and concentrate plant debris residing on the sediment surface. The observed chevron marks (*Plate 5, Figure 5*) have a drag mark diameter that is in range with the diameter of observed fossilised stems lending weight to this theory. The stems may have been transported in saltation, occasionally making contact with the sediment surface before being rapidly deposited into the underlying muddy strata or left in semi-suspension and deposited with the finer fraction of the turbidity current.

Grey Sandstone (Non-spotted)

Feldspar, biotite, muscovite and internally fractured quartz (*Plate 10, Figure 4*) as well as lithic fragments containing zoned and altered feldspar grains (albite) as well as chert point towards a gneissic sediment source. Nicols (2009) states that quartz, mica, feldspar, calcite and lithic fragments containing any of the aforementioned minerals are the principal components of volcaniclastic sedimentary rocks. Northward subduction and subsequent volcanism along the southern margin of Gondwana at ca. 330 Ma as proposed by Johnson *et al.* (2006), is most likely the source of the Collingham Formation rhyodacitic tuff layers as well as the possible source of the felsic volcaniclastic sediment observed in the Ripon Formation. Metamorphism, due to subduction related volcanism, of a granitic parent rock would account for the observed mineralogy as well as the internally fractured quartz grains. The Cape Fold Belt had not developed during Ecca Group deposition (Johnson *et al.,* 2006; Flint *et al*., 2011), and thus may be ruled out as a possible sediment source. Flint *et al*. (2011) states that granitic rocks exposed in Patagonia could be a source for the uniformly fine grained sandstones of the Laingsburg Formation which is stratigraphically similar to the Ripon Formation.

The very well rounded to sub-rounded shape of the grains (*Plate 11, Figure 2*) is testament to the long duration/distance and moderate to high level of energy experienced by the grain during transport from its source (hinterland) by a river to an accumulation point (shallow marine upper shelf) then to the site of deposition (deep marine lower shelf/basin floor). Large clastic submarine fan complexes are all composed of terrigenous material supplied by large river systems (Nicols,

2009). The distance travelled by the grain combined with the energy of transport will dictate the rounding, or lack thereof, of a grain.

The rapid transport and relatively short transport distance of turbidity currents combined with rapid deposition accounts for the poorly sorted nature of the sediment. Sorting is a function of the origin and transport history of the detritus (Nicols, 2009). Gradually waning energy levels would allow sediment to be sorted according to size and density but the coarser fraction of the sediment being transported in turbidity currents (medium grained sand) is deposited rapidly, and thus poor levels of sorting are experienced.

Glauconite observed in the Ripon Formation is an indicator of a marine depositional setting (*Plate 10, Figure 6*). Nicols (2009) states that glauconite is a reliable indicator of deposition in a shallow marine environment. It can be reworked into deeper water and occasionally into shallower environments by currents. Nicols continues to state that glauconite is authigenic and forms on the sea floor on substrates at the interface between slightly oxidising seawater and slightly reducing interstitial waters usually between water depths of 50 to 500 m on the outer part of continental shelves and upper parts of continental slopes. It is plausible that glauconite formed in the sediment during accumulation on the shelf prior to transport by turbidity currents. Transport by turbidity currents to the lower shelf would account for the sub-rounded shape of the grains that usually form in between clastic grains.

The high percentage of clay and organic matter observed (*Plate 10, Figures 5 & 6*) in some of the samples was most likely deposited as a result of pelagic 'rain' on the shallow to deep marine shelf as well as deep marine basins. High energy turbidity currents would have incorporated the organic and clay rich sediment by scouring the unlithified sea floor sediment during periods of increased turbidity current activity. During periods of low activity the organic and clay rich pelagic 'rain' would accumulate and result in the thick shale layers observed in the outcrop between turbidites.

Classification

Classification of non-spotted sandstone based on the Selley (1984) classification scheme (quartz, clay, lithic fragments) results in the majority of samples falling within the quartz greywacke section (*Figure 4.8*). Classification based on the Pettijohn (1975) classification scheme (quartz, feldspar,

lithic fragments) results in the majority of samples falling within the lithic arkose section (*Figure 4.9*).

Classification based on a ternary diagram is slightly biased in that it can only take into account three main components, whereas rocks such as the Ripon Formation sandstones contain more than three principal components with organic matter accounting for a large percentage of the rock. It makes sense then to add the prefix 'organic' to both the Selley and Pettijohn classifications e.g. 'organic quartz greywacke' and 'organic lithic arkose'.

Spotted Sandstone

A lithology, composed of medium grained dark grey sandstone, containing white match head sized spots, often concentrated in bands up to 30cm thick, is observed in the upper parts of the Ripon Formation stratigraphy (*Plate 11, Figures 3-6*). Johnson (1966; 1976) also observed similar white 'mottling' and conceded that the cause of the mottling is not obvious. Johnson (1966; 1976) states that mottling characterises roughly half of the sandstone in the Ecca Group with noticeable local variation. The dark material in between the spots (referring to the dark grey sandstone) probably contains a certain amount of carbonaceous material. Reynolds (1971) proposed that the whitish spots were formed as a result of migration of the dark material away from the spots, to become concentrated in the intervening areas.

An alternative explanation may be that the white material is volcanic in origin. Proposed ash layers of rhyodacitic origin are observed in large quantities in the underlying Collingham Formation as well as the overlying Fort Brown Formation. Johnson *et al*. (2006) reports the presence of a crystal tuff from the Fort Brown Formation containing 90% plagioclase and 10% quartz indicating contemporaneous dacitic-andesitic volcanism. It is not unreasonable to suggest that the volcanic activity present in the Collingham and Fort Brown formations may be active during the intermediate Ripon Formation. The white spotted strata may be coarse grained ash/tuff layers resulting from an increase in sediment supply of volcanic origin, with the white spots being leucocratic minerals such as feldspars. The purely white layers may represent sediment supply periodically being composed of only volcanic sediment whilst 'mottled' sandstone may represent only a portion of the sediment supply being composed of volcanic sediment that mixes with the normal sediment that constitutes the Ripon Formation sandstones. Sandstones that contain no

white spots may have been deposited during a hiatus in volcanic activity or during a period when conditions were not optimal for the accumulation of volcanic sediment and subsequent transport to the environment of Ripon Formation deposition.

Spotted sandstone differs from non-spotted sandstone in that the quartz and feldspar grains are larger and angular to sub-angular in shape. Quartz grains in the spotted sandstone lack the internal fracturing present in the non-spotted sandstone. The absence of clay and organic material in the spotted sandstone is another major difference. Mineralogically the differences are less obvious with both sandstone types containing quartz, feldspar, biotite and muscovite with glauconite being absent in spotted sandstone.

The lack of rounding of the grains is indicative of a short transport distance from the sediment source to the site of accumulation on the shallow marine shelf. The sediment source must have been more proximal to the shallow marine shelf compared to that of the non-spotted sandstone.

The lack of glauconite suggests that either the conditions for glauconite formation were not met, i.e. correct water depth and chemical conditions, or that the sediment did not accumulate on the shallow marine shelf for a period of time long enough for glauconite to form, prior to transport via turbidity currents.

The absence of internally fractured quartz grains in the spotted sandstone hints at a different sediment source compared to that of the non-spotted sandstone. A granitic sediment source would account for the observed mineralogy in the spotted sandstones namely quartz, biotite, muscovite and feldspar.

Classification

Spotted sandstone was not plotted on a ternary diagram due to the small sample size (n=1), however a tentative classification based on Pettijohn (1975) would classify the spotted sandstone as arkose to subarkose.

6.2 Palaeoenvironmental Interpretations

6.2.1 Prince Albert and Whitehill Formations

Geel (2013) proposed that the Prince Albert, Whitehill and Collingham formations formed as a result of accumulation of starved sediments in a stratified, anoxic water column.

The depositional setting of the Prince Albert Formation was unlikely to be totally anoxic based on the lack of abundant black shales, gypsum, sulphides etc. It is possible that it could have been sub-oxic due to the fact that the sediment appears to contain organic matter in some abundance. Sulphides may have formed during phases of increased anoxia based on the iron and manganese oxides detected in the rock. Fluctuations in organic matter input may alternatively explain the lack of black shales observed in the Prince Albert Formation if it was deposited in an anoxic basin as proposed by Geel, (2013).

Black shales can form in numerous depositional settings such as deep-marine anoxic basins, reduced or anoxic swamps, tidal flat zones, estuaries, lakes, lagoons with high nutrient supply, shelves and upper continental slopes under zones of coastal upwelling (Einsele, 1992; Reading, 1996; Nicols, 2009).

The Whitehill Formation is laterally extensive in the Karoo Basin which covers approximately 700 000 km² (Johnson *et al.*, 2006). The large lateral extent eliminates all speculative depositional settings with the exception of a deep marine anoxic basin (*Figure 6.2*) and possibly a very large lacustrine setting. The possibility of a large lacustrine setting can be eliminated due to the marine signature of the Ecca Group based on the presence of Foramnifera (Geel, 2013), fluorescent amorphous organic matter (AOM) (Götz, pers. comm. 2014) and glauconite.

Johnson *et al.* (2006) states that the black, laminated carbonaceous shales were deposited by suspension settling in a basin under anoxic bottom conditions. The high concentration of organic matter in the water body and restricted oceanic circulation in the basin probably created anoxia in the water column and thus preservation of organic matter was high with an absence of benthic fauna. Observations and interpretations from the Whitehill Formation exposures in the Ecca Pass study locality concur with the generally accepted model of an anoxic basin (Johnson *et al.*, 2006; Geel, 2013). No other plausible depositional settings can account for the features observed.

6.2.2 Collingham Formation

Three possibilities exist for the formation of the Collingham Formation shales. The first is that the shales were deposited by pelagic settling in a deep water setting. According to Nicols (2009) pelagic sediment comprises terrigenous airborne particulates, clay and silt sized particles blown from land combined with the remains of calcareous organisms such as Formanifera, Coccoliths and siliceous organisms such as Radiolaria. Pelagic sediments may be mobilised by bottom currents and re-deposited as contourites. Contourites are sheets of fine muddy and silty sediments that cover vast areas tens to hundreds of metres thick. Reading (1996) states that deep marine sediments are composed of a variety of clay minerals chiefly illite and montmorillonite with lessor kaolinite and chlorite plus windblown quartz. Ferromanganese nodules and siliceous oozes also occur in deep marine pelagic deposits.

The second is that shale formation occurred as a result of hemipelagic settling of the fine grained silt fraction left in suspension after the passage of a mixed sand-mud turbidity current. Nicols (2009) states that mixing of a density current (turbidity current) with the ocean water results in the temporary suspension of the fine material long after the turbidite has been deposited. Most of the sediment is brought into the ocean by currents from the adjacent landmass and is deposited at much higher rates than pelagic deposits. The provenance of the hemipelagic deposit will be the same as that of the turbidite in such cases. Hemipelagic sediments contain varying proportions of fine silt along with dominantly clay-sized material. Bottom currents can also remobilise hemipelagic sediment from the shelf areas and re-deposit them on the abyssal plain. The distinction between muddy contourites and associated hemipelagites is very difficult (Reading, 1996).

The third possibility is that the shales were deposited as a result of mud-rich turbidity currents. According to Nicols (2009), mud-rich systems are the largest fan systems in modern oceans and are over 1000 km in radius. Nicols (2009), states that channels are the dominant architectural element and channels are seen to follow a largely sinuous course. Deposits of this type grade from predominantly sandy channels near the inner fan through to intercalated thin sandstones and mudrocks at the outer fan. No channel-fill deposits were observed and no intercalated sandstones were observed thus eliminating the possibility of a mud-rich submarine fan being the setting for Collingham Formation shale deposition.

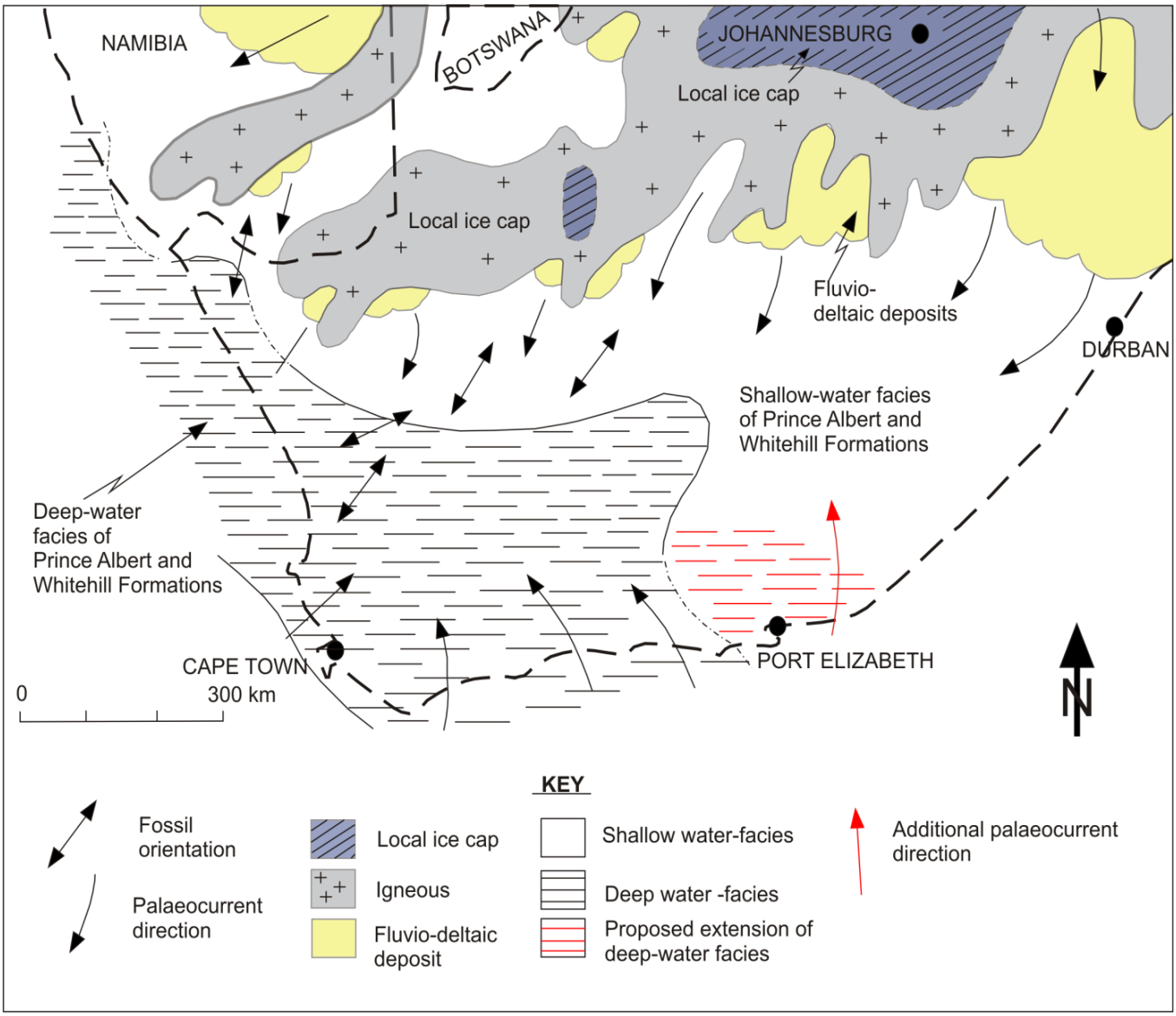

Figure 6.2: Palaeocurrent directions and facies distribution of the Prince Albert and Whitehill formations. **NOTE**: Proposed extension to deep-water facies and additional palaeocurrent data. Diagram modified from Visser (1994).

The shales of the Collingham Formation of the Ecca Pass study locality contain quartz and muscovite grains visible in thin sections (airborne particulates?) as well as calcite, illite and montmorillonite which is in agreement with a pelagic settling model. The Matjiesfontein chert bed may be the result of siliceous ooze formed from Radiolarians which also supports the theory of pelagic settling as the dominant contributor to the Collingham Formation shale deposition. Hemipelagic settling can largely be ruled out due to the fact that mudrocks interbedded with sandy turbidites are commonly of hemipelagic origin (Nicols, 2009), and no sandy turbidites are observed in the Collingham Formation. The most likely scenario is that pelagic settling combined with

occasional input from hemipelagic settling of the suspended fine silt fraction, possibly mobilised by contourite drifts, is responsible for the shale formation. These interpretations based on observations from the Ecca Pass study agree with Johnson *et al.* (2006). Johnson states that the lack of traction current indicators, the trace fossil assemblage and the great lateral extent of individual beds points towards deposition from suspension in relatively deep water with low density turbidites most likely being responsible for deposition of the thin siltstone layers. Geochemistry and clay mineral assemblage identification can be used to distinguish hemipelagic and pelagic sedimentation based on the provenance of the material.

6.2.3 Ripon Formation

Facies associations are defined according to architectural elements of submarine fans based on components of the depositional system i.e. sediment input type- mud-rich, mixed sand and mud, or sand-rich and according to different processes and sub-environments based physiographic location on the submarine fan i.e. inner fan, middle fan and outer fan. (Nicols, 2009; Bouma, 2000).

Johnson *et al*. (2006) proposed a model for basin floor fan systems (*Figure 6.3*) that subdivides a fan into four physiographic zones, from proximal to distal. Each zone is characterised by a facies assemblage dictated by processes operating within that 'zone' during deposition.

The Ripon Formation of the Ecca Pass study site is characterised by laterally extensive upwards fining sequences of sandstone and shale with erosive bases. Internally the sequences contain structure in accordance with the Bouma Sequence.

The Ripon Formation likely represents an inter-channel deposited based on the laterally extensive sandstone bodies and the lack of channel-fill deposits observed. The erosive contacts combined with the sediment grain size (medium to fine sand) suggest a position in the middle-fan region between proximal and distal- close enough to the sediment source to account for the medium grained sand and high energy deposition, but far enough away to account for the massive-bedded style. A position more proximal to the source would eliminate large inter-channel areas, and a position more distal would eliminate the erosive power of the turbidity current. Thus a position indicated by the red circle (*Figure 6.3*) in Zone 3 is the most plausible physiographic location for deposition of the Ripon Formation of the Ecca Pass study site.

The increasing percentage of sand relative to mud with increase in stratigraphic height through the Ripon Formation (*Plate 3*) may either be as a result of; changing physiographic position on the fan from a distal position to a more proximal location, or due to a change in sediment input from a mixed sand-mud source to a more sand rich source.

A change in physiographic position on the fan is the least plausible option. An up-fan shift in position of deposition would be expected to be accompanied by a change in facies associations and sedimentary structures from tabular laterally extensive sheets to more channel-fill and laterally inextensive interchannel sheets as proposed by Johnson *et al*. (2001). No such changes were observed, only the percentage of sand-rich layers relative to mud-rich layers was documented.
Thus, a shift from a predominantly mixed sand-mud system to a sand-rich system is the most likely explanation for the observed features.

6.2.4 Karoo Basin Fill History

The lithologies and structures exposed in the Prince Albert, Whitehill, Collingham and Ripon formations record the changing environments of deposition associated with the infilling and gradual shallowing of the Karoo Basin. The glacial-marine sediments of the Dwkya Group are overlain by the very deep-marine Prince Albert and Whitehill formations. The Prince Albert and Whitehill formations are stratigraphically overlain by the deep marine to distal fan deposits of the Collingham Formation followed by the mid-fan deposits of the Ripon Formation. Observations from the studied formations document the initial shallowing of the Karoo Basin by sediment infill related to climate change and agree with the generally accepted model of Karoo Supergroup.

The Ripon Formation is overlain by the Fort Brown Formation which represents distal delta-front deposits and continued shallowing (Johnson *et al.*, 2006). The Ecca Group is followed by the Beaufort Group which marks the transition from a marine to terrestrial environment with deposition occurring in deltas, meandering rivers and, floodplains (McCarthy and Rubidge, 2005).

The Stormberg Group follows the Beaufort Group and represents continued infill and subsequent aridification with deposits of the Molteno, Elliot and, Clarens formations characterising a shift from braided rivers with localised swamps to desert conditions (McCarthy and Rubidge, 2005).

ZONE 1	ZONE 2	ZONE 3	ZONE 4
This area is dominated by multi-storey and multi-lateral channel complexes. Channels are erosive and rarely depositional with extensive rip-up clasts, local slumped deposits and many erosive contacts. In early fan development sediments mainly bypass this area. Channel fill is aggradational to retrogradational in later stages of fan development.	This zone is a mixture of erosive channels and laterally-extensive interchannel sheets. Channels have massive to thick-bedded fills and overbanks are rippled, thin- to thick-bedded amalgamated sheets.	A complex zone with architecture controlled by geographic position and up-dip to down-dip relationships. Largest proportion of interchannel deposition in this zone is characterised by extensive tabular sheets of rippled bedded sandstone. Dominant sedimentation occurs in depositional channels and associated interchannel areas. In the down-dip areas of this zone extensive tabular sheets can develop with a massive-bedded style.	In this zone down-dip of extensive sheet deposits, deposition is characterised by isolated broad, thin channels and laterally inextensive- to moderately-extensive thin-bedded sheets. Fan deposition in the pinch out area is ultimately only represented by a thin silt unit
Sequence boundary is erosive to sharp with channels overlying the sequence boundary.	Sequence boundary is erosive to sharp. Channels and some sheet like deposits overlie the sequence boundary.	Variable sequence boundary expression in this zone: Erosive below channels; Sharp below sheets; Gradational below thin-bedded turbidites and silts.	Sequence boundary expression s dominated by gradational and sharp styles in this zone. Rare sharp to erosive sequence boundary expression at the base of localised channels.

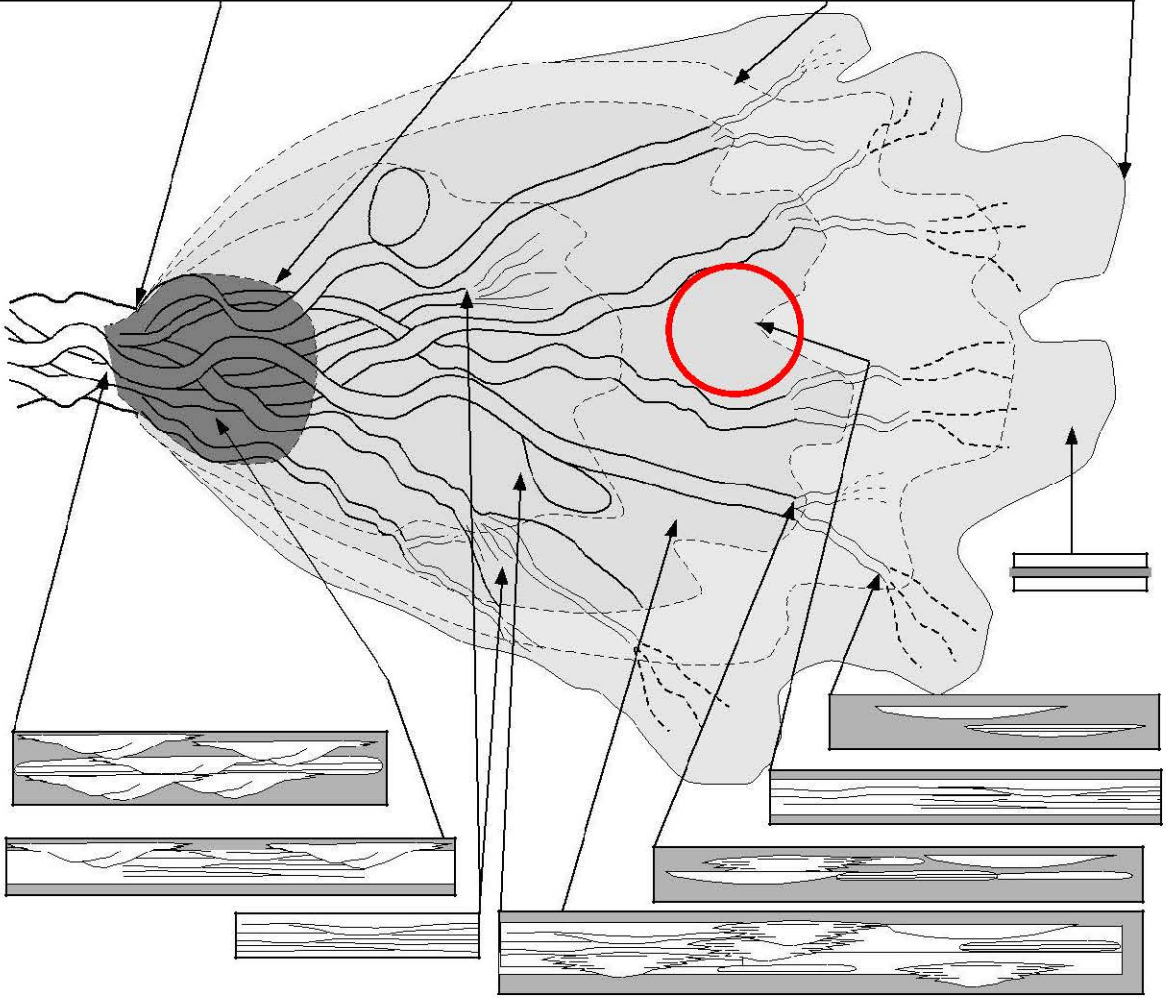

Figure 6.3: Model for basin-floor fan systems with schematic map view and expected cross-sectional profiles at specific points on the fan. NOTE: Red circle indicates proposed setting of Ripon Fm. deposition at study site. From Johnson *et al*. (2001).

6.3 Reservoir Characteristics

6.3.1 Unconventional Reservoirs

Unconventional reservoirs are defined as rocks, such as black shales, that generate hydrocarbons as a consequence of burying large volumes of plant and animal matter under reducing conditions in marine, deltaic or lacustrine environments. Over time and increases in temperature, the organic remains may alter to oil and gas based on the intensity and duration of post- depositional heating or burial metamorphism due to maximum depth of burial. The hydrocarbons are stored in the source rock (Geel, 2013).

The recorded TOC values for the Whitehill Formation of the Ecca Pass are low with a maximum value of 0.9 wt% compared to TOC values of between 0.77-8.15 wt% recorded in fresh core material from a nearby locality (Geel, 2013) and compared to up to 17% organic carbon (Johnson *et al.*, 2006). Average TOC is 4.5% and the Whitehill Formation contains a mixture of Type II and Type III kerogen with a Tmax of $\geq$563°C (Decker, 2013; Geel, 2013).

The low TOC from the outcrop is due to intense weathering (Cole, pers. comm, 2014). The exercise of performing TOC analysis on material from an outcrop is not entirely without merit. The values recorded in an outcrop represent the absolute minimum in total organic carbon due to weathering. These values are useful because fresh material from the same formation extracted from a core can be expected to contain TOC values several times higher than the values attained from the outcrop as demonstrated. Therefore, TOC analysis of outcrops should be used as a preliminary tool before any cores are drilled. Formations exposed in outcrops with promising TOC values can be targeted in drill cores.

TOC values of the Collingham Formation range between 0.2-0.6 wt% with an average of 0.4 wt%. These values are comparable with values recorded by Geel (2013) from core material with TOC values ranging from 0.15-1.07 wt% with an average of 0.62 wt%. The Collingham Formation is probably less susceptible to weathering due to an overall lower organic matter content compared to the Whitehill Formation. This is could be a result of the Collingham Formation being deposited in oxic to sub-oxic conditions with reducued organic matter input.

Table 5: The Whitehill Shale exposure of the Ecca Pass compared to the Whitehill cores of the Greystone Area, and the Posidonia, Marcellus Shale, and Barnett shales. Table modified from Geel (2013).

Property	Whitehill (Permian shale, Ecca Pass, RSA) Outcrop (This study)	Whitehill (Permian shale, Greystone Area, RSA) Core (Geel, 2013)	Posidonia (Lower Toarcian Shale, Luxembourg/ Netherlands) (Verreussel *et al.,* 2013; Song *et al.,* 2013)	Marcellus (Devonian Shale, Appalachian Basin USA) (Bruner and Smosna, 2011)	Barnett (Mississippian shale Fort Worth Basin, USA) (Bruner and Smosna, 2011; Hoelke, 2011)
TOC (%)	0.9	0.7-8.15	2.8-15	1-10	2-6
Tmax	-	≥563°C	426°C	≥475°C	≥465°C
Porosity (%)	-	0.83	2.3	3-6	3-6
Vitrinite Reflectance (R_o)	-	4	0.55	1.6 (max 3.5)	1.2 (max 1.9)
Thickness of Formation	31 m	28 m	30 m	15 m	107 m
Estimated size of shale gas play	155 000-183 000 km²	155 000-183 000 km²	110 000 km²	129 499 km²	23 310 km²
Estimated potential yield	906 billion - 13.7 tillion m³	906 million-13.7 trillion m³	116 million m³	1.4-25 trillion m³	70 million -1.1 trillion m³

Pay-zone Identification

A general assessment of the gas in place (GIP) can be given based on a number of general assumptions. The average TOC is 4.5%. The average thickness of the Whitehill Formation in the southern portion of the basin is 30 m with a basin wide thickness range of 10 – 80 m. The Whitehill Formation is laterally extensive over 200 000 km² but the estimated size of the shale gas play has been reduced to between 155 000 and 183 000 km² due to the increased abundance of silt and sand in the formation as well as thinning in the northern section of the basin combined with decreased burial depth and thermal maturity of the organic matter (Johnson *et al.*, 2006; Geel 2013; Verreussel *et al.,* 2013). The Whitehill Formation is rich in brittle quartz (up to 50%) allowing increased fracturing and has a vitrinite reflectance (R_o) between 1-4, well within the range of mature gas (Decker, 2013). The GIP was initially estimated at between 906 billion and 13.7 trillion cubic meters but was reduced to 11 trillion cubic meters due to additional factors impacting on the potential of the reservoir (EIA, 2013).

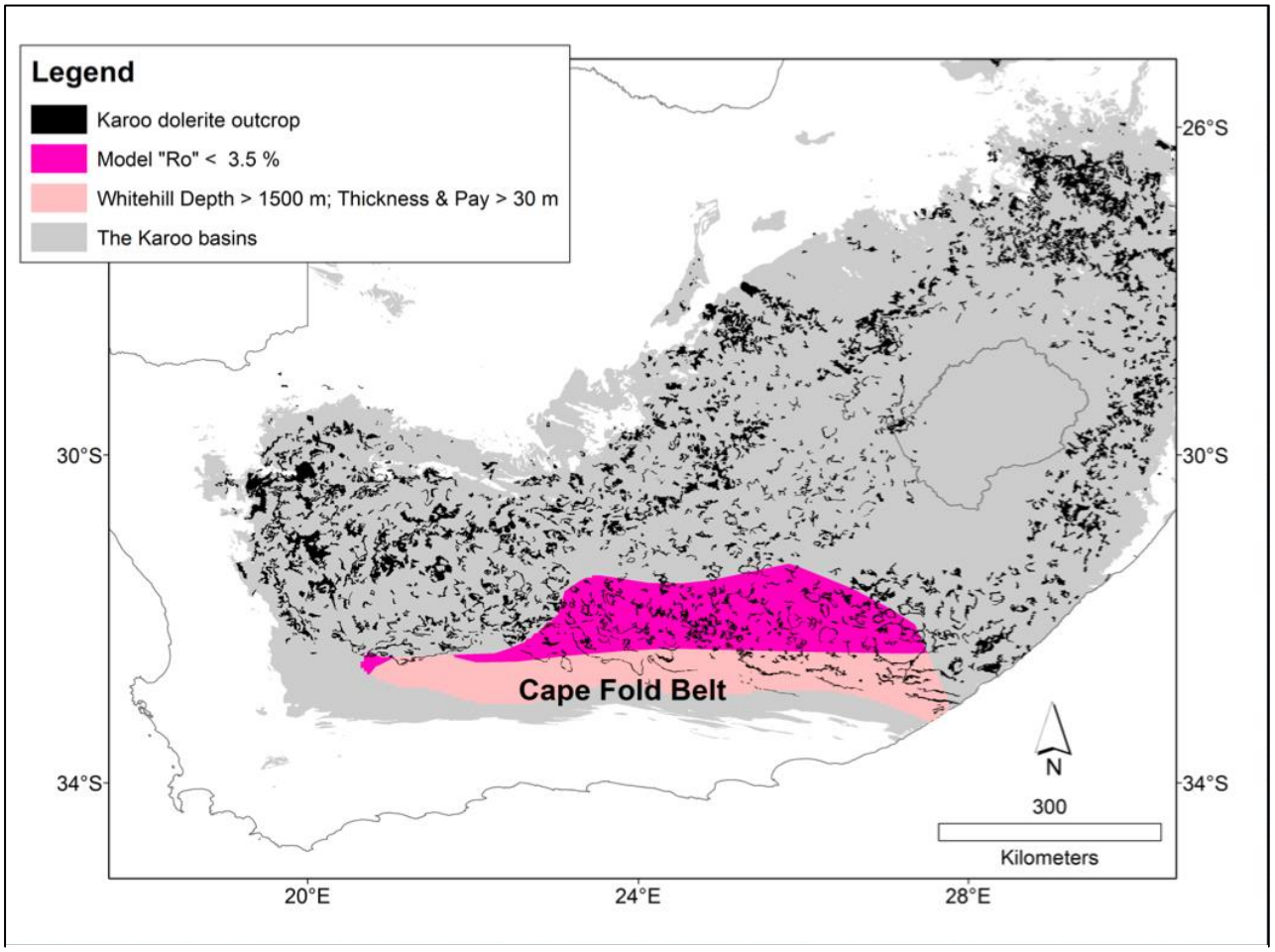

Figure 6.4: Map of South Africa with Karoo Basin, Karoo dolerites and zone of greatest shale gas potential based on depth, thickness, pay and, vitrinite reflectance. Diagram from Decker (2013).

Additional factors that have to be taken into account are the metamorphic effects of the Cape Fold Belt in the southern portion of the basin, as well as the effect of the dolerite dykes that intruded the Karoo stratigraphy. The southern parts of the basin, which would be the most prospective (*Figure 6.4*), are located proximal to the Cape Fold Belt (CFB). The CFB was deformed, along with the lower groups of the Karoo Supergroup, during orogeny between 230 and 280 Ma reaching a maximum temperature of 300°C (mid Greenschist Facies) (Johnson *et al.*, 2006; EIA, 2013; Büttner *pers. comm.* 2014).

Regional metamorphism may have destroyed organic matter or at least resulted in over maturity in the southern portion of the basin. Metamorphism and deformation may have resulted in substantial distortion of the deep structure and thermal history of the rocks, with possible significant implications for any volatile hydrocarbon deposits that may have been 'cooked off' and escaped through microstructural cleavage and larger faults. The rock strata in this area are also not

horizontal, which may have assisted further in escape of any volatiles. Also, this southern area coincides with the deepest part of the basin and some shales could be over-mature for gas generation due to excessively deep burial (EIA, 2013).

Dolerite dykes of the Karoo Igneous Province intruded the basin at approximately 183 Ma due to the breakup of Gondwana. The Karoo Igneous Province represents one of the largest flood basalt events in Earth's history and could have substantially raised the geothermal gradient within the Karoo sedimentary rocks at the time when they were most deeply buried, with further consequences for volatile hydrocarbons. The dolerites intruded often as ring complexes. The impermeable dolerite ring complexes serve to compartmentalise and metamorphose the immediate sedimentary rocks, a feature that is well known from shallow aquifer studies, with the impermeable dolerites often preventing vertical and horizontal migration of water over significant distances (EIA, 2013). Potential shale gas reservoirs may have been compartmentalised by the ring complexes therefore limiting the hydraulic stimulation potential of the target formation as well as destroying the organic matter contained in the rock. However, according to Marsh *Pers. Comm.* (2014) the ring complexes appear to intrude the stratigraphically higher Beaufort Group with normally dykes and sills intruding the Ecca Group.

The Collingham Formation should be considered for shale gas exploration if TOC values are consistently found to be above 3% over large areas of the basin (Decker, 2013). Organic matter in the Collingham Formation should have been subject to the same temperature and pressure conditions as that of the Whitehill Formation so hydrocarbon generation should largely depend on amount and type of kerogen contained in the formation. The organic matter in the Collingham Formation has however been diluted by input of large amounts of volcanic ash. Dolerite dykes and proximity to the Cape Fold Belt will also affect potential reservoir properties of the Collingham Formation.

Comparison

The Whitehill Formation has a similar TOC range compared to other shale gas yielding basins in Europe and the United States (*Table 5*). However, the vitrinite reflectance of the Whitehill Formation is significantly higher than other basins, suggesting that the organic matter may be over-mature due to the proximity of the CFB in combination with depth of burial. In comparison, the Posidonia Shale has lower vitrinite reflectance indicating that the hydrocarbons may still fall within

the oil window of maturity. The Whitehill Formation has a larger lateral extent than the Posidonia, Marcellus and, Barnett shales with a similar thickness. The lateral extent, thickness and, TOC content of the Whitehill Formation result in an estimated potential yield of between 32-458 tcf provided the organic matter of the formation has not been 'burnt off', these values are within the same range of the Posidonia and Marcellus shales. The Barnett Shale has an estimated potential yield of up to 40 tcf due to the thickness of the formation (107 m).

6.3.2 Conventional Reservoirs

Accessible and commercially viable conventional hydrocarbon reservoirs feature two essential elements: reservoir rock and a hydrocarbon trap. The reservoir rock, which is porous and permeable, contains the hydrocarbons generated by a source rock such as organic rich shale; determining the nature of this rock and its geometry is the goal of conventional hydrocarbon exploration. A hydrocarbon trap is a particular distribution of rocks in the subsurface that keeps the hydrocarbons inside the reservoir rock until they have been reached by the drilling and can therefore be extracted. The top of the trap consists of impermeable rock (sealing rock) which prevents the hydrocarbons from migrating towards the surface (Casnedi, 2005).

The Ripon Formation has an average porosity of 1% and an average permeability of 0.05 mD. The Ripon Formation could potentially be targeted as a hydrocarbon reservoir due to the formations proximity to the organic rich Whitehill Formation. The Ripon Formation contains laterally extensive thick sandstone sequences capped by thick impermeable shales (cap rock). These features characterise an ideal hydrocarbon reservoir provided that the poroperm values are conducive to hydrocarbon storage.

The Ripon Formation falls within the category of tight-rock with 90% of studied sandstone reservoirs having poroperm values greater than that of the Ripon Formation (*Figure 4.11*). The low poroperm values are most likely due to the poorly sorted nature of the rock and the high percentage of organic matter (*Plate 10, Figures 5 & 6*), combined with slight metamorphism due to proximity of the CFB. Potential pore spaces are filled by smaller particles and organic matter thus limiting the potential hydrocarbon storage volume of the sandstone. No change in reservoir properties with changing stratigraphic height was observed (*Figure 4.12*). Secondary jointing may have increased the reservoir potential of the lower Ripon Formation (*Figures 4.3 & 4.4*) by

increasing permeability but in all likelihood artificial stimulation may be needed if the sandstones were to become productive reservoirs.

The Ripon Formation is thickest in the southern portion of the Main Karoo Basin (up to 1000 m) but pinches out from south to north. The southern part of the Main Karoo Basin, as previously mentioned, is over-mature due to proximity of the CFB and great burial depth resulting is marginal gas potential and no oil potential. The oil generation zone is located in the northern portion of the Karoo Basin where the Ripon formation is very thin or non-existent. The potential source rock, the Whitehill Formation, is also thinner with a lower TOC in the northern part of the basin limiting the reservoir potential of the Ripon Formation.

Table 6: The reservoir potential of the Ripon Formation compared to the Marnoso Arenacea Formation and the Foinaven Field.

Property	Ripon (Permian sandstone, Ecca Pass, RSA) (This Study).	Marnoso Arenacea Formation, (northern Italy) (Amy *et al*., 2009)	Foinaven Field (Palaeocene sandstone, Off-shore, Scotland) (Huggins, 2007)
Lithology	Medium to fine grained sandstone	Mixed sandstone, mudstone	Medium to fine grained sandstone
Thickness of Reservoir	200 m of up to 20 m thick sequences	1 m thick sequences	80 m
Porosity (%)	1	0.15	23-30
Permeability (mD)	0.045	<100	500- 2000

Comparison

The Ripon Formation does not compare well with globally productive and studied sandstone hydrocarbon reservoirs (*Table 6*). The primary differences are the aberrantly low porosity and permeability values. The productive Foinaven Field has porosity values up to 30 times higher than that of the Ripon Formation allowing for the effective storage of hydrocarbons. The Ripon Formation has virtually no porosity, compared to that of the recently studied Marnoso Arenacea Formation and the productive Foinaven Field, effectively limiting the migration potential of potential hydrocarbons.

Chapter 7 - Conclusion

The Whitehill Formation was deposited in an anoxic deep marine basin based on the laterally extensive organic-rich planar laminated mud and silt and the abundance of gypsum. The Collingham Formation was deposited in a deep-water setting such as a distal slope or an abyssal plain by pelagic settling, hemi-pelagic settling or a combination of both.

The Ripon Formation was deposited as a result of predominantly mixed sand-mud turbidites deposited in a mid-fan inter-channel area based on the almost complete Bouma Sequence. The non-spotted sandstones can be attributed to a granitic source such as the granites exposed in Patagonia. The source of the spotted sandstone is unknown but observations suggest that it is or contains components of a crystalline tuff probably with a similar source to the tuff layers of the Collingham Formation and the crystal tuff of the overlying Fort Brown Formation.

The lithologies, sedimentary structures and facies relationships observed in the Whitehill, Collingham, and Ripon formations of the Ecca Pass are indicative of a gradually shallowing environment of deposition. The abundance of structures depicting higher energy processes increase up-stratigraphy, from planar laminated laterally extensive mud and silt to medium-grained turbidites. Numerous authors have documented that the entire sequence of groups and formations of the Karoo Supergroup, from the Dwyka Group to the Clarens Formation, represent deposition in a basin gradually being filled with sediment transported from sediment sources in the south and in the north (Visser, 1994; McCarthy and Rubidge, 2005; Johnson *et* al., 2006).

Total organic carbon (TOC) testing of exposed and weathered black shale outcrops is useful in that it gives a base line TOC value of a prospective formation without the need to drill. Fresh core samples of the same formation can be expected to contain TOC several times higher than the weathered outcrop material.

The Whitehill Formation of the southern portion of the Main Karoo Basin is the main target for unconventional shale gas exploration. The Whitehill Formation has an average TOC of 4.5% and is laterally extensive with a thickness of up to 30 m producing an estimated yield of 390 tcf of gas. Over-maturity due to the proximity of the CFB and excessive burial may have resulted in the loss of potential hydrocarbons. Compartmentalisation of reservoirs and burning off of hydrocarbons due to the intrusion of numerous dolerite dykes and sills may have contributed to additional loss of

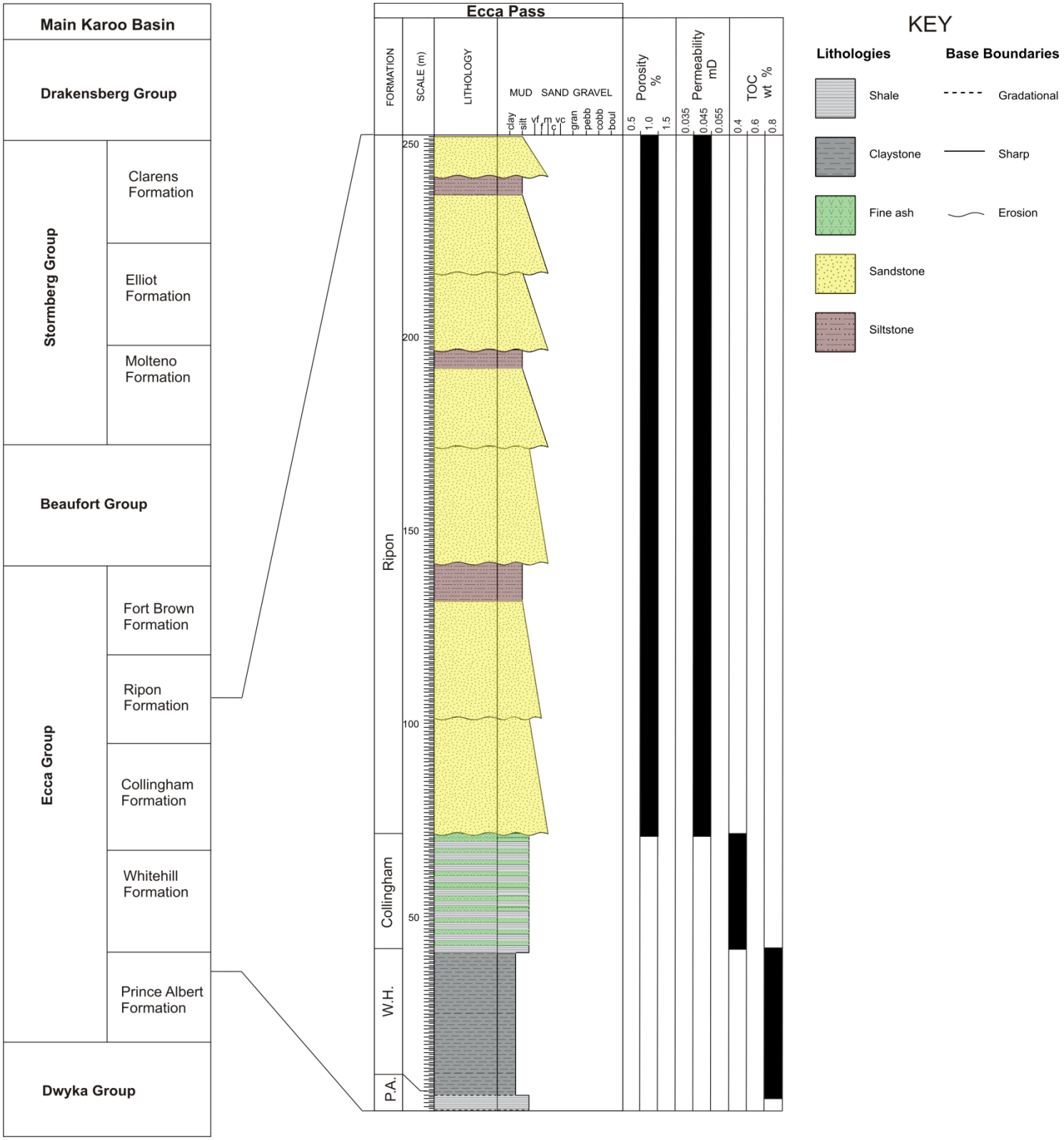

Figure 7.1: Generalised lithological log of the Ecca Pass study area with stratigraphic column and mean values of total organic carbon, porosity and permeability for individual formations. **Note**: The Collingham and Whitehill formations were not tested for porosity and permeability and the Ripon Formation was not tested for total organic carbon.

potential hydrocarbons. The Collingham Formation should be targeted for shale gas exploration if future studies indicate TOC values above 3% in fresh core material.

The Ripon Formation along the southern Karoo Basin boundary contains unfavourable conventional (turbidite) hydrocarbon reservoir characteristics being poorly located and plotting in the field of a tight rock. The southern Ripon Formation is also located in an over-mature gas window thus limiting the potential of conventional hydrocarbon storage.

Chapter 8 - Outlook

The Ecca Pass study site contains numerous possibilities for further research that, unfortunately due to the scope of the M.Sc thesis, were not pursued.

Suggested further research includes:

- A detailed provenance study should be conducted on the spotted sandstone portion of the Ripon Formation. Geochemical comparisons can be made with the Collingham Formation tuff as well as the crystal tuff in the Fort Brown Formation.
- Continuous TOC measurements and micro poro-perm measurements within the Whitehill Formation.
- The fossil rich horizon located at the base of the Ripon Formation identified in this study should be thoroughly studied in order to further document possible plant and insect remains.
- The formation of the Whitehill Formation gypsum nodules should be studied and geochemical analysis performed to ascertain if barium has replaced calcium in some samples as proposed in this study.
- A geochemical investigation into the formation of concretions in the Ripon Formation with an emphasis on concretion-rich versus concretion-poor layers should also be undertaken.
- Conducting sulphur isotope studies on shales of the Whitehill, Collingham and, Ripon formations in order to investigate a marine signature based on isotopic variations in pyrite.
- An investigation in to the potential geothermal potential of the southern portion of the Karoo Basin.

Chapter 9 - Reference List

Amy, L.A., Peachy, S.A., Gardiner, A.A. and Talling P.J. (2009) Prediction of hydrocarbon recovery from turbidite sandstones with linked-debrite facies: Numerical flow simulation studies. *Marine and Petroleum* Geology, **26**, 2032–2043.

Bordy, E.M. (2000) Sedimentology of the Karoo Supergroup in the Tuli Basin (Limpopo River Area, South Africa). PhD thesis, Rhodes University.

Bordy, E.M., Hancox, P.J. and Rubidge, B.S. (2004) Basin development during the deposition of the Elliot Formation (Late Triassic - Early Jurassic), Karoo Supergroup, South Africa. *South African Journal of Geology*, **107**, 395-410.

Bouma, A.H. (1962) Sedimentology of some Flysch Deposits: A Graphic Approach to Facies Interpretation. Elsevier, Amsterdam, 168.pp.

Bouma, A.H. and Stone, C.G. (eds.) (2000) Fine-grained turbidite systems. AAPG Memoir 72/SEPM Special Publication 68.

Branch, T., Ritter, O., Weckmann, U., Sachsenhofer, R. F. and Schilling, F. R. (2007) The Whitehill Formation - a high conductivity marker horizon in the Karoo Basin. *South African Journal of Geology*, **110,** 465-476.

Bruner, K.R., and Smosna, R., (2011) A Comparative Study of the Mississippian Barnett Shale, Fort Worth Basin, and Devonian Marcellus Shale, Appalachian Basin. U.S. Department of Energy (DOE). National Energy Technology Laboratory (NETL), pp.118.

Casnedi, R. (2005) Geological Characteristics of Hydrocarbon Reservoirs. *Encyclopedia of Hydrocarbons,* Volume I, Exploration, Production and Transport. pp. 85-104.

Catuneanu, O., Hancox, P.J. and Rubidge, B.S. (1998) Reciprocal flexural behaviour and contrasting stratigraphies: a new basin development model for the Karoo retroarc foreland system, South Africa. *Basin Research*, **10**, 417-439.

Catuneanu, O., and Elango, H.N. (2001) Tectonic control on fluvial style: the Balfour Formation of the Karoo Basin, South Africa. *Sedimentary Geology*, **140**, 291-313.

Catuneanu, O., and Bowker, D.M. (2002) Sequence stratigraphy of the Koonap and Middleton fluvial formations in the Karoo foredeep, South Africa. *Journal of African Earth Science*, **33**, 570-595.

Cole, D.I. and Basson, W.A. (1991) Whitehill Formation, in Johnson M.R., ed, Johnson. M.R. (Ed.), Catalogue of South African Lithostratigraphic Units. South African Committee for stratigraphy, 51-52.

Decker, J. and Marot, J. (2012) Investigation of Hydaulic Fracturing in the Karoo of South Africa. Annexure A, Resource Assessment, Pertoluem Agency SA 2012. [Online] Available at: http://www.dmr.gov.za/publications/viewdownload/182/854.html

Decker, J. (2013) The Karoo Basin's Shale Gas Potential. Petroleum Agency SA. GeoForum, Johannesburg.

De Wit, M.J. and Ransome, I.G.D. (1992) Regional inversion tectonics along the Southern Margin of Gondwana. In: De Wit M.J., Ransome I.G.D (eds) Inversion tectonics of the Cape Fold Belt, Karoo and Cretaceous Basins of Southern Africa. A.A Balkema, Rotterdam, pp. 15-21

Einsele, G. (1992) Sedimentary Basins: Evolution, Facies and Sediment Budget. Springer, Berlin, 792

Energy Information Administration (2013) Technically Recoverable Shale Oil and Shale Gas Resources: An Assessment of 137 Shale Formations in 41 Countries Outside the United States. [Online] Available at: http://www.eia.gov/analysis/studies/worldshalegas/

Faure, K. and Cole, D. (1999) Geochemical evidence for lacustrine microbial blooms in the vast Permian main Karoo, Paraná, Falkland Islands and Huab basins of southwestern Gondwana. *Palaeogeography, Palaeoclimatology, Palaeoecology*, **152**, 189–213.

Flint, S.S., Hodgson, D.M., Spraque, A.R., Brunt, R.L., Van Der Merwe, W.C., Figueiredo, J., Prelat, A., Box, D., Di Celma, C. and Kavanagh, J.P. (2011) Depositional Architecture and Sequence Stratigraphy of the Karoo Basin Floor to Shelf Edge Succession, Laingsburg Depocenture, South Africa. *Marine and Petroleum Geology*, **28**, 658-674.

Geel, C., Schulz, H.M., Booth P., De Wit, M. and Horsfield B. (2013) Shale Gas Characteristics of Permain Black Shales in South Africa: Results From Recent Drilling in the Ecca Group (Eastern Cape). *Energy Procedia*, **40**, 256-265.

Gess, R.W. (2013) The Earliest Record of Terrestrial Animals in Gondwana: A scorpion from the Famennian (Late Devonian) Witpoort Formation of South Africa. *African Invertebrates*, **54** (2), 373-379.

Goggin, D.J., Thrasher, R.L. and Lake, L.W. (1988) A theoretical and experimental analysis of minipermeameter response including gas slippage and high velocity flow effects. *In Situ*, **12**, 79-116.

Götz, A.E. and Lenhardt, N. (2011) The Anisian carbonate ramp system of Central Europe (Peri-Tethys Basin): sequences and reservoir characteristics. *Acta Geologica Polonica*, **61**(1), 59-70.

Götz, A.E. and Ruckweid, K.C. (2013) Palynological Records of the Early Permian Post Glacial Climate Amelioration (Karoo Basin, South Africa). Paleobiodiversity and Palaeoenvironment DOI 10.1007/s12549-013-0134-8.

Götz, A.E., Török, Á. and Sass, I. (2014) Geothermal reservoir characteristics of Meso- and Cenozoic sedimentary rocks of Budapest (Hungary). Zeitschrift der Deutschen Gesellschaft für Geowissenschaften (German Journal of Geoscience).

Haughton, S. H. (1925) Exhibit: tracks of animals preserved in the Ecca Shales of Cape Province. *Transactions of the Royal Society of South Africa*, **13**, 28-29 [Minutes of the proceedings 1924-1925 published in 1926]

Haughton, S.H. (1928) The geology of the county between Grahamstown and Port Elizabeth. Explanatory Notes to Cape Sheet 9 Geological Survey, Department of Mining, South Africa.

Hoelke, J.D., (2011) Chemostratigraphy and Paleoceanography of the Mississippian Barnett Formation, Southern Fort Worth Basin, Texas, USA. Master Degree of Science in Geology submitted by the University of Texas, Arlington, pp. 96.

Horne, R.R. and Taylor, B.J. (1969) Calcareous Concretions in the Lower Cretaceous Sediments of South-Eastern Alexander Island. British Antarctic Survey Bulletin.

Huggins, P. (2007) Heterogeneity and flow barriers in turbidites, Foinaven Field, UKCS. 69th EAGE Conference & Exhibition, WO11 North Sea Core Workshop.

Johnson, M.R., van Vuuren, C.J., Visser, J.N.J., Cole, D.I., de V. Wickens, H., Christie, A.D.M., Roberts, D.L. and Brandl, G. (2006) Sedimentary Rocks of the Karoo Supergroup. In: Johnson M.R., Anhaeusser C.R. & Thomas R.J. (Eds)(2006). The Geology of South Africa. Geological Society of South Africa, Johannesburg/Counsel for Geoscience, Pretoria pp. 691.

Johnson, M.R. (1976) Stratigraphy and Sedimentology of the Cape and Karoo Sequences in the Eastern Cape Province. PhD thesis, Rhodes University.

Johnson, M.R. (1966). The Stratigraphy of the Cape and Karoo Systems in the Eastern Cape Province. MSc thesis, Rhodes University.

Johnson, S.D., Flint, S., Hinds, D. and De Ville Wickens, H. (2001). Anatomy, geometry, and sequence stratigraphy of basin floor to slope turbidite systems, Tanqua Karoo, South Africa. *Sedimentology*, **48**, 987-1023.

Kingsley, C.S. (1979) A composite turbidite-delta-fluvial model for the Permian sedimentation in the Ecca and lower Beaufort of the Eastern Cape Province: a new link with Gondwanaland. 18th Congree of the Geological Society of South Africa, Part 2 (abstracts), Karoo Basin Symposium, 96-105.

Kingsley, C. S. (1981) A composite submarine fan-delta-fluvial model for the Ecca and lower Beaufort Groups of Permian age in the Eastern Cape Province. *Transactions of the Geological Society of South Africa*, **84**, 27-40.

Lindeque, A., De Wit, M.J., Ryberg, T., Weber, M. and Chevallier, L. (2011) Deep Crustal Profile Across the Southern Karoo Basin and Beattie Magnetic Anomaly, South Africa: An integrated interpretation with tectonic implications. *South African Journal of Geology*, **114**, 265-292.

Nichols, G. (2009) Sedimentology and Stratigraphy. 2nd Edition, Wiley Blackwell, Chichester, pp. 419.

Martin, J. P., Hill, D.G., Lombardi, T.E. and Nyahay, R.E. (2008) A Primer on New York's Gas Shales, New York State Geological Association: Field Trip Guidebook- 80th Annual meeting.

McCarthy, T. and Rubidge, B. (2005) The Story of Earth and Life. A Southern African Perspective on a 4.6 Billion-Year-Journey. Struik Publishers, Cape Town.

Miall, A.D. (1996) The Geology of Fluvial Deposits. Sedimentary Facies, Basin Analysis, and Petroleum Geology. xvi + 582 pp.

Moore, D.M. and Reynolds, R.C (1989) X-ray diffraction and the identification and analysis of clay minerals, pp. 332.

Mountain, E.D. (1946) The geology of an area east of Grahamstown. An explanation of sheet no. 136 (Grahamstown). Geological Survey of South Africa.

Oelofsen, B.W. (1987) The biostratigraphy and fossils of the Whitehill and Irati shale formations of the Karoo and Paraná Basins. In G. D. McKenzie (ed): Gondwana Six: *Stratigraphy, Sedimentology and Paleontology.* Geophysis Monograph, American Geophysical Union **41**, 131-138.

Pangaro, F., and Ramos, V.A. (2012) Palaeozoic Crustal Blocks of Onshore and Offshore Central Argentina: New pieces of the south-western Gondwana collage and their role in the accretion of Patagonia and the evolution of Mesozoic south Atlantic sedimentary basins. *Marine and Petroleum Geology*, **37**, 162-183.

Reading, H.G. (1996) Sedimentary Environments: Processes, Facies, Stratigraphy. 3rd Edition. Blackwell Science, Oxford pp. 688.

Reed, F.S. and Mergner, J.L. (1952) Preparation of rock thin sections: 1184-1203. US Geological Survey, Washington D.C.

Reynolds, I.M. (1971). The Predominantly sandstone member of the Ecca Pass Formation. Unpublished BSc (Hons.) project, Rhodes University, Grahamstown.

Rossouw, P.J. (1953) General Geology: The Southern Karoo. In: Hauton, S.H., *et al*. Results of an Investigation into the the Possible Presence of Oil in Karoo Rocks in part of the Union of South Africa. *Memoir of the Geological Survey of South Africa*, **45**, 14-36.

Santos, R.V., Souza, P.A., Souza de Alvarenga, C.J., Dantas, E.L., Pimentel, M.M., Gouveia deOliveira C. and Medeiros de Araújo, L. (2006) Shrimp U–Pb zircon dating and palynology of bentonitic layers from the Permian Irati Formation, Paraná Basin, Brazil. *Gondwana Research*, **9**, 456–463

Sass, I. and Götz, A.E. (2012) Geothermal reservoir characterization: a thermofacies concept. *Terra Nova*, **24**, 142-147.

Scheffler, K., Buehmann D. and Schwark L. (2006) Analysis of late Palaeozoic glacial to postglacial sedimentary succession in South Africa by geochemical proxies-Response to climate evolution and sedimentary environment. *Palaeogeography, Palaeoclimatology, Palaeoecology*, **240**, 184-203.

Song, J., Littke, R., Maquil, R. & Weniger, P. (2014) Organic facies variablilty in the Posidonia Black Shale from Luxembourg: Implications for thermal maturation and depositional environment. *Palaeogeography, Palaeoclimatology, Palaeoecology*, **410**, 316-336.

Stow, D.A.V. (1994) Deep-sea processes of sediment transport and deposition. In: *Sediment Transport and Depositional Processes.* Blackwell Science, Oxford; 257-291.

Stollhofen, H., Stanistreet, I.G., Bangert, B. and Grill, H. (2000) Tuffs, tectonism and glacially related sea- level changes, Carboniferous-Permian, southern Namibia. *Palaeogeography, Palaeoclimatology, Palaeoecology*, **161**, 127-150.

Suarez-Ruiz, I. (2012) Organic Petrology: An Overview. Intechopen, Instituto Nacional del Carbõn (INCAR-CSIC) Oviedo, Spain, 200-217. Available at: <http://www.intechopen.com/download/get/type/pdfs/id/26096> (viewed 19-08- 14)

Tankard, A., Welsink H., Aukes P., Newton R. and Stattker E. (2012) Geodynamic interpretation of the Cape and Karoo basins, South Africa. Phanerozoic Passive Margins, Cratonic Basins and Global Tectonics Maps. USA & UK: Elsevier 869.

Thomas, C.G.C. (2001) Sedimentology and Stratigraphy of the Falkland Islands Permian with comparisons to Gondwana stratigraphy of South Africa and South America. Unpublished PhD Thesis, University of Aberdeen, [various pages]

Trewin, N. H., Macdonald, D. I. M. and Thomas, C. G. C. (2002) Stratigraphy and sedimentology of the Permian of the Falkland Islands: lithostratigraphic and palaeoenvironmental links with South Africa. *Journal of the Geological Society*, London **159**, 5-19.

Veevers, J.J., Cole D.I. and Cowan E.J. (1994) Southern Africa: Karoo Basin and Cape Fold Belt. In: Veevers J.J., Powell C.Mc.A. (ed) Permian-Triassic Pangean Basins and fold belts along the Panthalassan Margin of Gondwanaland. *GSA Memoir*, **184**, 223-279.

Verreussel, R., Zijp, M., Nelskamp, S., Wasch, L., de Briun, G., ter Heege, J. and ten Veen, Johan. (2013) Pay-zone identification workflow for shale gas in the Posidonia Shale Formation, the Netherlands. *first break*, **31**,63-69.

Visser, J.N.J. (1996) Controls on Early Permian Shelf Deglaciation in the Karoo Basin of South Africa. *Palaeogeography, Palaeoclimatology, Palaeoecology,* **125**, 129-139.

Visser, J.N.J. (1994) A Permian argillaceous syn- to post-glacial foreland sequence in the Karoo Basin, South Africa. In Deynoux, M., Miller, J.M.G., Domack, E.W., Eyles, N. & Young, G.M. (Eds.) Earth's Glacial Record. International Geological Correlation Project Volume **260**,193-203. Cambridge University Press, Cambridge.

Visser, J.N.J. (1992) Deposition of the Early to Late Permian Whitehill Formation during a sea-level highstand in a juvenile foreland basin. *South African Journal of Geology*, **95**, 181-193.

Weimer, P., Slatt, R.M., Coleman, J., Rosen, N.C., Nelson, H., Bouma, A.H., Styzen, M.J., and Lawrence, D.T. (Eds.) (2000) Deep-Water Reservoirs of the World. Gulf Coast Section. SEPM 20th Bob F. Perkins Research Conference.

Appendix A

Checklist for Description of Clastic Sedimentary Rocks in Hand Specimen

1. Colour (not dark or light)
2. Grain size (diameter of the most common grains with special mention to max and min sizes if not sorted- document grain size in both mm and words).
3. Sorting
4. Shape of grains (rod, disk, sphere)
5. Rounding and sphericity of grains
6. Clast: matrix ratio (clast or matrix supported)
7. Type of cement (not of matrix)(eg. Silica, calcite, Fe-oxides, -use acid test).
8. Textural maturity (including clay content).
9. Fossil content, bioturbation (trace fossils)
10. Sedimentary structures
11. Weathering
12. Rock name

Appendix B

Checklist for Petrographic Description of Sandstones in Thin Section

I. Sample Number

II. Texture

A. Most dominant grain size

If polymodal, what are the modal sizes?

B. Sorting *very well s. well s. moderately s. poorly s. very poorly s.*

C. Grain shape

Idiomorph xenomorph

Low sphericicty high sphericicty

Very angular angular/subangular subrounded rounded very well rounded

Relation of roundness to grain size and mineralogy

Roundness sorting

D. Stage of textural maturity

Immature sediment = >5% clay matrix: poorly-sorted and not well rounded grains

Submature sediment = < 5% clay matrix: poorly-sorted and not well rounded grains

Mature sediment = little or no clay matrix: well-sorted but not well rounded grains

Supermature sediment = no clay matrix: well-sorted and well rounded grains

E. Fabric

Homogenous (massive) Laminated (cause and scale of lamination)

Ratio of grain:matrix (grain or matrix supported).

Grain orientation (lineation, imbrication)

Grain packing (closely p, loosely p)

Grain contacts (point ct. concavo-convex ct. sutured ct.)

Percent of porosity (i.e pore-filling cement plus present porosity)

Etching of grains by cement

Bioturbation

III. Mineral Composition

A. Percentage of quartz

Monocrystalline polycrystalline

Undulatory nonundulatory

Polycrystalline grains

Grain size xtl size xtl number xtl texture and boundary

Mean grain size (relation btw quartz type and grain size (eg mono qtz coarser than poly)

B. Percentage of feldspar

Twinned untwined

Type of twinning

Degree and type of alteration

Mean grain size (relation between mineralogy and grain size)

C. Percentage of lithic fragments

Types of fragments and relative abundances

Plutonic rf volcanic rf metamorphic rf sedimentary rf

Mean grain size (relation btw fragment type and grain size)

D. Percentage of micas

Types of mica and relative abundances

Biotite muscovite (+ other white micas)

Mean grain size (relation btw mica type and grain size)

E. Percentage of other terrigenous minerals

Types of terrigenous minerals and relative abundances

Fe-oxides tourmaline zirzon

Mean grain size (relation between mineralogy and grain size)

IV. Matrix- total percentage

Percentage of: Clay qtz mica

V. Classification

VI. Provenance

Appendix C

XRD Mineral Data

MINERAL DATA BASE	SAMPLE			
	CH5a	Wh2	Pa1b	R4a
Illite: Wavellite				
Oneilite	xx			xx
Mendipite				x
Leadhillite				
Devilline		x		
Bobtraillite				
Afwillite			x	
Sanidine			x	x
Quartz	x	x		
Pyrite			x	
Biotite: Phlogopite				
Anite				
Oligoclase				
Muscovite			x	
Montmorillonite				
Calcite	x			
Albite				x
Siderite				
Chamosite				
Dolomite	x			
hematite				x
goethite	x		x	x
chloritoid				
clinochlore				
fayalite				
magnetite	xx	x	xx	
Baryte	xx	xx	x	
gypsum				
chlorapatite				
flourapatite	xx			xx
Birnessite	xx		xx	
Pyrolusite	x			
Bixbyite				
Hausmannite	x			
Hollandite				
gold			x	
xx	High Probability			
x	Low Probablity			

Appendix D

Total Organic Carbon Data

Sample	EP1	EP2	CH5	CH6
Formation	Whitehill	Whitehill	Collingham	Collingham
Lithology	Black shale	Black shale	Shale	Shale
TOC (wt%)	0.6	0.9	0.6	0.2
Sulphur (wt%)	0.0	0.0	0.0	0.0
Tmax (°C)	No Tmax	No Tmax	No Tmax	No Tmax
S1 (mg/g)	0.00	0.00	0.00	0.00
S2 (mg/g)	0.03	0.07	0.01	0.01
S3 (mg/g)	0.79	1.16	0.66	0.33
PI	0	0	0	0
HI	5.0	7.78	1.67	5.00
OI	131.67	128.89	110.00	165.00

Appendix E

Porosity and Permeability Data

Sample	Lithology	Grain Density	Porosity	Permeability	Permeability
		[g/cm³]	**[%]**	**Ø[mD]**	**Ø[m²]**
1	Medium grained sandstone	2.7268	0.645	0.01	7.2148E-18
2	Fine grained sandstone	2.6737	1.08	0.01	1.1201E-17
3	Medium grained sandstone	2.6574	0	0.06	5.8148E-17
4	Medium grained sandstone	2.6395	3.7	0.07	6.9131E-17
5	Medium grained sandstone	2.6349	1.453	0.1	9.9368E-17
6	Medium grained sandstone	2.6905	0	0.01	8.7353E-18
7	Fine grained sandstone	2.6495	0.943	0.01	1.3741E-17
8	Very fine grained sandstone	2.6932	1.437	0.08	8.0935E-17
9	Medium grained sandstone	2.638	0.813	0.03	3.2666e-17
10	Very fine grained sandstone	2.6750	0.02	0.07	9.2227E-17
	Mean	**2.6704**	**1.0091**	**0.045**	**4.7337E-17**